UNIVERSITÀ DEGLI STUDI DI TRENTO

Doctoral School in Civil, Environmental and Mechanical Engineering

Topic 3. Modelling and Simulation

Benedetta Calusi

Penetration Mechanics of Plant Roots and Related Inspired Robots

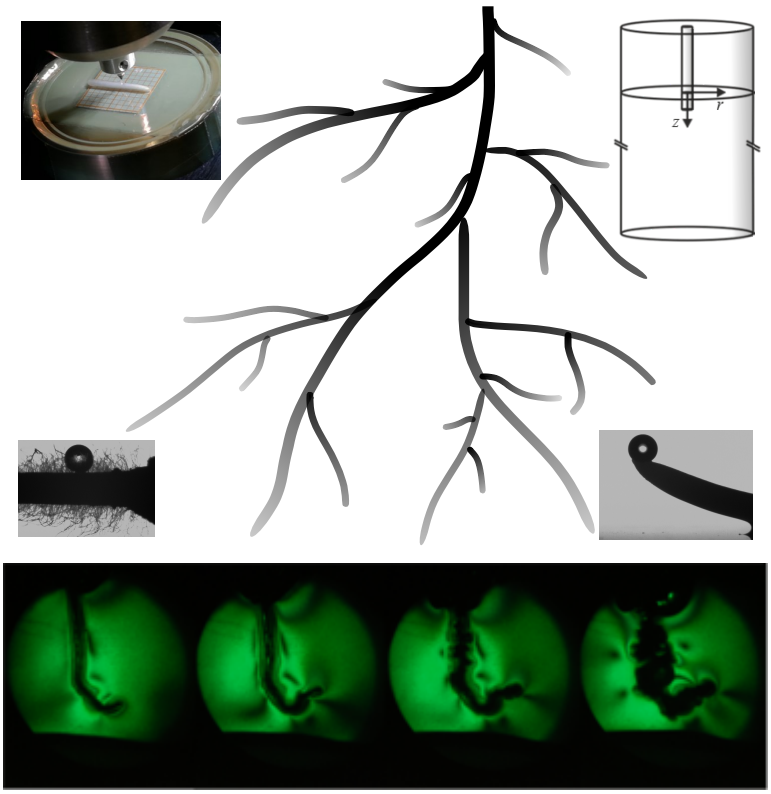

2017 - Doctoral thesis

UNIVERSITY OF TRENTO - Italy
Department of Civil, Environmental
and Mechanical Engineering

Doctoral School in Civil, Environmental and Mechanical Engineering
Topic 3. Modelling and Simulation - XXX cycle 2015/2017

Doctoral Thesis - June 2018

Benedetta Calusi

Penetration Mechanics of Plant Roots and Related Inspired Robots

Supervisors
Barbara Mazzolai, CMBR of the Istituto
Italiano di Tecnologia
Nicola Maria Pugno, University of Trento

Credits of the cover image: Benedetta Calusi

University of Trento
Doctoral School in Civil, Environmental and Mechanical Engineering
http://web.unitn.it/en/dricam
Via Mesiano 77, I-38123 Trento
Tel. +39 0461 282670 / 2611 - *dicamphd@unitn.it*

Dedicated to my little sweet Chiara,
to my little adventure buddy,
and to those who always had faith in me.

Acknowledgements

I wish to thank various people for their support and encouragement that I have received throughout my educational and professional career. In particular, I would like to express my sincere gratitude to Angiolo Farina, Fabio Rosso, and Lorenzo Fusi of the University of Firenze for inspiring and encouraging me during my master degree with their love for science, that got me into the world of research. I would also like to thank Alice Berardo and Maria Fiorella Pantano of the University of Trento for their friendship, constant support, and guidance during my PhD studies. My sincere thanks go also to Francesca Tramacere of the Italian Institute of Technology for her encouragement, constructive suggestions, and useful critiques. Furthermore, I would also like to extend my thanks to some new colleagues and friends that I have met during my PhD. Finally, I would like to thank my current advisors, Barbara Mazzolai and Nicola Maria Pugno, for the opportunity to improve, discover and explore connections between biology, engineering, and mathematics.

Trento, March 8, 2018

Benedetta Calusi

Table of Contents

List of Figures

List of Tables

Summary

The ability of plant roots to penetrate soils is affected by several stimuli from the surrounding medium such as mechanical stresses and chemical changes. Therefore, roots have developed multiple responses to the several outer stimuli. Since plant roots have to face very complex problems to grow deeply into the ground, they are remarkable examples of problem-solving behaviour and adaptation to the outer constraints. The adaptation strategies of a natural root are not yet completely known and understood with exhaustive explanations. For this reason, mathematical models and experimental techniques applied to biological phenomena can perform a key role in translating the Nature adaptive solutions into engineering applications. The aim of this thesis is therefore to provide further insights in understanding biological phenomena for the development of new potential technologies inspired by the adaptive ability of plant roots, e.g. for environmental exploration, monitoring systems, rescue tasks, and biomedical fields. Accordingly, we proposed both theoretical and experimental explanations to the adaptive behaviour of plant roots. The mathematical modelling is based on a modified version of the extended (Guiot, Pugno and Delsanto, 2006) West, Brown and Enquist universal law (West, Brown and Enquist, 2001), considering the root growth as an inclusion problem. We showed that the proposed equation has as a particular case a growth equation exploiting an approach similar to Lockhart (Lockhart, 1965) taking into account the soil impedance. We studied the influence of mechanical stresses and nutrient availability on the root growth. Firstly, we applied the developed theoretical framework for the strategy adopted by plant roots of a growing tip in natural soils and of the root behaviour in response to different soil impedances with data from both natural and artificial soils. The model predicted a different variation of the root final length in artificial and real soils. Unexpectedly, we obtained a greater elongation in the highest compaction for the case of artificial soils and a lower elongation in the highest compaction for real soils. The results were in agreement

with experimental data. Secondly, by coupling mechanical stress with nutrient stimuli, we adopted an activation mechanism of the root response to the nutrient availability in order to model the radial expansion. In particular, we proposed an extension of the previous mathematical model by including a radial expansion through a critical threshold. We compared the numerical solution of the analytical model with experimental data collected in artificial soils.

In addition, we investigated the theories and hypotheses of the root ability to grow in the apical region through nanoindentation, wettability, and photoelasticity. The first technique provided insights for the possible role and function at both different tissues levels and distances from the tip in the root movement and penetration during the growth. The investigation of root tissue properties revealed that the penetration and adaptation strategies adopted by plant roots could be enhanced by a combination of soft and stiff tissues. The second technique aimed to highlight the wettability of the apical zone and root hairs for the acquisition of water and nutrients. Finally, photoelastic experiments provided a non-invasive and *in situ* observation of plant roots growth and, by exploiting the fringe multiplication, we proposed a set up for the study of plant roots growing in edible gelatine.

Chapter 1

1. Introduction

1.1. Bioinspired Engineering

In their evolution, humans have developed several methods, design and materials to improve the quality of their life. However, such solutions could frequently have a negative impact on the environment, e.g. the presence of pollutants in both air and water damaging all species living on the Earth. On the contrary, Nature has developed effective mechanisms by continuously adapting in order to withstand the environment changes. Specifically, several examples of optimal efficiency in design and fabrication can be found in Nature, such as bees' honeycomb, spider's web, gecko adhesion and lotus' self-cleaning, see e.g. (Bar-Cohen, 2006; Cranford *et al.*, 2012). Moreover, it is relevant how animals and plants evolved strategies to adapt and maintain stability during their movements, from climbing abilities to soil anchorage. Therefore, science and engineering are both interested in the principles exploited by Nature (Darwin and Darwin, 1880; Dougal, 1987; Full, 2002; Goriely and Neukirch, 2006; Baluška *et al.*, 2009; Isnard and Silk, 2009; Roppolo *et al.*, 2011; Margheri *et al.*, 2011; Crouzy, Edmaier and Perona, 2014; Tramacere *et al.*, 2014; Edmaier *et al.*, 2014; Mazzolai, Beccai and Mattoli, 2014; Popova, Tonazzini, *et al.*, 2016). The transfer of such biological mechanisms into novel technologies and solutions can lead to a great improvement in engineering applications (Laschi *et al.*, 2012; Hawkes *et al.*, 2014; Tricinci *et al.*, 2015; Pope *et al.*, 2017). In particular, the translation of Nature's adaptive strategies into engineering applications could provide smart solutions with tunable properties, e.g. films with controlled surface wettability (Wang *et al.*, 2017). In addition, the use of a bioinspired approach could lead to the development not only of efficient devices but also of environment-friendly technologies. The nest of birds and silk fabrication, e.g. of spiders and silkworm, are remarkable examples of Nature's ability to produce sustainable, smart and effective solutions. In this regard, a recent

study shows the existence of worms eating plastic that leads to a potential solution for plastic degradation (Bombelli, Howe and Bertocchini, 2017). Furthermore, another recent research investigates and translates the hairy structure of aquatic plant leaves for oil/water selective separation with biodegradable and recyclable polymers (Kavalenka *et al.*, 2017; Zeiger *et al.*, 2017). Therefore, Nature is the perfect teacher for the creation of robust, efficient, and optimized ideas which provide benefits to both the environment and the economy. The study and translation of Nature's adaptive strategies could have a positive effect on the sustainability and economic development.

Recently, plant roots have inspired new principles and new technological solutions: plant-inspired robots, called PLANTOIDs (Mazzolai, 2017), which aim at efficiently moving into the soil by artificial roots that can grow, sense, and bend (Sadeghi *et al.*, 2014, 2017), by exploiting the adaptive penetration strategies of the natural counterpart. One of the main challenges in describing the penetration of plant roots is the active interaction between the root and the soil, i.e. the presence of a simultaneous and mutual dependence on their evolutions and changes (*Figure 1.1.1*). In fact, roots adapt themselves to unexpected environment changes with several responses, e.g. the shrinking of the diameter, the root-structure architecture, the secretion (Barley, 1963; A. G. Bengough and Mullins, 1990; Li *et al.*, 2014; Popova, van Dusschoten, *et al.*, 2016), by leading further changes in the surrounding medium. Thus, plant roots move inside the soil by growing at the apical zone with several and not yet completely known regulation mechanisms. One of the first steps towards a better understanding of the root penetration is the knowledge and definition of the key parameters to simplify the variables involved. The penetration mechanisms and adaptation can be investigated by means of mathematical modelling and experimental techniques. Theoretical studies have been developed to investigate and to explain possible regulation processes that govern the root growth, by exploiting either the control of hormone production, the root water uptake, the root distribution on space, or the mechanical behavior at the cellular to tissue scale, e.g. see (Chavarría-Krauser, Jäger and Schurr, 2005; Dupuy,

Gregory and Bengough, 2010; Dyson and Jensen, 2010; Blengino Albrieu, Reginato and Tarzia, 2015). In this regard, experimental investigations can estimate essential aspects which mathematical models could predict and exploit, i.e. chemical and morphological properties and variations that may depend on the environment changes, e.g. see (Hamza *et al.*, 2006; Peaucelle, 2014; Colombi *et al.*, 2017; Dietrich *et al.*, 2017).

For the theoretical approach, two simple models from continuum mechanics have been proposed to characterize the mechanical and nutrient influence of the surrounding medium on the root during its growth. In addition, the root mechanical properties, wettability of root surface and the stress distribution developed by plant roots inside the surrounding medium have also been investigated.

Experimental frameworks will allow further to extend the proposed mathematical modelling by considering a more complete scenario of the root growth inside a soil medium.

Indeed, the linkage of theoretical and experimental studies could provide not only the means to better understand the root control mechanisms (e.g. tissue bending, mucilage secretion, and hormones production), but also contribute in defining which aspects should be translated with artificial smart materials in devices. For this reason, cross-disciplinary studies are crucial to shed light on the root adaptive capability during the penetration through the soil. On this basis, a future challenge is to inspire an effective design based on the biological phenomenon and, consequently, to describe the connection between natural and artificial roots.

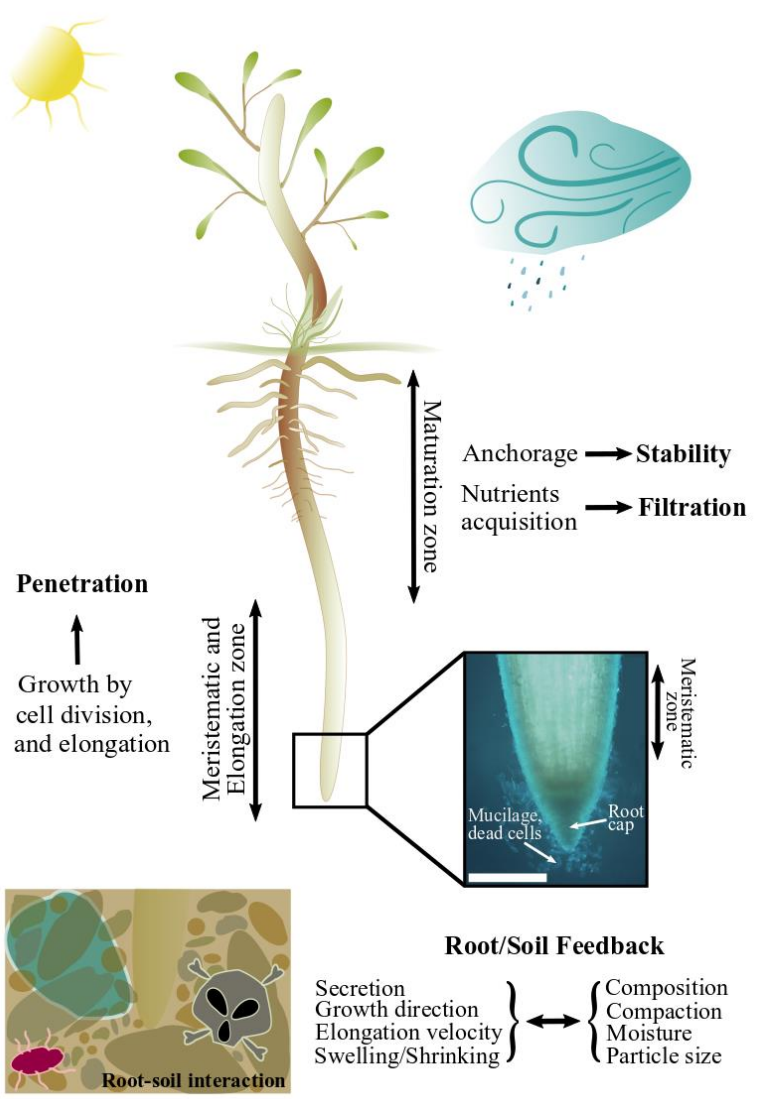

Figure 1.1.1 Schematic diagram of plant root structure with a simplified overview of the interaction between plant roots and environment (e.g. climatic and soil influences). The growth phenomenon occurs at the apical region through cell growth and elongation. The growing region is constituted by the elongation zone and the meristem, separated by a transitional zone, namely the transition zone. Therefore, the growing tip with mucilage and cell secretion at the root cap enables the root penetration into the soil. The maturation zone is stationary and it is characterized by the presence of lateral hairs on the roots. The presence of hairs and lateral roots in the mature zone provides nutrients acquisition and anchorage. In the latter zone, the cells begin their differentiation to become a more specialized type. The growth phenomenon is strictly connected to the root structure organization, i.e. the development of specialized zones allows roots to penetrate the soil with adaptive movements.

1.2. Outline

The present work focused on providing further insights in understanding Nature's adaptive solutions for the development of innovative technologies inspired by the penetration mechanics of plant roots. This thesis aims at studying such strategies through mathematical modelling and experimental methods and translating them into potential engineering applications.

Chapter 2 and 3 are devoted to mathematical modelling developed to describe the root growth in presence of mechanical and nutrient stimuli. In fact, the ability of plant roots to penetrate soils is affected by different stimuli, which are exerted by the surrounding medium. In literature, studies undertook in real soils have shown conflicting results. We supposed that this discrepancy was mainly due to the experiment in real soils, which are intrinsically characterized by several chemical and physical stimuli. We then compared the two growth models with experimental data.

In particular, in Chapter 2 we investigated and modelled the biomechanical response of the primary root of *Zea mays L.*, grown in artificial soils at several levels of compactness. Unlike in heterogeneous real soils, in artificial soils the mechanical stimulation can be distinguished from all other stimuli. We developed a mathematical model of the dynamic evolution of plant roots, based on a modified version of the extended universal law of West, Brown and Enquist. The theoretical results confirm the used experimental data. Our model highlighted that root behaviour is strongly affected by the mechanical properties of the surrounding medium and may provide a plausible theory explaining the root behaviour during the growth inside the surrounding soil medium. This study provides further insights for the adaptive ability of plant roots to various soil impedance constraints.

In Chapter 3, we explored the root growth with different nutrient concentrations in artificial soils. In fact, in presence of high concentration of chemicals plants show thicker and shorter root apparatus. This physiological enlargement of the root

transversal section becomes anomalous in presence of toxic elements. In this case, an abnormal swelling of the root diameter and an inhibition of the root elongation occur in the apical region. Thus, we studied the response of *Zea mays* roots to different nutrient concentrations in artificial soils and proposed a hypothesis of mechanism which can be used by plants to control nutrient changes. In this regard, we extended the model developed in Chapter 2 by including both axial and radial growth and we proposed that the radial expansion occurs through a critical threshold.

The exploited experimental results showed that an excess of nutrients concentration can result toxic for the plants, which, in fact, show a shorter root system with abnormal enlargement in the apical region.

Our experimental and theoretical findings may improve the current knowledge of the root response to nutrient stress. In particular, this study could describe how plant roots may regulate both the root elongation and radial expansion due to nutrient concentrations.

Chapters 4 and 5 are devoted to experimental activities.

In Chapter 4, we analysed the mechanical properties and surface features of *Zea mays* primary roots, exploiting dynamic nanoindentation and wettability tests. We used the indentation in the apical region and measured the contact angle close both to the tip and the seed. The mechanical results revealed higher storage modulus along the outer wall with respect to the central skeleton. Therefore, the outer tissue could provide a coating to induce rigidity along the whole root and inner core could help in case of unexpected fractures of the outer wall, e.g. for the excavation of tunnels by burrowing animals or water flow. Moreover, the contact angle tests showed that the apical region is characterized by low wettability and the hairy surface close the seed seem to be a highly hydrophobic surface.

The aim of this work is to implement these features into robots inspired by natural roots. Accordingly, a soft robot with adaptable mechanical and wettability

properties for both efficient penetration and selective filtration could be useful in several fields, e.g. soil monitoring and exploration, chemical and toxic material spill and medical applications.

In Chapter 5, we explored the growth of *Phaseolus vulgaris L.* primary roots in homogeneous birefringent media using the photoelastic technique. The growth medium is edible gelatine. The creation of an artificial growing medium with photoelastic properties allows to directly observe the root development and to analyse the stresses of the growing root at the same time. Plant roots generate small stresses at the growing tip, thus only low fringe orders can be seen. Therefore, we showed the advantages of fringe multiplication applied to the study of plant roots growing in edible gelatine.

In Appendix, we present an additional related study. In particular, it is devoted to mathematical modelling of instability phenomena affecting the performance of load sensor in MEMS-based tensile testing devices.

Chapter 2

2. Mathematical Model for Axial Root Growth under Soil Confinement

Plants do not follow a rigid predefined growing plan but adjust their strategy to environmental conditions. Upon germination, plant architecture is driven by a genetic post-embryonic program, which is at the basis of the plant plasticity (Foehse and Jungk, 1983; Sánchez-Calderón, Ibarra-Cortés and Zepeda-Jazo, 2013). The study in (Bradshaw, 1965) identified two types of plant plasticity based on morphological or physiological mechanisms. Morphological mechanisms require high energetic costs because new functional portions are produced. On the other hand, in the physiological mechanism, the modifications occurring in differentiated tissue are imperceptible, the process is completely reversible and the energetic cost is very low. The two types of plasticity are continuously expressed during plant life since they are fundamental for their own survival (Grime and Mackey, 2002). Root system is one of the more remarkable examples of plant plasticity because it can sense, move and respond to the external stimuli and transmit this information to the entire plant. The root architecture is led by the root tip, which has the entire control of root structure in the space of a few millimetres (Filleur *et al.*, 2005). Root tip consists of a meristematic and elongation area, separated by a region called the transition zone (*Figure 2.1*). The initial cells, namely the cells producing new tissues during root growth, are in the meristematic zone. Therefore, the apical region interacts with the surrounding medium and can move continuously adapting to the outer stimuli, e.g. soil impedance. Specifically, a growing plant root can exert an estimated maximum pressure up to 1MPa (Misra, Dexter and Alston, 1986). For maize root, the arrest of the growth has been reported with a penetration resistance of 0.8-2MPa (Clark, Whalley and Barraclough, 2003; Bengough *et al.*, 2011), and in (Popova, van Dusschoten, *et al.*, 2016) some maize plants did not grow beyond a penetrometer resistance of 0.25MPa. The growth

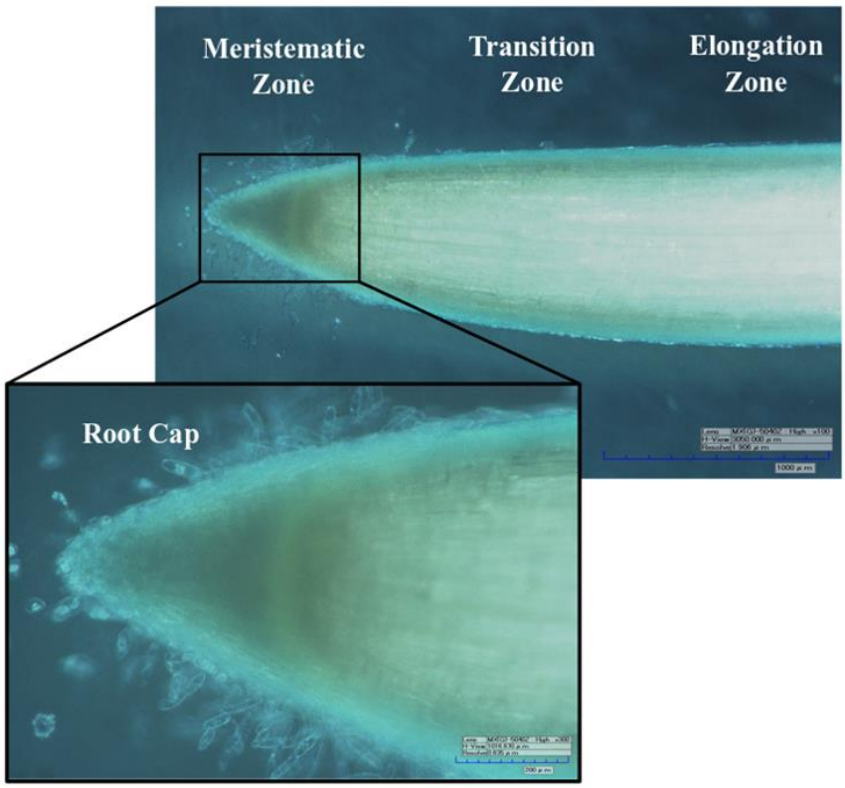

Figure 2.1 Optical image of the growth region of a *Zea mays L.* primary root. The zoom shows the root cap with mucilage and dead cells.

pressure is defined as the stress, acting normally at the root surface, which a root has to exert in order to deform the soil around it. Although a penetrometer probe is widely used to estimate the pressure that a root has to exert for penetrating soils, the studies in (Clark, Whalley and Barraclough, 2003) and (Misra, Dexter and Alston, 1986) demonstrated that this procedure overestimates the root growth strength. In literature, growth models for plant roots are mainly based on Lockhart's equation (Lockhart, 1965; Greacen and Oh, 1972). In (Dexter, 1987), expressions are proposed for the changes in root elongation rate with respect to soil water potential and soil mechanical resistance.

In this Chapter, we investigate the evolution of the primary root of maize in artificial soil with different concentration of Phytagel and in real soils with different

soil compactness. Furthermore, we formulate a mathematical model for root growth based on an elastic inclusion problem (Guiot, Pugno and Delsanto, 2006). By exploiting a continuum mechanics approach, we consider plant root as an elastic cylinder and soil as a homogeneous elastic fracturable matrix, in agreement with (Guiot, Pugno and Delsanto, 2006). Since we focus on the variation of the root elongation caused by the interactions with the surrounding environment, we consider a single isolated root growing in an axial direction. By comparing the theoretical results with experimental data, the goal of the present work is to investigate how the root behaviour can be affected by the mechanical interaction between the growing root and the surrounding soil medium.

2.1. Theoretical Model

We present a mathematical model describing the effect of mechanical stresses on plant root growth. The model shows how the axial stress at the contact affects the plant roots growth in the surrounding environment. When the environment is hard to penetrate, an individual root may stop growing (Popova, van Dusschoten, *et al.*, 2016). Therefore, a Fracture-Regrowth Cycle, FRC, was used as in (Guiot, Pugno and Delsanto, 2006) by including also the condition that the root stops its growth when a threshold axial pressure is reached. If $\overline{p}_{fr}^{*}$ is the fracture stress of the surrounding elastic medium and $\overline{p}_{c}^{*}$ is the maximum pressure that a root can exert to grow, two cases can occur:

(a) $\overline{p}_{c}^{*} \leq \overline{p}_{fr}^{*}$. The elastic root can grow until the axial stress $\overline{p}^{*}$ reaches the critical value and there is no fracture of the elastic matrix; i.e. the root stops growing when $\overline{p}^{*} = \overline{p}_{c}^{*}$. It may be the limit case of a root growing in very strong soils.

(b) $\overline{p}_{c}^{*} > \overline{p}_{fr}^{*}$. The medium strength tolerance is reached and the root relaxes. Therefore, the growth process starts with a new initial length.

In the present study, we focus on case (b).

Figure 2.1.1 shows a flow chart for the implementation of both the concept of FRC and the stop growth condition.

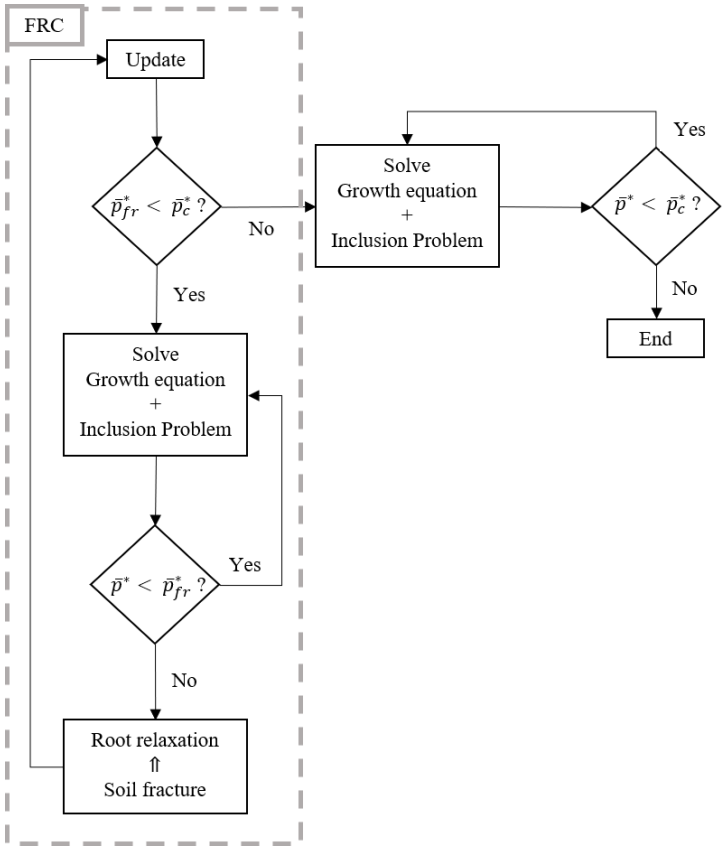

Figure 2.1.1 Flow chart of FRC (Fracture Regrowth Cycle) and the condition of the threshold axial pressure. Each cycle starts with the initial length equal to the growing zone length and ends when the axial stress, $\overline{p}^*$, at the contact reaches soil failure, $\overline{p}^*_{fr}$. Therefore, the root relaxes, the increase in root length is stored, and a new cycle starts with the updated root length. Otherwise, the root can grow until the growth critical pressure, $\overline{p}^*_c$, and there is no fracture of the elastic matrix.

2.2.1. Mechanical Problem and Interpretation

We treat both the root and the surrounding medium as a linearly elastic, homogeneous, and isotropic material. Since the time-scale of growth is longer than

the time-scale of the elastic response, this latter is hypothesized as being a quasi-static phenomenon, thus inertial forces are negligible. We denote the plant root domain of the growing zone C, the surrounding matrix as M, and we split M into two subdomains $C^+, C^-, C^+ \cup C^- = M$ as in *Figure 2.1.2*.

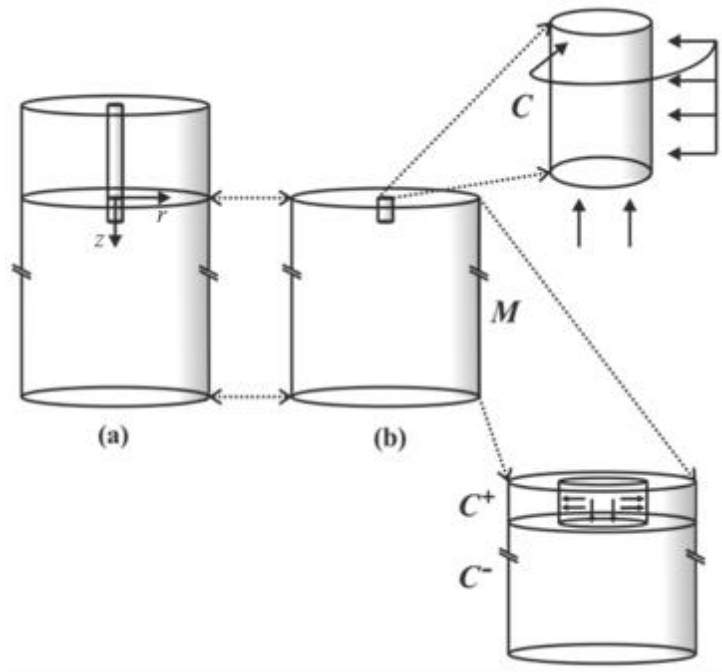

Figure 2.1.2 Diagram of (a) the domain for the plant root and soil, and (b) the inclusion problem applied to the domain related to the growing region. The growing zone of the root is a cylinder, *C*, and is subjected to axial and radial pressure. The surrounding soil, *M*, is such that $M = C^+ \cup C^-$ with the cylindrical hole subjected to axial and radial pressure.

We assume that the plant root domain, C, is cylindrical, with radius[1] R^*, and that the growth occurs only in the axial direction. The cylinder is closed at both ends and subjected to the outer pressure $\overline{p}^*$ on the bottom surface at $z^* = L^*$ and p^* in the radial direction. The upper part of the matrix is a linear elastic isotropic thick-walled cylinder, C^+, of inner and outer radii R_1^* and R_2^*, respectively. p^* is the

[1] The superscript "*" denotes dimensional variables.

pressure applied at R_1^*. We then consider a linear elastic isotropic cylinder, C^-, of radius R_2^*. We suppose that the cylinder C^- is closed at bottom end (at $z^* = L_2^*$) and the top end is subjected to axial pressure $\overline{p}^*$ over a circle of radius R_1^*. In order to meet the experimental conditions, we require that there is no displacement over the whole outer surface of M. We assume that the displacement vector is

$$\boldsymbol{u}^*(r^*, \theta^*, z^*) = (u_{r^*}^*, u_{\theta^*}^*, u_{z^*}^*) = \left(u_{r^*}^*(r^*), 0, u_{z^*}(z^*)\right), \tag{1}$$

thus, for the cylinders $C^{\pm}, C$ we have

$$\nabla^* \times \boldsymbol{u}^* = 0. \tag{2}$$

First, we compute stresses and displacements in the elastic matrix, M, with a cylindrical hole, and then in the elastic cylinder, C.

In the case of elastic matrix, the equation (2) has the following solution[2]

$$\begin{cases} {u_{r^*}^*}^+(r^*) = \dfrac{C_1^+ r^*}{2} + \dfrac{C_2^+}{r^*} & in\ C^+, \\ {u_{z^*}^*}^+(z^*) = C_3^+ z^* + C_4^+ & in\ C^+, \\ {u_{r^*}^*}^-(r^*) = \dfrac{C_1^- r^*}{2} & in\ C^-, \\ {u_{z^*}^*}^-(z^*) = C_3^- z^* + C_4^- & in\ C^-, \end{cases}$$

where u^{*+}, u^{*-} are the displacements of the upper and lower part of the matrix, respectively. Thus, we look for values of the constants such that the following boundary conditions

$$\begin{cases} {\sigma_{r^* r^*}^*}^+ = -p^* & r^* = R_1^*,\ z^* \in (0, L_1^*), \\ {u_{r^*}^*}^+(R_2^*) = 0 & z^* \in (0, L_1^*), \\ {u_{r^*}^*}^+(R_2^*) = 0 & z^* \in (L_1^*, L_2^*), \\ u_{z^*}^{*-}(L_2^*) = 0 & r^* \in (0, {R_2}^*), \\ {u_{z^*}^*}^+(L_1^*) = u_{z^*}^{*-}(L_1^*) & r^* \in (R_1^*, R_2^*), \\ {u_{z^*}^*}^+(0) = 0 & r^* \in (R_1^*, {R_2}^*), \end{cases}$$

[2] All the derivatives with respect to θ^* vanish and there is no dependence of the angle θ^*.

and the following equilibrium

$$\pi\sigma^{*\,+}_{z^*z^*}\left(R_2^{*\,2}-R_1^{*\,2}\right)-\pi\overline{p}^{*}R_1^{*\,2}=\pi\sigma^{*\,-}_{z^*z^*}R_2^{*\,2}\qquad z^*=L^*,\ \ r^*\in(0,R^*),$$

are satisfied. By neglecting the terms of higher order then ε^2, we obtain

$$\begin{aligned}
C_1^+ &= \frac{-2p^*\epsilon^2}{E_m}(1+\nu_m),\\
C_2^+ &= \frac{R_1^{*2}(1+\nu_m)}{E_m}\left\{\bar{p}^*\frac{\epsilon^2\nu_m(1-\chi)}{1-\nu}+p^*\left[1+\frac{\epsilon^2}{1-2\nu_m}\left(-1+\frac{2\nu_m^2(1-\chi)}{1-2\nu_m}\right)\right]\right\},\\
C_3^- &= \frac{\epsilon^2\chi}{E_m(1-\nu_m)}\left(\bar{p}^*+p^*\frac{2\nu_m}{1-2\nu_m}\right),\\
C_1^- &= 0,\\
C_4^- &= 0,
\end{aligned}$$

where $\chi=L_1^*/L_2^*$, $\epsilon=R_1^*/R_2^*$, υ_m, E_m are the Poisson ratio and Young modulus of the elastic medium, respectively.

In a similar way, in the case of the elastic cylinder, the solution of the equation (2) is given by $u^*_{r^*}(r^*)=\frac{C_1r^*}{2}$ and $u^*_{z^*}(z^*)=C_3z^*$ with $(r^*,z^*)\in C$. By imposing the following boundary conditions

$$\begin{cases}\sigma^*_{r^*r^*}=-p^* & r^*=R^*,\ \ z^*\in(0,L^*),\\ \sigma^*_{z^*z^*}=-\overline{p}^* & z^*=L^*,\ \ r^*\in(0,R^*),\\ u^*(0)=0,\end{cases}$$

the solution, in the case of the elastic cylinder, is given by $C_1=\frac{-p^*(1-\nu_c)+\nu_c\overline{p}^*}{E_c}, C_3=\frac{2\nu_cp^*-\overline{p}^*}{E_c}$, where υ_c, E_c correspond to the elastic cylinder coefficients, respectively. In order to have the contact at the interface between the matrix and the elastic cylinder, we require the following compatibility equation

$$\begin{cases}R^*+u^*_{r^*}(R^*)\ =\ R_1^*+u^{*\,+}_{r^*}(R_1^*),\\ L^*+u^*_{z^*}(L^*)=\ L_1^*+u^{*\,+}_{z^*}(L_1^*),\end{cases}$$

the radius and length of the deformed elastic root are equal to the radius and length of the deformed matrix, respectively. By exploiting the compatibility conditions at

the contact and after some algebra, we obtain the expressions for radial, p^*, and axial pressure, $\overline{p}^*$, in a dimensional form

$$\bar{p}^* = E_c \frac{(1-\nu_c)(R^* + R_1^* A_2)(L^* - L_1^*) + 2\nu_c (L^* - L_1^* A_1)(R^* - R_1^*)}{(1-\upsilon_c)(R^* + R_1^* A_2)(L^* + L_1^* B_1) - 2\nu_c^2 (L^* - L_1^* A_1)(R^* - R_1^* A_1)}, \quad (3.1)$$

$$p^* = E_c \frac{\nu_c (R^* - R_1^* A_1)(L^* - L_1^*) + (L^* - L_1^* B_1)(R^* - R_1^*)}{(1-\upsilon_c)(R^* + R_1^* A_2)(L^* + L_1^* B_1) - 2\nu_c^2 (L^* - L_1^* A_1)(R^* - R_1^* A_1)}, \quad (3.2)$$

where

- $A_1 = \epsilon^2 \frac{E_c}{E_m} \upsilon_m \frac{(1-\chi)(1+\upsilon_m)}{\nu_c(1-\upsilon_m)}$,
- $\mathrm{A}_2 = \frac{E_c}{E_m} \frac{(1+\upsilon_m)}{(1-\upsilon_c)} \left[1 - \epsilon^2 + \frac{\varepsilon^2}{1-2\upsilon_m} \left(\frac{2\upsilon_m^2(1-\chi)}{1-\upsilon_m} - 1\right)\right]$,
- $\mathrm{B}_1 = \epsilon^2 \frac{E_c}{E_m}(1-\chi)(1+\upsilon_m)$
- $\epsilon = \frac{R_1^*}{R_2^*}, \chi = \frac{L_1^*}{L_2^*}$.

2.2.2. Axial Growth Equations

By exploiting a similar approach to Lockhart (Lockhart, 1965) and by taking into account the soil impedance as in (Greacen and Oh, 1972; Dexter, 1987; Bengough, Croser and Pritchard, 1997; Bengough *et al.*, 2006), we can describe the growth process with the following model[3]

$$\frac{1}{V^*}\frac{dV^*}{dt^*} = \Phi^* \left(\overline{p}_c^* - \overline{p}^*\right)_+, \quad (4)$$

where $\Phi^*, [\Phi^*] = (\mathrm{MPa} \cdot \mathrm{s})^{-1}$, is related to the extensibility of wall of a plant cell and $\overline{p}_c^*$ is the threshold value introduced at the beginning of Section 2.1. The model (4) captures the most commonly accepted phenomenon related to the influence of

[3] $(f(x))_+ = \max(f(x),0) = \begin{cases} f(x), & f(x) > 0 \\ 0, & otherwise \end{cases}$ is the positive part of $f(x)$.

soil physical properties on root growth, i.e. roots grow slower in denser soils. Proceeding as in (Guiot, Pugno and Delsanto, 2006), we introduce a second growth model based on energy considerations, namely

$$\eta^* \frac{dN}{dt^*} + \overline{p}^* \frac{dV^*}{dt^*} + \beta^* N = \gamma^* N^\rho , \tag{5}$$

where

- $N = M^*/m^* = V^*/v^*$ represents the total number of cells in the growing zone of the plant root; and M^* (V^*), m^* (v^*) are the mass (volume) of the root growing zone and average mass (volume) of a single cell, respectively;
- η^* is the energy required to create a new cell;
- β^* is the metabolic rate for a single cell;
- $\gamma^* N^\rho = \alpha^* (m^*)^\rho N^\rho = \alpha^* M^\rho$ is the input power from the surrounding matrix and $\rho = 3/4$. Since we focus on the growth of the primary root, we assume that the plant seed continuously supplies nutrients and the surrounding matrix is only an external source of water. In the case of older plant roots, we can consider the matrix is a continuously-replenished medium.
- $\overline{p}^*$ is the axial pressure experienced by the growing root tip at the boundary between root and matrix.

For simplicity, we consider a uniformly distributed growth at the apical zone through cell division and cell extension. It is worth noting that the effect of turgor pressure, which is regarded as the driving force for cell extension, can be implicitly considered in both the axial and radial pressures.

The equation (5) is a modified version of the growth equation proposed by (Guiot, Pugno and Delsanto, 2006). This approach has been applied to a wide range of

biological phenomena (West, Brown and Enquist, 1997; Bettencourt *et al.*, 2007). For example, the authors of (Guiot, Pugno and Delsanto, 2006) developed a model for tumour invasion, considering the effect of interfacial pressure as an extension of the West, Brown and Enquist law (West, Brown and Enquist, 2001). The root elongation rate is sensitive to variations in axial pressure (Bengough and Mackenzie, 1994; Bengough, 2012), but insensitive to radial pressure (Kolb, Hartmann and Genet, 2012). This aspect explains the presence of the mechanical term in equations (4) and (5) due to the axial pressure. We will further assume that root is cylindrical (as in *Figure 2.1.2*) and grows only in length. Therefore, an increase in length is related to an increase in volume and in the number of cells through

$$\frac{dL^*}{dt^*} = \frac{1}{\pi R^{*2}} \frac{dV^*}{dt^*} = \frac{v_0^*}{\pi R^{*2}} \frac{dN}{dt^*}, \tag{6}$$

where v_0^* is the single cell volume that we consider constant. Note that if $\rho = 1$ and if $\overline{p}^*$ is small, with proper values of $v_0^*, \eta^*, \gamma^*, \beta^*$ we can recover the equation (4) from the equation (5).

2.2.3. Adimensionalization

We scale the variables by writing

$$L^* = L_0^* L, \qquad t^* = t_{ref}^* t,$$

where L_0^* represents the length of the growing region from the tip to the end of the elongation zone and t_{ref}^* is the duration of the experiment. We assume $L_0^* = 3\text{mm}$ and $t_{ref}^* = 3\text{days}$.

We notice that L_1^* represents the initial length of the elastic cylinder in each cycle and we assume zero pressure at both ends of the cycle. Therefore, we can write $L_1^* = L_0^* L(t_0)$, where the adimensional length $L(t_0)$ is "updated" at the beginning of each cycle.

Assuming the axial growth, i.e. $R^* = R_1^*$, we can rewrite equations (3.1) and (3.2) as

$$\begin{cases} \overline{p}^* = \Theta_1^* \dfrac{L - \Theta_2}{L + \Theta_3}, \\ p^* = \Theta_4^* \dfrac{L - \Theta_2}{L + \Theta_3}, \end{cases}$$

where

- $\Theta_1^* = E_c \, \frac{\alpha}{\beta}$,
- $\Theta_2 = L(t_0)$ is the root length at the beginning of the FRC;
- $\Theta_3 = \frac{\gamma}{\beta} \epsilon^2 \frac{E_c}{E_m} \, L(t_0)(1-\chi)(1+\upsilon_m)$,
- $\Theta_4^* = \frac{E_c}{\beta} \left[\upsilon_c - \epsilon^2 \frac{E_c}{E_m} \, (1-\chi) \frac{\upsilon_m(1+\upsilon_m)}{(1-\upsilon_m)} \right]$,
- $\alpha = 1 - \upsilon_c + \frac{E_c}{E_m}(1+\upsilon_m) \left[1 - \epsilon^2 + \frac{\varepsilon^2}{1-2\upsilon_m} \left(\frac{2\upsilon_m^2(1-\chi)}{1-\upsilon_m} - 1 \right) \right]$,
- $\beta = \alpha + \frac{E_c}{E_m}(1+\upsilon_m) \frac{2\upsilon_m \upsilon_c \varepsilon^2 (1-\chi)}{(1-\upsilon_m)^2} - 2\upsilon_c^2$,
- $\gamma = \alpha - \frac{E_c}{E_m}(1+\upsilon_m) \frac{2\upsilon_m^2 \varepsilon^2 (1-\chi)}{(1-\upsilon_m)^2} - \frac{2\upsilon_m \upsilon_c}{1-\upsilon_m}$,

and $[\Theta_1^*] = [\Theta_4^*] =$ MPa and $[\Theta_2] = [\Theta_3] = 1$.

By considering the stop of the root growth when $\overline{p}^*$ reaches the critical value $\overline{p}_c^*$, from the equation (5) the following relation

$$\beta^* = \gamma^* \left(\frac{\Theta_2 + \Theta_3 \dfrac{\overline{p}_c^*}{\Theta_1^*}}{1 - \dfrac{\overline{p}_c^*}{\Theta_1^*}} \right)^{\rho - 1} ,$$

holds and we introduce the scaling parameter Θ_1^* for the adimesionalization of the axial pressure, $\overline{p}^*$, as an upper bound for $\overline{p}_c^*$.

2.2.4. Stress Effects on Root Penetration

This Section focuses on how the axial stress at the contact affects the biomechanical properties of plant roots penetration depending on the surrounding matrix. Since the change in length is slow, every moment of the growth process can be represented as a static state and we can interpret the mechanical process of root growth as an inclusion model. The inclusion model analyses in detail the mechanical expansion of an elastic cylinder in a cylindrical hole of an elastic fracturable medium. In particular, we study the sensitivity of the root length to the variation in the fracture stress, $\overline{p}_{fr}^*$, and the Young modulus, E_m, of the surrounding matrix. Therefore, we analyse the variation in the root length, L_{fr}^*, when the axial contact pressure is equal to $\overline{p}_{fr}^*$.

From the inclusion problem, we can obtain the expression of root length in the dimensionless form (see Subsection 2.2.3) at $\overline{p}^* = \overline{p}_{fr}^*$

$$L_{fr} = \frac{L(t_0) + \Theta_3 \dfrac{\overline{p}_{fr}^*}{\Theta_1^*}}{1 - \dfrac{\overline{p}_{fr}^*}{\Theta_1^*}}, \qquad \forall\, \overline{p}_{fr}^* < \Theta_1^*, \tag{7}$$

where

- $L(t_0)$ is the root length at the beginning of FRC;
- $\Theta_1^* = E_c \, \frac{\alpha}{\beta}$,
- $\Theta_3 = \frac{\gamma}{\beta}\epsilon^2 \frac{E_c}{E_m} \, L(t_0)(1-\chi)(1+\upsilon_m)$,
- $\alpha = 1 - \upsilon_c + \frac{E_c}{E_m}(1+\upsilon_m)\left[1 - \epsilon^2 + \frac{\varepsilon^2}{1-2\upsilon_m}\left(\frac{2\upsilon_m^2(1-\chi)}{1-\upsilon_m} - 1\right)\right]$,

- $\beta = \alpha + \frac{E_c}{E_m}(1+\upsilon_m)\frac{2\upsilon_m\upsilon_c\varepsilon^2(1-\chi)}{(1-\upsilon_m)^2} - 2\upsilon_c^2$,
- $\gamma = \alpha - \frac{E_c}{E_m}(1+\upsilon_m)\frac{2\upsilon_m^2\varepsilon^2(1-\chi)}{(1-\upsilon_m)^2} - \frac{2\upsilon_m\upsilon_c}{1-\upsilon_m}$.

Since $L_1^* \ll L_2^*$, we consider $\chi = L_1^*/L_2^* \to 0$, but we maintain the order of approximation of $\epsilon = R_1^*/R_2^*$.

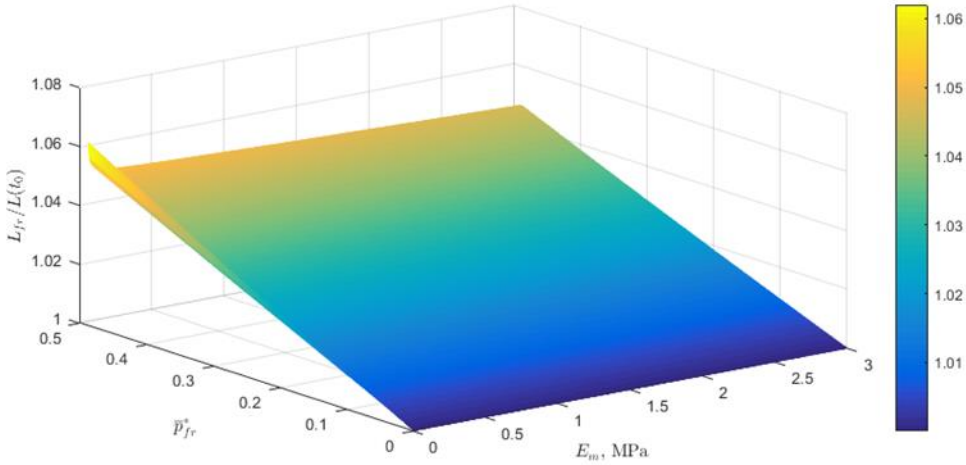

Figure 2.1.3 Plot of the ratio between the root length at $\overline{p}^* = \overline{p}^*_{fr}$ and the root initial length in adimensional form, $L_{fr}/L(t_0)$, considering the 'stop growth' pressure as $\overline{p}^*_c = 0.5$MPa, the root Young modulus, $E_C = 10$MPa, the Poisson ratio for both root and soil as $\upsilon_m = \upsilon_c = 0.49$, the root and hole radius as $R^* = R_1^* = 0.588$mm, and the outer radius of the soil as $R_2^* = 50$mm.

We consider $L_{fr} = L_{fr}(\overline{p}^*_{fr}, E_m)$, i.e. as a function of both failure stress, $\overline{p}^*_{fr}$, and the elastic modulus of the surrounding medium, E_m. The plot of $L_{fr}(\overline{p}^*_{fr}, E_m)$ is shown in *Figure 2.1.3*, which highlights that when

1. $\overline{p}^*_{fr} = k \cdot E_m$, L_{fr} is an increasing function of E_m for values of E_m enough small such that $L_{fr} > 0$ and $\overline{p}^*_{fr} < \overline{p}^*_c$;
2. $E_m = constant$, L_{fr} is an increasing function of $\overline{p}^*_{fr}$ such that $L_{fr} > 0$ and $\overline{p}^*_{fr} < \overline{p}^*_c$;

3. $\overline{p}_{fr}^{*} = constant < \overline{p}_{c}^{*}$, L_{fr} is a decreasing function of E_m such that $L_{fr} > 0$.

The above analysis highlights the importance of considering the concept of failure stress at a small value for Young's modulus of the elastic matrix.

In order to determine the growth, we employ the model given by the equation (5) to the experiments in artificial soils (the experimental work related to this Chapter has been performed by IIT). In addition, we compare our theoretical results with data from experiments in different real soil compactions (for more details see (Popova, van Dusschoten, *et al.*, 2016)).

2.2. Theoretical Results

In this analysis, the surrounding medium is assumed to be an infinite body with respect to the plant root, so that $R^*, R_1^* \ll R_2^*$ and $L^*, L_1^* \ll L_2^*$. Therefore, to obtain the numerical solutions, we set $\chi = L_1^*/L_2^* = 0$, and we assume $R_2^* = 50\text{mm}$ for both artificial and real soils. We then assume that the growth critical pressure $\overline{p}_c^* = 0.5$ MPa (for the value range of $\overline{p}_c^*$ see, e.g., (Misra, Dexter and Alston, 1986; Clark, Whalley and Barraclough, 2003; Bengough *et al.*, 2011; Popova, van Dusschoten, *et al.*, 2016)), and the root Young modulus $E_c = 10\text{MPa}$ (Forterre, 2013). We assume that $R_1^* = R^*$ are equal to the values of the root apex radius at the third day of life (the related experimental work has been performed by IIT) for artificial soil, and $R_1^* = R^* = 0.6\,\text{mm}$ for real soils. Both Poisson's ratios are $\nu_{m,c} = 0.49$ for Phytagel and $\nu_c = 0.49, \nu_m = 0.45$ for soils (Bowles, 1997; Normand *et al.*, 2000; Das, 2014). The values used for $\gamma^*, E_m, \overline{p}_{fr}^*$ are reported in Table 1 ($E_m, \overline{p}_{fr}^*$are obtained by means of compression tests). In order to estimate only the variation of γ^* with respect the different soil media, a constant value for the parameter η^*, $\eta^* = 35\,\text{MPa} \cdot \text{mm}^3$, has been chosen. *Figure 2.2.1- Figure 2.2.3* show the evolution of the root length with time for artificial and real soils, respectively.

The value of the scaling parameter γ^* of the energy released from the seed increases in the medium hardness for both artificial and real soils. By using artificial growth media, roots, which were grown in harder soils, were longer than the roots grown in softer soils, while in real soils this was not the case. Using 0.6% Phytagel (Group C) we obtain a lower final length in both the numerical (*Figure 2.2.4*b) and experimental results (the related experimental work has been performed by IIT). In order to assess the influence of γ^* on the variation of the final root length, we carry out the theoretical predictions in both artificial and real soil using all the combinations of the value for γ^* listed in Table 1. The results by means of equation (5) are given in *Figure 2.2.4*.

Phytagel is a hard and brittle homogeneous gel (Schiavi, Cuccaro and Troia, 2016) and, because of its homogeneity, we can assume that the increase in Young modulus leads to an increase in the fracture stress (see Subsection 2.2.4). In addition, *Figure 2.2.4*c shows that γ^* increases linearly with respect to the Phytagel concentration. Therefore, in the presence of artificial soils the increase in energy availability and the soil mechanical properties may enhance root penetration.

Table 1 Values of parameters used in the analytical results for the growth model.

		E_m (MPa)	$\overline{p}^*_{fr} \pm$ SD (MPa)	γ^*(MPa·mm^3/s)
Phytagel Artificial soil	**Group A (0.15% Phyt. conc.)**	$1.02 \cdot 10^{-2}$	$0.0025 \pm 7.278 \cdot 10^{-4}$	$7.53 \cdot 10^{-4}$
	Group B (0.3% Phyt. conc.)	$1.82 \cdot 10^{-2}$	0.0053 ± 0.0012	$1.94 \cdot 10^{-3}$
	Group C (0.6% Phyt. conc.)	$4.23 \cdot 10^{-2}$	0.0089 ± 0.0016	$2.56 \cdot 10^{-3}$
	Group D (0.9% Phyt. conc.)	$7.43 \cdot 10^{-2}$	0.0140 ± 0.0018	$4.76 \cdot 10^{-3}$
	Group E (1.2% Phyt. conc.)	$8.09 \cdot 10^{-2}$	0.0141 ± 0.0017	$6.7 \cdot 10^{-3}$
Real soil	**Low compaction**	2	0.02	$1.2 \cdot 10^{-2}$
	Medium compaction	25	0.04	$2.19 \cdot 10^{-2}$
	High compaction	50	0.25	0.1021

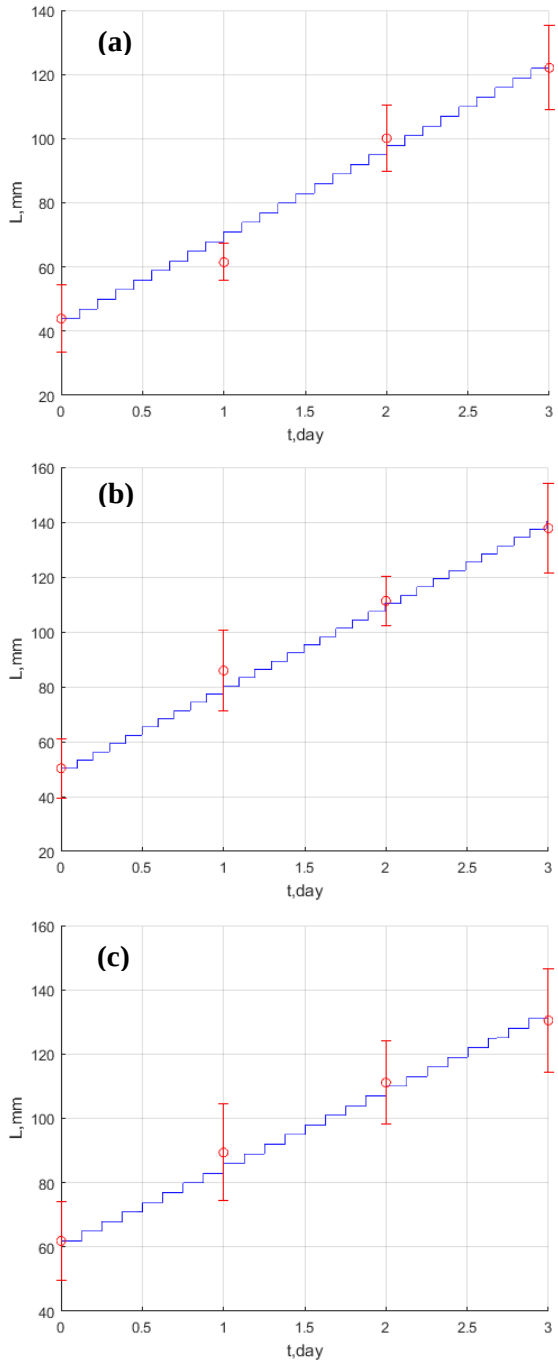

Figure 2.2.1 Comparison of the experimental data (red circles) in artificial soils (mean values ±SD) and analytical solution (blue line) in (a) 0.15%, (b) 0.3%, (c) 0.6% Phytagel concentration. Each step of the analytical solution represents a cycle, which ends with the fracture of the soil and begins after the relaxation of the root.

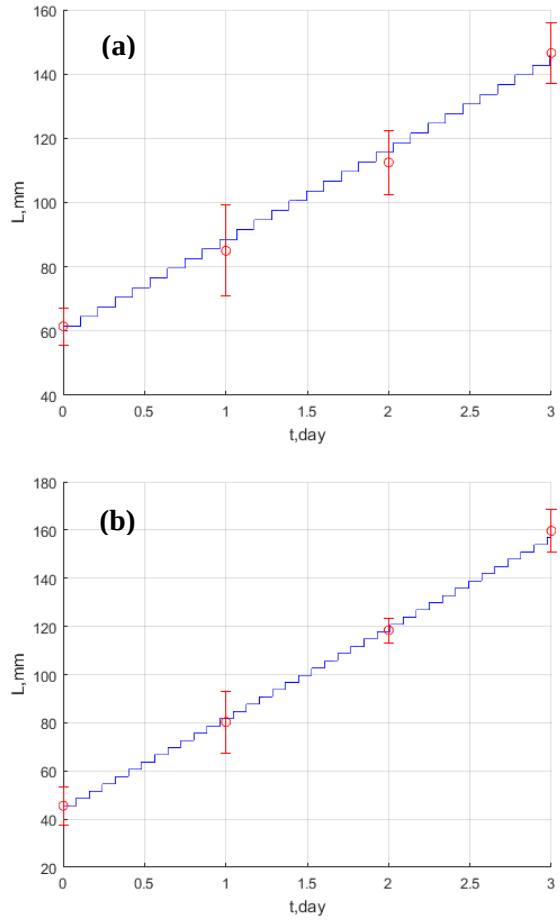

Figure 2.2.2 Comparison of the experimental data (red circles) in artificial soils (mean values ±SD) and analytical solution (blue line) in (a) 0.9% and (b) 1.2% Phytagel concentration. Each step of the analytical solution represents a cycle, which ends with the fracture of the soil and begins after the relaxation of the root.

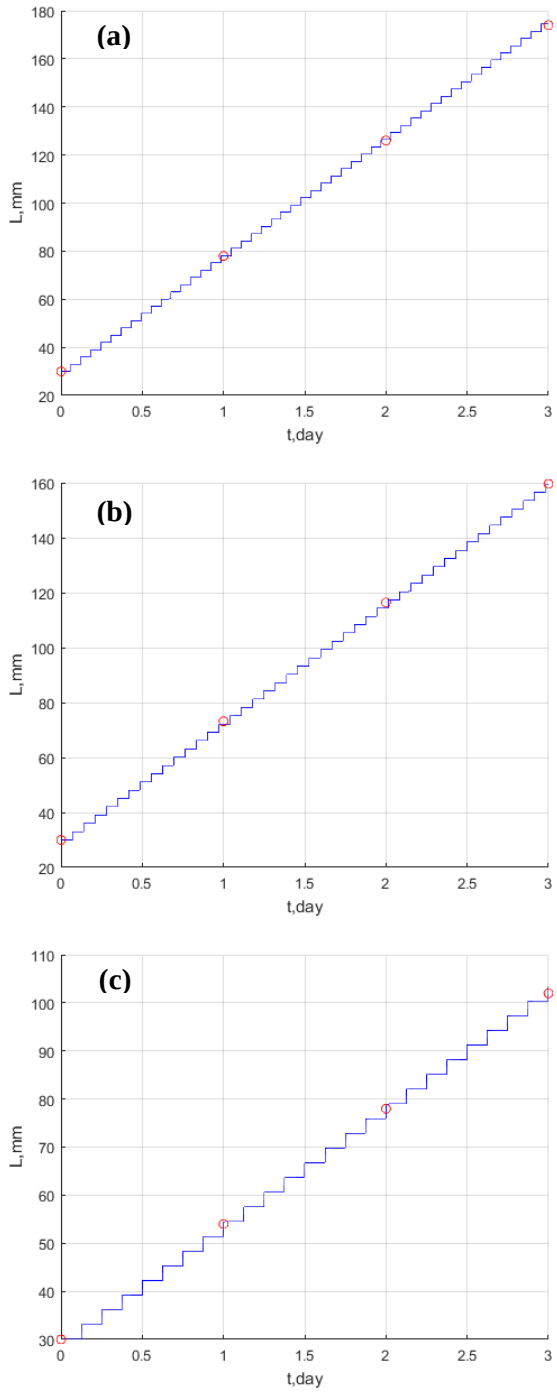

Figure 2.2.3 Comparison of the experimental data (red circles) in real soils and analytical solution (blue lines) in (a) low, (b) medium, and (c) high compaction. Each step of the analytical solution represents a cycle, which ends with the fracture of the soil and begins after the relaxation of the root.

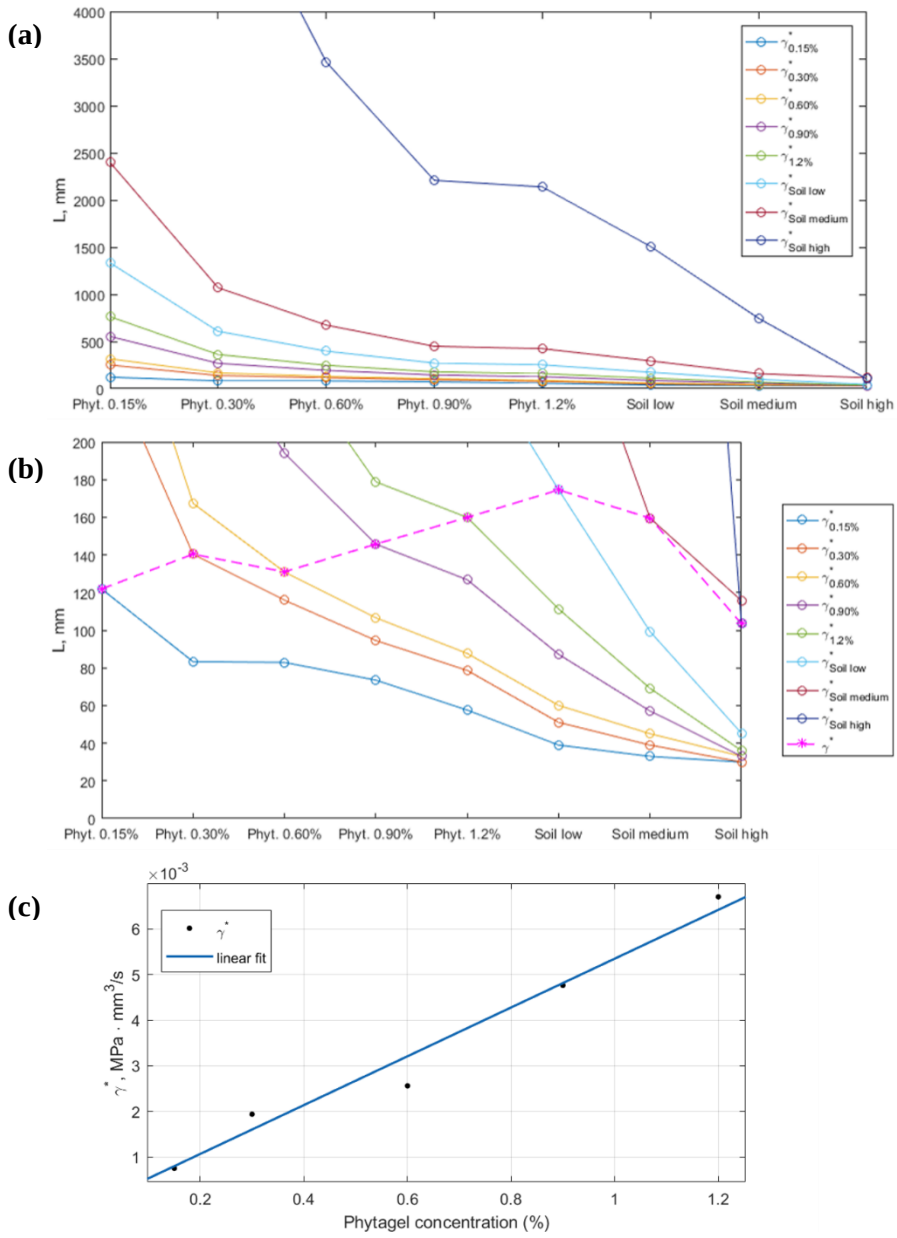

Figure 2.2.4 (a) In each soil medium we evaluated the variation of the root length at the sixth day of life, by considering all the combinations of the values for the scaling parameter γ^* of the input power from the plant seed, exploited in the numerical solution (Table 1); (b) The dotted line represents the variation in the root length in the numerical solutions of Figure 2.2.1-Figure 2.2.3; (c) The linear fit of γ^* and different concentrations of Phytagel (R-squared: 0.97; $y = a \cdot x$, $a = 5.346 \cdot 10^{-3}$ MPa·mm^3/s).

2.3. Interpretation and Discussion

The first week of plant life is a fundamental period to establish a strong anchorage and develop a complete radical apparatus. The primary root thus represents an interesting model to study the soil impedance response (Goodman and Ennos, 1999). By using real soils, conflicting results on the increase or decrease in root length by varying the soil compaction and root species have been found (Barley, 1963; Taylor and Ratliff, 1969; Wilson, Robards and Goss, 1977; Wilson and Robards, 1978; Atwell, 1989; A. Bengough and Mullins, 1990; Pietola and Smucker, 1998; Alessa and Earnhart, 2000). Decodifying a univocal cause–effect behaviour between root growth and soil hardness is difficult. In fact, previous studies have been carried out in real soil, which is intrinsically characterized by several physical and chemical complex interactions (soil aerations, water, oxygen availability, etc.).

Alternative protocols to the use of real soil have been proposed, such as wax layers or vertical oriented agar plates (Okada and Shimura, 1990; Materechera, Dexter and Alston, 1991; Clark *et al.*, 1996). One of the most common approaches is to use transparent gelling agents such as agar and agarose, commonly used to prepare growth media for botanical and bacterial applications. For example, (Zacarias and Reid, 1992; Volkmar, 1994; Clark *et al.*, 1999) all used the agar gels to study mechanical impedance in roots because agar gel impedes the root system and visualizes it at the same time. In accordance with these studies, we analyse the growth kinetics of *Zea mays L.* primary root exploiting artificial soils (Phytagel) with different levels of concentrations. Accordingly, we investigated the first interaction of plant root with the soil, preventing the interference of any other physical and chemical stimulus.

Unexpectedly, the experimental results showed that the primary roots grown in higher concentrations of Phytagel (i.e. higher levels of compactness in the soil) have greater elongation. In order to ascertain the plausibility of these findings in comparison with experiments in real soils, we developed a theoretical model for

the mechanical process of root growth with the root-soil mechanical interaction. Our mathematical model combines plant roots growth and the mechanical contact with the soil through the modified version of the extended WBE universal law and the inclusion problem.

From the theoretical results, we found that an increase in the scaling parameter γ^* (Table1) could reveal an increase in the demand of plant nutrients when the soil medium is more compact. Since the experiments were carried out in the absence of nutrients in the soil, the nutrient demand was addressed to the reserves stored in the seed (primary roots) and the surrounding soil medium supplies continuously only water. Thus, our study may reveal a relation between nutrients from the seed and soil medium compactness. Since the mechanical impedance of the artificial soils is weaker than real soils in terms of inducing a change in root growth, the increase in the released energy can provide a more effective penetration in Phytagel (*Figure 2.2.4*). In fact, the inclusion problem could explain how, at the contact fracture pressure, the ability of plant roots to grow changes and is influenced by the mechanical properties of the surrounding environment.

The Young modulus of plant tissues takes typically a value of around 10 MPa (Forterre, 2013). We assume that E_c is constant so it does not change along the root axis (i.e. with age) and the surrounding soil. In addition, we notice that L_{fr}^* is a decreasing function of E_c , i.e. considering a fixed medium the increase in root stiffness seems to have a negative influence on the plant roots expansion as remarked in (Wei and Lintilhac, 2007). Indeed, the authors of (Wei and Lintilhac, 2007) investigated aspect of turgor-driven plant cell growth with a model derived from the Eulerian concept of instability and showed that increasing elastic modulus of plant cell has a negative effect on wall expansion.

In conclusion, we analyse the growth kinetic of the primary root (*Z. mays*) in artificial soils. In particular, we develop an *ad-hoc* setup and a theoretical framework to understand the contribution played by mechanical stimuli in the root growth. Our theoretical and experimental studies may be a further investigation to explain how plant roots could control the growth in response to the contact with the

surrounding medium and help to improve the current knowledge on the behavioural strategies of plant roots. The mathematical model is based on continuum mechanics and is a general formulation for the prediction of plant roots growth in soil media. The unexpected experimental results highlight the active response of plant roots to the changes in the surrounding medium as simulated by the theoretical model.

Chapter 3

3. Extension of the Mathematical Model including Root Radial Growth and Nutrient Influence

Plant roots have developed different defence responses to outer stimuli caused by the surrounding soil, e.g. increase or decrease in the elongation, swelling or shrinking of the diameter and root-structure tortuosity (Barley, 1963; A. Bengough and Mullins, 1990; Li *et al.*, 2014; Popova, van Dusschoten, *et al.*, 2016). Since the apical zone tissues are the most sensitive to the environment changes, the apex is the first zone of the root responding to external stimuli. For this reason, several investigations to understand how plant roots can modulate and control the effects of external chemical and physical (mainly mechanical) stimuli on their growth can be found, e.g. see (Wilson, Robards and Goss, 1977; Atwell, 1989; Baluska *et al.*, 1993; Baluska, Parker and Barlow, 1993; Baluška, Parker and Barlow, 1993; Baluška, Busti, *et al.*, 2001; Baluška, Jasik, *et al.*, 2001).

In particular, many studies illustrated the evolution of root system in nutrient-rich patches (Drew and Saker, 1978; Crick and Grime, 1987; Jackson and Caldwell, 1989, 1996; Gross, Peters and Pregitzer, 1993) analysing phenotypical reactions (branching, root elongation, lateral root emergence, root hairs proliferation, etc.). Since the majority of these studies were conducted in real soils (Kirby and Bengough, 2002; Pierret *et al.*, 2007), characterized by high heterogeneity, these findings have to be considered as a result of several physical and chemical stimuli. In fact, in order to properly investigate each phenomenon and carry out a rigorous cause-effect analysis, plants should be studied in environments that allow to distinguish each single stimulus. In order to discriminate indiscernible parameters in a real environment (Tian and Doerner, 2013) and ascertain the response of plant root to different nutrient concentrations, we used data of plants grown in artificial soils in the absence of other physical or chemical stimuli.

A recent research (Li *et al.*, 2014) explains that roots exploit an adaptive strategy to defend themselves by salt toxicity, increasing the number of stele tissue cell layers. Such a strategy causes an evident swelling of root apex that should help cells to up-take more water and create a stronger barrier to reduce Na^+ concentration. Furthermore, other studies show similar root apex swellings, e.g. after depletion of giberellic acid or ethylene and high calcium exposures (Baluska *et al.*, 1993; Baluška, Parker and Barlow, 1993; Baluska, Hauskrecht and Barlow, 1996). In addition, investigations on the depolymerization of F-actin with latrunculin B reveal also in very similar maize root apex swellings and inhibition of the root cell elongation (Baluška, Jasik, *et al.*, 2001). The root swelling and the reduction of primary root length were observed in maize and cotton (Kurth *et al.*, 1986; Zidan, Azaizeh and Neumann, 1990) and in several crop plants grown in media with high concentration of NaCl. Aluminium is considered a source of toxicity for plants as well, inducing structure deformation (Pietola and Smucker, 1998; Zhu, Ahn and Matsumoto, 2003; Kynast, 2012) and swelling phenomenon (Bennet, Breen and Fey, 1985a, 1985b; Budíková, 1999). One of the potential explanations of the observed phenomenon could be an adaptation strategy of plant roots. In fact, plants can be regarded as sensory and communicative organisms with active problem-solving behaviour (Baluška *et al.*, 2009). Although the molecular and cellular responses are still not known, we believe that such studies will provide insights in understanding the control and modulation of root development with several morphological adaptations.

In this Chapter we exploited the experiments in which the nutrient stress was produced by an excess of Murashige and Skoog Basal Salt Mixture, MS (Murashige and Skoog, 1962). Therefore, by using the aforementioned data, we focus on modelling the behaviour of plant roots in the presence of mechanical and nutrient stress (a schematic diagram is reported in *Figure 3.1.1*). Here we pursue such an approach, seeking to understand how the simultaneous mechanical and chemical properties of the surrounding medium may influence and contribute to the root

development such as morphometric changes, particularly root elongation and radial expansion. For this reason, we develop a modified version of the growth equation applied to model the tumour invasion proposed in (Guiot, Pugno and Delsanto, 2006) with a radial growth equation as an activation response to chemical-mechanical stimuli. The model illustrates how nutrients concentration may influence both the root length and radius.

3.1. Theoretical Model

3.1.1. Axial and Radial Growth Coupled Equations

We propose the following model

$$\eta^* \frac{dN}{dt^*} + \overline{p}^* \frac{dV^*}{dt^*} + \beta^* N = \gamma^* N^{\rho}\,, \tag{8.1}$$

$$\frac{dR^*}{dt^*}\frac{1}{R^*} = \left(1 - \frac{\gamma_{Cc}^*}{\gamma^*}\right)_+ \cdot \frac{dN}{dt^*} \cdot \frac{1}{N}\,. \tag{8.2}$$

The equation (8.1) has been proposed by (Guiot, Pugno and Delsanto, 2006) and we include both axial and radial growth. As reported in Subsection 2.2.2, in the equation (8.1) the parameters η^* and β^* refer to the energy required to create a new cell and the metabolic rate for a single cell of the root, respectively. The parameter γ^* is a scaling constant of the root metabolic rate and $\rho = 3/4$. Specifically, the axial pressure, $\overline{p}^*$, at the boundary between the root tip and matrix depends on both axial and radial growth (see Subsection 2.2.1). In the equation (8.2), we take into account the estimated value, γ_{Cc}^*, of the previous case, i.e. without nutrient in the soil, meaning that the plant seed furnishes nutrients and the surrounding medium supplies continuously only water (see Section 2.2, Table 1); γ_{Cc}^* corresponds to the parameter γ^* labelled as Control concentration in Table 2. In order to include the effect of the nutrient in the soil, the equation (8.2) considers that the radial swelling occurs only when the scaling parameter γ^* of the input power from the surrounding soil is higher than γ_{Cc}^* (*Figure 3.1.1*).

By assuming that the root is cylindrical, the increase in length, L^*, is given by

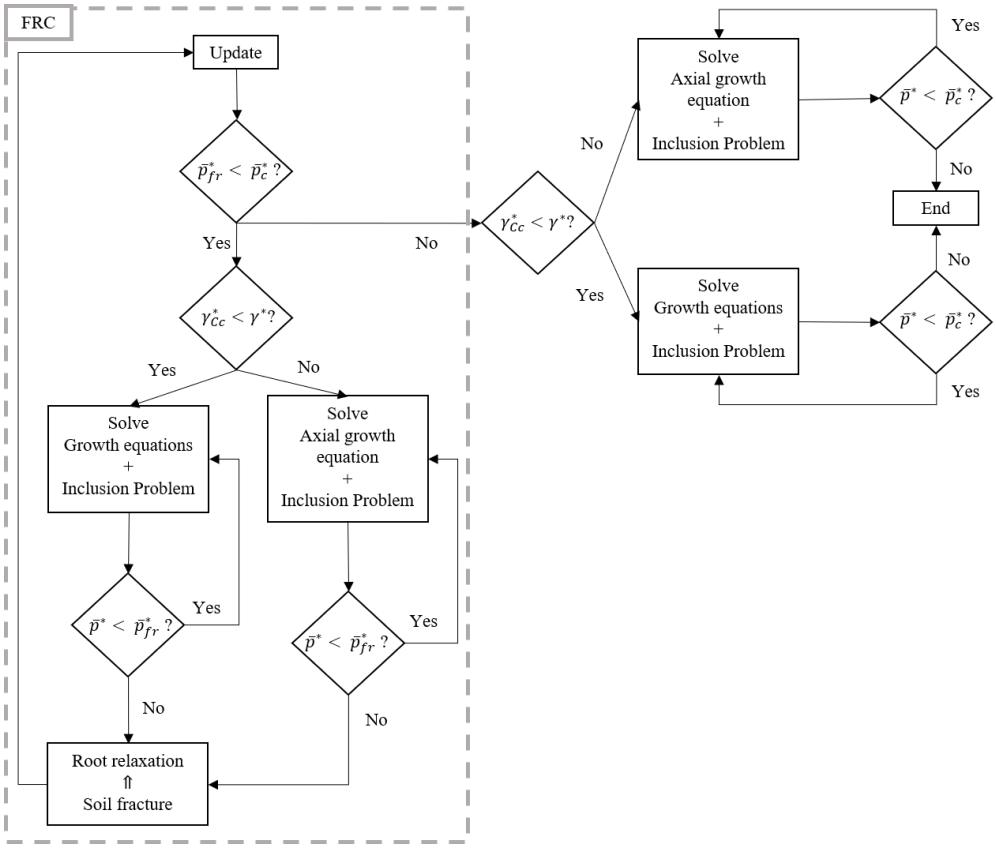

Figure 3.1.1 Schematic diagram of the root control mechanism to nutrient stress. This mechanism could be similar to salt toxicity as observed in (Li *et al*., 2014). A possible adaptive strategy to nutrient stress could be the enlargement of cells, inducing a swelling of root apex. This strategy should help cells to up-take more water and create a stronger barrier to reduce toxic nutrient concentration (Li *et al.*, 2014). The initial conditions are differently updated if the root activates the radial swelling as response to nutrient stress. In such a case, the initial root length, diameter, and cell volume are updated and stored, otherwise only the root initial length is stored. Specifically, each cycle starts with updated initial conditions and ends when the soil medium fractures, i.e. the axial stress, $\overline{p}^*$, at the contact equals the soil failure, $\overline{p}^*_{fr}$. Therefore, the root relaxes and a new cycle starts with the updated initial conditions. Otherwise the fracture in the matrix does not occur and the root grows until the growth critical pressure, $\overline{p}^*_c$.

$$\frac{dL^*}{dt^*} = \frac{v_0^*}{\pi {R^*}^2}\left(\frac{dN}{dt^*} - \frac{2N}{R^*}\cdot\frac{dR^*}{dt^*}\right). \tag{9}$$

We consider that the total number of cells in a plant root is $N = V^*/v_0^*$, where V^* is the root volume of the growing zone and v_0^* is the average of a single cell volume.

We update v_0^* with the non-dimensional initial root radius at each FRC to indicate the possible thickening of cells due to the chemical stimulus.

3.1.2. Adimensionalization

We scale the variables by writing

$$L^* = L_0^* L, \qquad R^* = R_0^* R, \qquad t^* = t_{ref}^* t,$$

where L_0^* represents the length of the growing region from the tip to the end of the elongation zone and t_{ref}^* is the duration of the experiments. We assume $L_0^* = 3\text{mm}$, and $t_{ref}^* = 3\text{days}$ as in Chapter 2. We consider for R_0^* the values of the top diameter at the third day of life (the related experimental work has been performed by IIT).

L_1^*, R_1^* represent the initial length and radius of the elastic cylinder, respectively, in each cycle and we assume zero pressure at both ends of the cycle. Therefore, we can write

$$L_1^* = L_0^* L(t_0), \quad R_1^* = R_0^* R(t_0),$$

where the adimensional length $L(t_0)$ and radius $R(t_0)$ are "updated" at the beginning of each cycle. By assuming the same length growing zone (from the meristematic to the elongation region) and number of cells at the beginning of each FRC with an increasing radius ($v_0^* N(t_0) = \pi L^*(t_0) {R^*}^2(t_0)$), we update the single cell volume v_0^* with the non-dimensional initial root radius in each FRC, i.e. $v_0^* \propto R^2(t_0)$.

Furthermore, by assuming that the root growth ends when $\bar{p}^* = \bar{p}_c^*$, from the equation (8.1) we obtain

$$\beta^* = \gamma^* {N_c}^{\rho - 1}, \quad \rho = \frac{3}{4},$$

where

$$N_c = N(t_0)\frac{1+\frac{\bar{p}_c}{E_c}\left(\frac{U_1B_1-U_2A_1}{U_1}\right)}{1-\frac{\bar{p}_c}{E_c}\left(\frac{U_1-U_2}{U_1}\right)}, \tag{10}$$

and

- $U_1 = (1-\nu_c)(1+A_2)$,
- $\mathrm{U}_2 = 2\nu_c^2(1-A_1)$,
- $A_1 = \epsilon^2\frac{E_c}{E_m}\upsilon_m\ \frac{(1-\chi)(1+\upsilon_m)}{\nu_c(1-\upsilon_m)}$,
- $\mathrm{A}_2 = \frac{E_c}{E_m}\frac{(1+\upsilon_m)}{(1-\upsilon_c)}\left[1-\epsilon^2+\frac{\varepsilon^2}{1-2\upsilon_m}\left(\frac{2\upsilon_m^2(1-\chi)}{1-\upsilon_m}-1\right)\right]$,
- $\epsilon = \frac{R_1^*}{R_2^*},\ \chi = \frac{L_1^*}{L_2^*}$.

In the case of axial growth, the equation (10) corresponds to the equation (7) Chapter 2.

3.2. Theoretical Results

The theoretical results are performed by means of the equations (8.1) and (8.2) applied to the growing zone of the root and the related surrounding medium (*Figure 2.1.2*, Subsection 2.2.1). We suppose that the soil is greater than the root, i.e. $R^*, R_1^* \ll R_2^*$ and $L^*, L_1^* \ll L_2^*$ (*Figure 2.1.2*, Chapter 2). Therefore, we set the values of the parameters $\chi, R_2^*, \overline{p}_c^*, E_c, \nu_{m,c},$ and η^*as in Chapter 2. The values used for the matrix Young modulus, $E_m,$ and the fracture pressure, $\overline{p}_{fr}^*$, are obtained by means of compression tests and are reported in Table 1, Section 2.2. The estimated values of γ^* for *Zea mays* roots grown in artificial soil with and without nutrient are in Table 2.

The four different MS concentrations are labelled MS1, MS2, MS3, and MS4 and correspond to increasing MS concentration.

The value of the scaling parameter γ^* of the input power from the surrounding matrix increases with both the Phytagel concentration (used in the previous Chapter) and the MS concentration (only the MS2-Group B and Group C have a lower estimated value than the corresponding MS1). The results from the equations (8.1) and (8.2) are given in *Figure 3.2.1*. Since we have observed that the radial swelling of 17% at the height of meristematic area occurs in the 5-6-day old roots for the MS4 concentration with respect to the mature region, we consider the increase of 17% in the top diameter at the 6-day age for the comparison with the numerical solutions (the related experimental work has been performed by IIT). The numerical result of the MS4-Group B is smaller than the measured data for the same elongation reduction.

Figure 3.2.2-Figure 3.2.4 present the numerical solutions of the MS1-MS3 concentrations. It is worth noting that the equation (8.2) cannot allow a decrease in root radius, since γ_{Cc}^* represents the parameter related to the energy released by seed without nutrients in soil and the soil medium is only an external source of water.

Table 2 Estimated value of the parameter γ^* related to the nutrient availability. In the control concentration, i.e. without nutrient in the soil medium, the plant seed furnishes the nutrient for the growth and is the parameter labelled as γ_{Cc}^* in the current Section.

	γ^* (MPa mm^3 s^{-1})				
	Control conc.	**MS1 conc.**	**MS2 conc.**	**MS3 conc.**	**MS4 conc.**
Group B (0.3% Phyt. conc.)	$1.94 \cdot 10^{-3}$	$2.18 \cdot 10^{-3}$	$1.955 \cdot 10^{-3}$	$2.531 \cdot 10^{-3}$	$3.098 \cdot 10^{-3}$
Group C (0.6% Phyt. conc.)	$2.56 \cdot 10^{-3}$	$2.932 \cdot 10^{-3}$	$2.666 \cdot 10^{-3}$	$2.937 \cdot 10^{-3}$	$4.093 \cdot 10^{-3}$
Group D (0.9% Phyt. conc.)	$4.76 \cdot 10^{-3}$	$4.783 \cdot 10^{-3}$	$5.638 \cdot 10^{-3}$	$6.429 \cdot 10^{-3}$	$6.888 \cdot 10^{-3}$

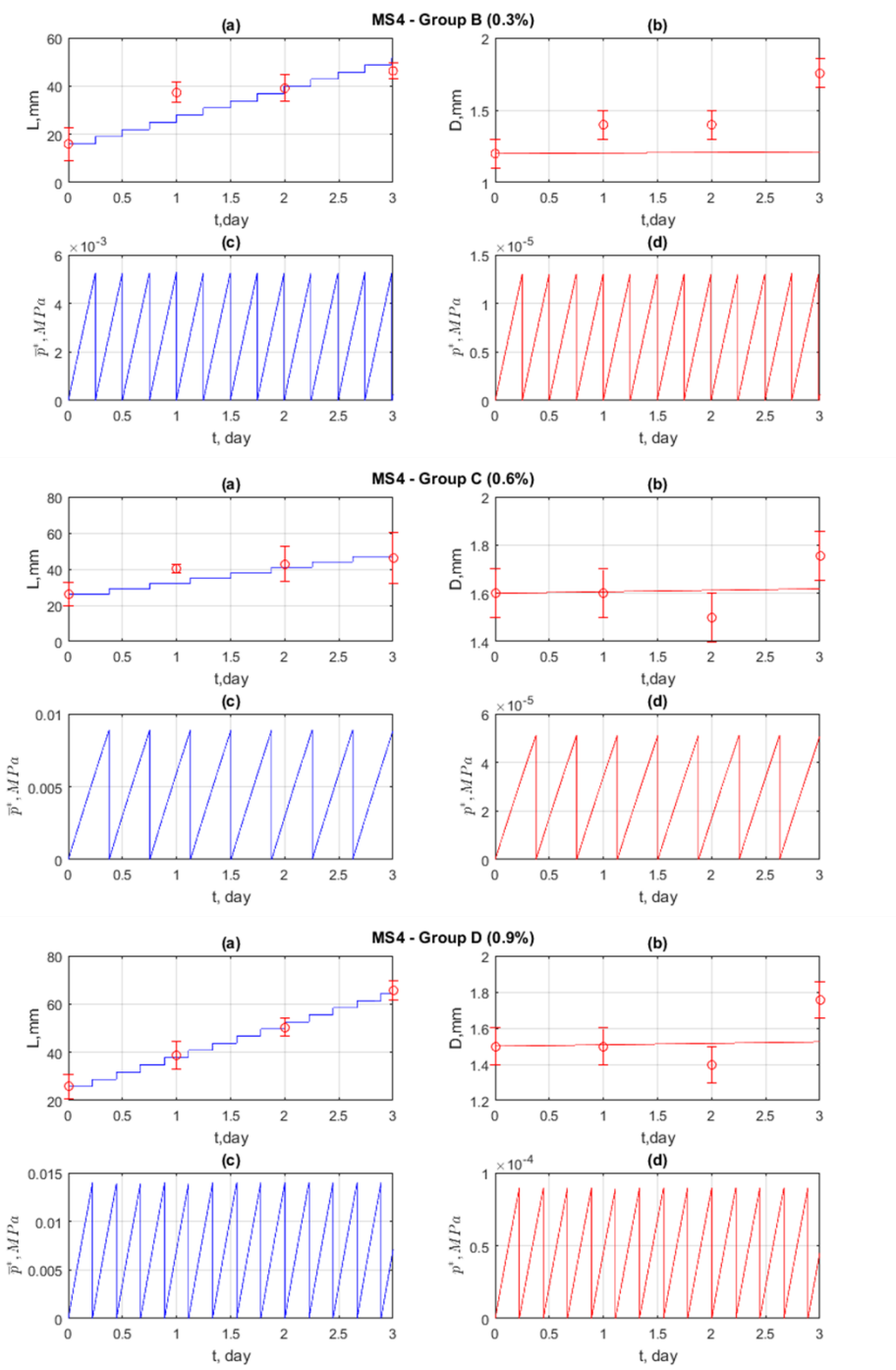

Figure 3.2.1 Numerical solution of length (a) and radius (b) evolution and axial (c) and radial (d) pressure against time. The red circles are the experimental data (mean values ±SD) in MS4 concentration.

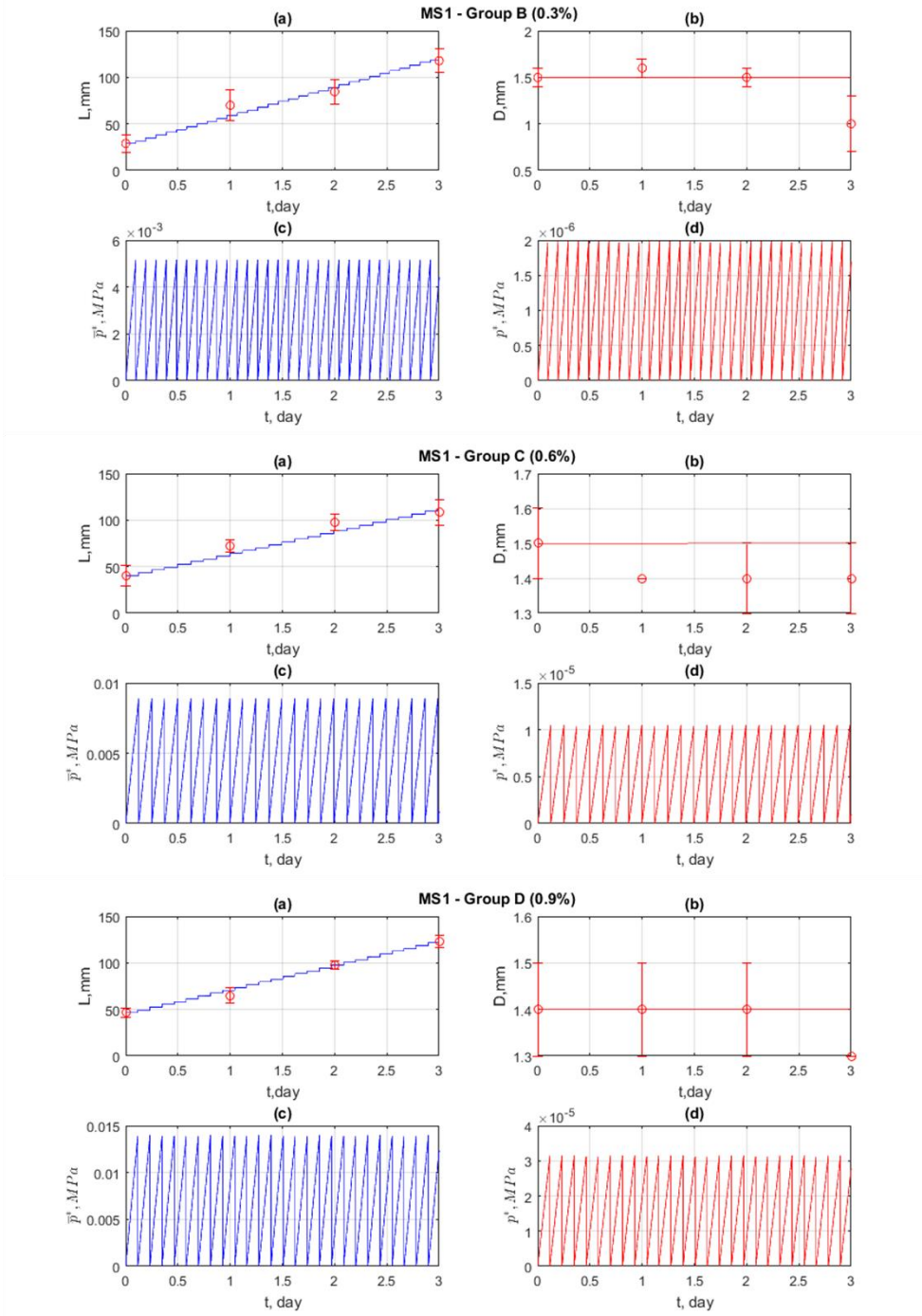

Figure 3.2.2 Numerical solution of length (a) and radius (b) evolution and axial (c) and radial (d) pressure against time. The red circles are the experimental data (mean values ±SD) in MS1 concentration.

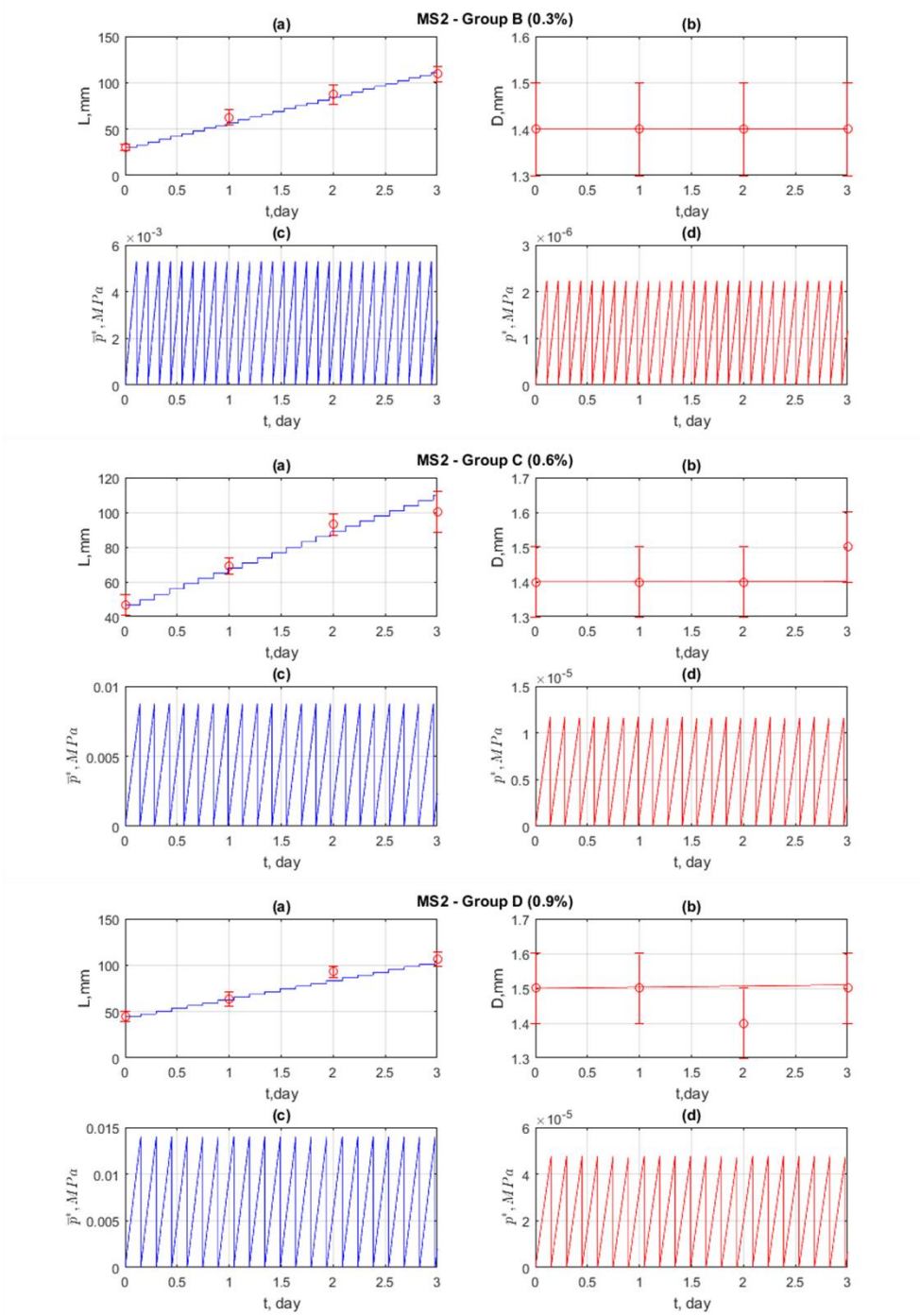

Figure 3.2.3 Numerical solution of length (a) and radius (b) evolution and axial (c) and radial (d) pressure against time. The red circles are the experimental data (mean values ±SD) in MS2 concentration.

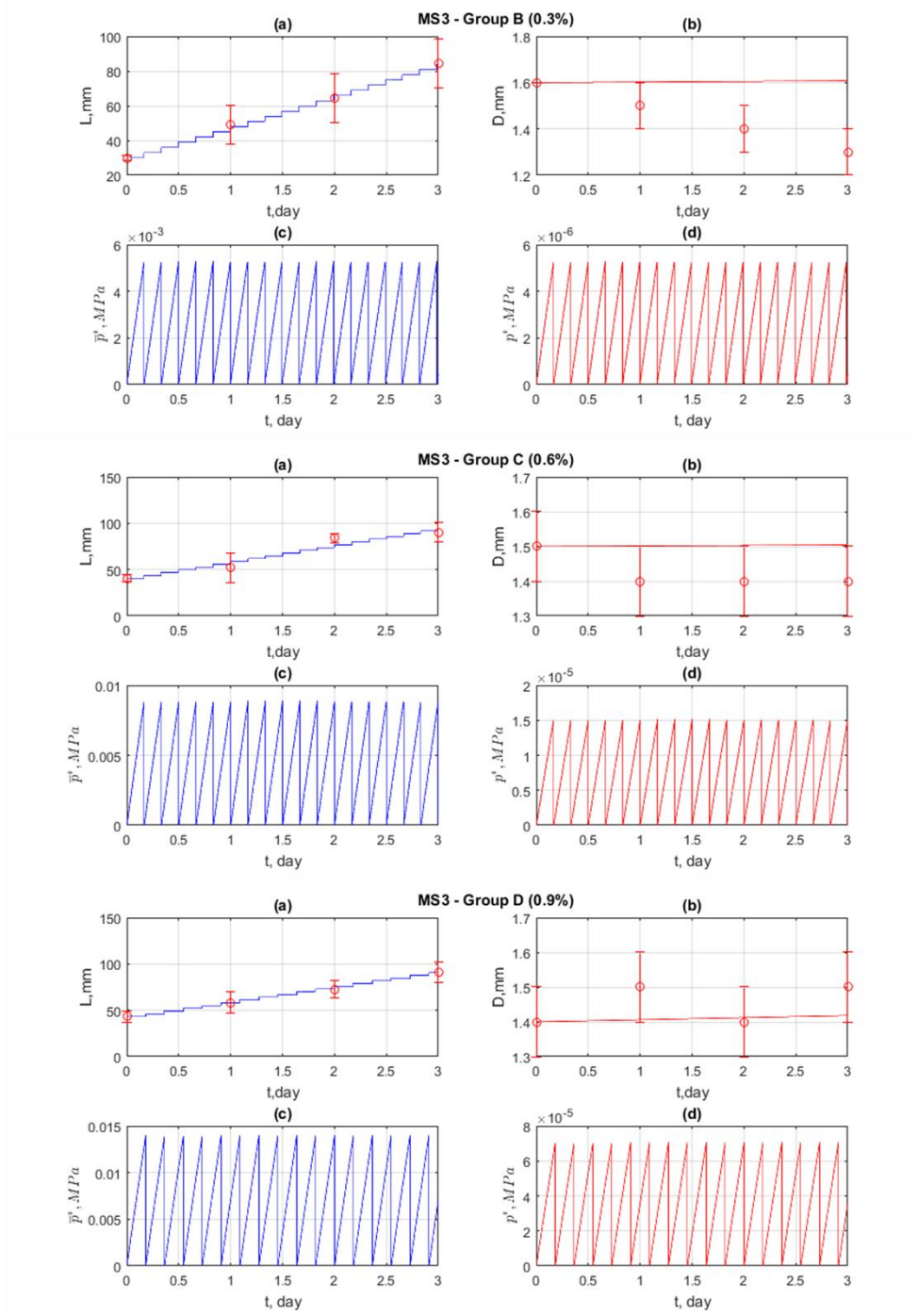

Figure 3.2.4 Numerical solution of length (a) and radius (b) evolution and axial (c) and radial (d) pressure against time. The red circles are the experimental data (mean values ±SD) in MS3 concentration.

3.3. Interpretation and Discussion

We observed the behaviour of *Zea mays* roots in artificial soils with different nutrient concentrations. Plants grown inside soil media with high concentrations of nutrients developed shorter and thicker root apparatus. The experiments have been repeated using soils with three different Phytagel concentrations and, in all the three cases, the root elongation rate decreased with the increase of nutrient concentrations.

It was possible to notice a visible enlargement for roots grown in media with higher concentrations of nutrients. The swelling was localized at the height of the meristematic area, which was the most sensitive area to the environment changes, e.g. to salt stress (Huang and van Steveninck, 1990). The experimental data showed that the excess of Murashige and Skoog Basal Salt Mixture, MS (Murashige and Skoog, 1962), in soil produces an abnormal radial swelling and elongation reduction and it can have a similar interpretation to the root swelling, due to NaCl stress (Li *et al.*, 2014). Therefore, the swelling of root observed in our study in the presence of MS4 concentration might be a further example of root sensibility to mineral nutrients stress.

The aim of this study is to couple experimental with theoretical results to gain a better understanding of how plant roots face nutrient stress. In order to explain such morphological and strategical adaptation of plant roots, we proposed a growth model by considering also the mechanical pressure due to the interaction between the root and the surrounding soil medium. In particular, we modelled the radial expansion through a critical threshold to describe the radial swelling as found in the experiments. Therefore, we formulated a hypothesis that the root radial expansion can be activated in the presence of an excessive nutrient concentration in the soil medium as an adaptation mechanism of response to nutrient availability. In fact, the equation (8.2) represents an activation equation for radial growth with a threshold level for the scaling parameter related to the nutrient availability, γ^*. In accordance with the experiments, γ^* increased with the Phytagel and MS

concentration. Specifically, the decrease in root length and the increase in root diameter occurred with respect to the increase in the values of γ^* and MS concentration in the soil medium for both our analytical and experimental results, respectively. One of the limits in our modelling approach is the underestimation of the radial expansion. Nevertheless, there is a significant scope to extend the theoretical model to incorporate other constitutive equations, e.g. more complex mechanical properties of root tissues and soil medium, the potential regulation of hormones and the osmotic effect at cellular level due to the outer medium. Such factors will be addressed in future studies by measuring further key parameters under experimental control. This study could lead to deeper investigations into the root behaviour mechanisms used to convert such adaptive strategies into bio-inspired approaches.

Chapter 4

4. Nanoindentation and Wettability Tests on Plant Roots

Several examples of adaptive strategies and solutions are in Nature kingdom to inspire engineering applications, e.g. see (Bar-Cohen, 2006). The question of how the efficient mechanisms by means of which plant roots respond and adapt to environmental stimuli has not completely answered, e.g. the endodermal specification and adaptation. Specifically, it is not completely understood how the root endodermis evolves according to the simultaneous and mutual dependence and interaction between the root and the soil medium. In fact, almost completely unknown mechanisms regulate such adaptive behaviours, such as the deposition of hydrophobic cell wall material (Roppolo *et al.*, 2011). Plant roots continuously sense and adapt their growth according to the surrounding medium through cell growth, secretion, elongation, differentiation and maturation (Kolb, Legué and Bogeat-Triboulot, 2017) (*Figure 4.1*).

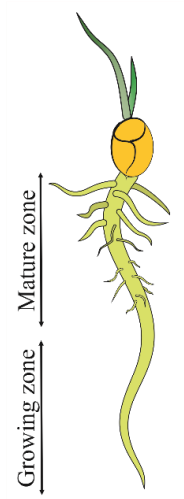

Figure 4.1 Plant root structure. In the maturation zone, the cells complete their differentiation and, providing anchorage and nutrient acquisition, lateral roots and root hairs grow. Then, in the growing zone, cell division and elongation occur. Therefore, the root elongates and penetrates the soil in the apical region. The penetration is due to the movements localized from the root tip to the beginning of the maturation region.

The addition, the growth, and the elongation of new material occur at the apical zone of the root between the meristematic and the elongation area, allowing the penetration in the soil. Then, the main differentiation of cells results in the mature zone with also the onset of hairs and lateral roots. Thus, the growing tip could control, coordinate and enhance the root system development and ability to face and withstand the unexpected physical and chemical obstacles. In fact, roots are extremely smart to resist to chemical and mechanical stimuli during the growth and, thus, to adjust their penetration direction and ability with a wide range of "active" responses, e.g. through radial swelling and reduction in elongation due to a toxic level of salt (Li *et al.*, 2014) and high soil impedance (A. Bengough and Mullins, 1990), respectively. Recent studies remark that plants can be regarded as sensory and communicative organisms with active problem-solving behaviour, as C. Darwin and F. Darwin firstly hypothesised in "*The power of movement in plants*" (Darwin and Darwin, 1880; Baluška *et al.*, 2009; Gagliano, 2017). In the latter manuscript a root tip that bends away when is irritated by contact is depicted (*Figure 4.2*).

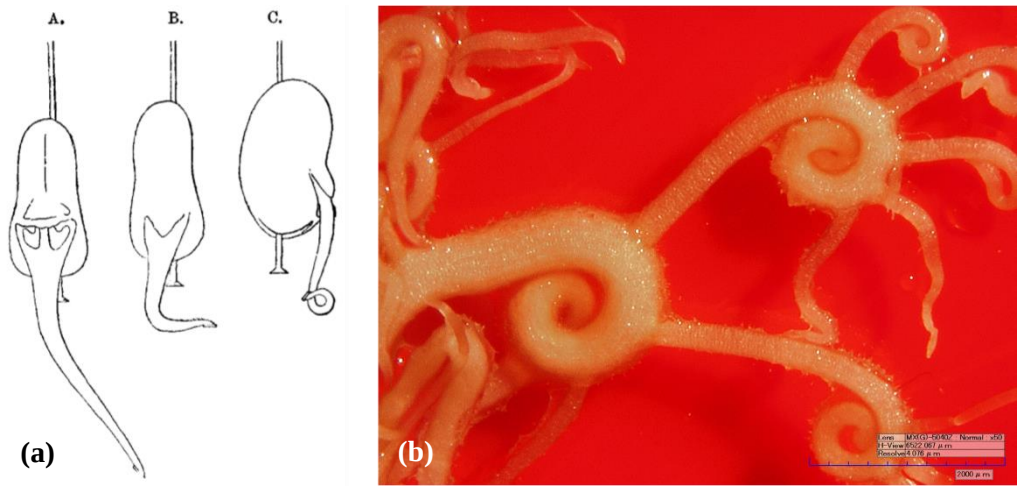

Figure 4.2 (a) "*Vicia faba: A, radicle beginning to bend from the attached little square of card; B, bent at a rectangle; C, bent into a circle or loop, with the tip beginning to bend downwards through the action of geotropism.*" from (Darwin and Darwin, 1880). (b) A Borlotti Lamon bean (*Phaseolus vulgaris L.*) exposed to light during growing in a 2D-confinement. The scale bar equals 2000 µm.

Therefore, we aim to reveal such adaptive behaviour through mechanical and surface characterization tests. In particular, we conducted dynamic indentation to shed light on the mechanical properties of the inner tissue and the intact root at the apical region. This technique allows localized measurements especially close the root tip, in which the standard setups for tensile test fail simply due to physical limitations. In addition, we performed wettability tests to investigate the capability of the root surface close to the root tip and seed. In the latter region, the presence of root hairs has a key role for the acquisition and selection of the nutrient and water uptake by roots.

This Chapter is devoted to experimental activities aiming to shed light on the adaptive strategies of plant roots during the penetration. Specifically, the mechanical tests, conducted at IIT (Pontedera) and reported in this thesis, arise from tensile tests on plant roots driven by curiosity (performed in our laboratory). *Figure 4.3* shows different responses of root tissue close to and far from the root tip.

In Section 4.1, we present a study on the mechanical properties of *Zea mays* primary root, at level of its outer surface, inner part, and cap, by using a dynamic indentation technique. Then, wettability tests were performed and reported in Section 4.2.

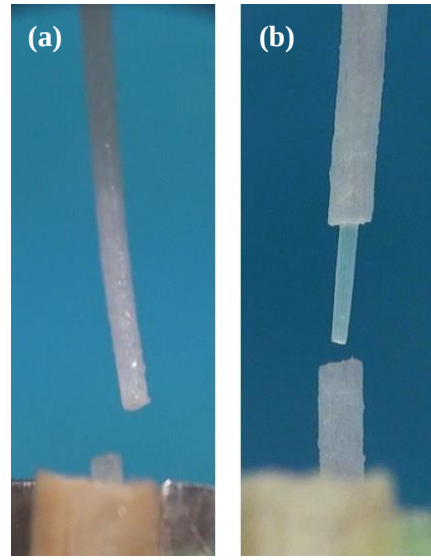

Figure 4.3 Tensile tests performed on *Zea mays* primary roots: (a) close to and (b) far from the tip.

4.1. Dynamic Nanoindentation Tests

4.1.1. Experimental Procedure

The experiments were performed using 3/4-day old *Zea mays L.* roots. The seeds were placed on filter paper with tap water and kept into a growth chamber at 25˚C. We measured the mechanical properties in correspondence of the outer wall and inner core of the root by dynamic indentation technique in 1-200 Hz frequency range with an indenter tip of 109 µm and 198.5 µm diameter, employing an iNano indentation system (Nanomechanics, Inc.). We used a dynamic nanoindentation technique to measure the storage modulus, E', and the loss modulus, E'', i.e. the real and complex part of the complex modulus which characterizes the material's ability to store and damp energy, respectively. E' provides information about the material ability to store energy elastically and E'' gives information about the material ability to dissipate energy (Pharr, Oliver and Brotzen, 1992; Herbert, Oliver and Pharr, 2008; Herbert *et al.*, 2009). In fact, E' and E'' are related to the storage stiffness and loss stiffness of the sample, respectively. E' is comparable to the Young's modulus if damping is negligible.

The experiments were carried out in distilled water and were made on roots (we cut the samples ~1cm in length from the tip) fixed on the bottom of the holder by means of attack (Loctite) at different distances from the tip (2, 3, 4, 5, 6, and 7 mm) in correspondence of the wall, the inner core, and the root cap (*Figure 4.1.1*, *Figure 4.1.2*). Due to the complex geometry of root tip, an *ad hoc* sample holder with two inclinations was built to perform tests in the root tip area (*Figure 4.1.1*b). In order to extract the root core, we made a circumferential incision of the root at the base of the seed, thus the outer wall can be easily separated from the inner core (*Figure 4.1.1*d). Then, we performed tests by exploiting the indenter tip of 198.5 µm diameter on both the intact root and the inner core and the indenter tip of 109 µm diameter near the root cap.

The results and the measurements number of the nanoindentation tests along the three root regions are reported in Tables 3-5. *Figure 4.1.3* and *Figure 4.1.4* show

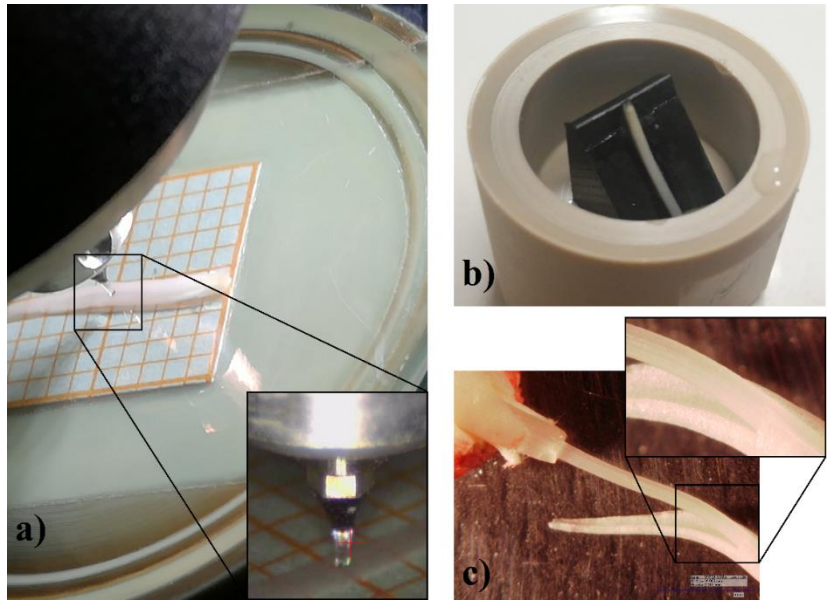

Figure 4.1.1 View of a nanoindentation experiment. a) A nanoindentation test. The zoom shows the indenter tip; b) and c) a sample holder used to test mechanical properties of root tissues near to the cap, and in outer and inner areas, respectively; d) separation procedure of the outer wall from the inner core.

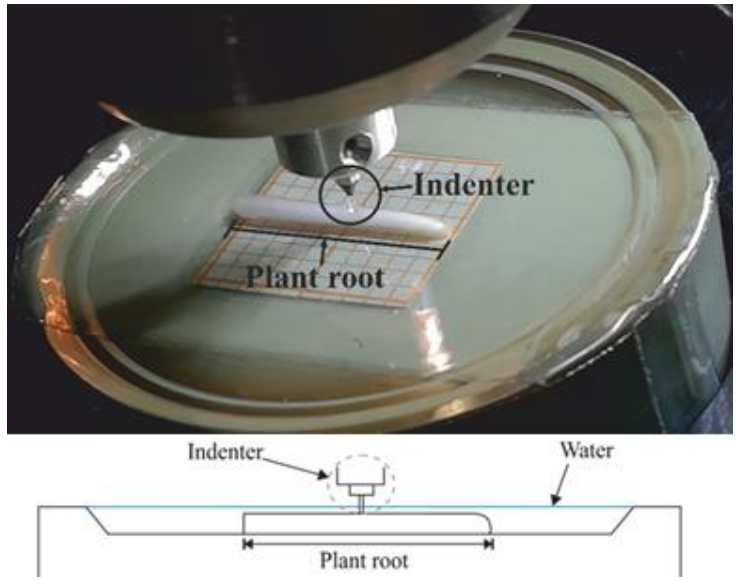

Figure 4.1.2 Schematic of the setup used for testing along the root in water at different distances from the tip.

graphical results of the storage and loss moduli for both the intact root and the inner tissue level.

4.1.2. Statistical Analysis

We performed statistical analysis to quantify the storage modulus (E') and the loss modulus (E'') changes with respect to the distance/frequency from the tip and at different tissue level (i.e. outer and inner tissues) for each frequency/distance.
The most appropriate statistical method is the ANOVA test in order to assess the statistical significance of the different response in the measurement of the moduli depending on the distance from the tip, frequency and tissue level. This test assumes that the data in the groups at various levels of effects are normally distributed, statistically independent and have the same variance. However, since our data showed some deviations from normality and/or homoscedasticity, we also performed different statistical tests when appropriated: the non-parametric Kruskal-Wallis test when the normality assumption failed, the Welch test when the data showed a strong heteroscedasticity.
In this regard, we exploited the Kruskal-Wallis test and the Welch test to verify the significance of the storage and loss modulus measurements, respectively, at both the intact root and inner core. We used the one-way ANOVA to test the significance of the measurements near the cap for both the storage and loss moduli.

The statistical analysis is at the 95% confidence level and performed in R.

We obtained significant E' difference with respect to distance from the tip (2mm-5mm) for each frequency for both intact root and inner tissue level (Table 6). While, we had significant E' differences with respect to frequency for each distance, except for the inner core at 2mm and 3mm from the tip and for the intact root at 2mm, 5mm and 7mm from the tip ($p > 0.05$, Table 7).
In addition, the results of the Welch tests showed significant E'' difference with respect to distances from the tip (2mm-7mm) for intact root at each frequency and (2-5mm) for inner tissue at 1-35Hz (Table 8). Moreover, the measurements of E'' changes are significant with respect to the frequency influence at both intact root

and inner core at each distance from the tip, except for the inner core at 2mm-3mm and for the intact root at 7mm ($p > 0.05$, Table 9).

The one-way ANOVA results pointed out significant E' and E'' differences near the root cap with respect to the frequency (Table 10).

Table 3. Storage and loss moduli (mean value ± SD) of the root cap for all frequencies (1, 3, 10, 15, 35, 85, 200 Hz). A total of 7 indentations on 4 roots were performed.

Freq. (Hz)	**E' (MPa)**	**E'' (MPa)**
200	4.23±1.53	0.61±0.22
85	3.9±1.29	0.6±0.22
35	3.65±1.22	0.56±0.18
15	3.39±1.15	0.55±0.17
10	3.27±1.13	0.55±0.16
3	2.81±1.01	0.54±0.17
1	2.49±0.93	0.55±0.2

Table 4 Storage modulus measurements (mean value ± SD) along the inner core at different distances from the tip (2, 3, 4, 5 mm) and the intact root tissue (2, 3, 4, 5, 6, 7 mm) for all frequencies (1, 3, 10, 15, 35, 85, 200 Hz). The measurements number for each distance is reported.

Freq. (Hz)	**Tissue level**	**Storage Modulus, E' (MPa)**					
		2mm (N=15)	**3mm** (N=15)	**4mm** (N=15)	**5mm** (N=15)	**6mm** (N=10)	**7mm** (N=10)
200	**intact**	8.06±1.95	7.28±1.41	5.94±1.39	5.23±1.51	4.4±0.9	3.86±1.03
	core	5.24±1.7	4.92±1.7	4.56±1.34	3.56±0.85	/	/
85	**intact**	7.74±1.88	6.98±1.35	5.66±1.38	4.99±1.53	4.16±0.89	3.6±1.04
	core	4.97±1.66	4.65±1.29	4.27±1.06	3.4±0.83	/	/
35	**intact**	7.51±1.87	6.74±1.33	5.47±1.33	4.83±1.5	4.02±0.87	3.46±1.03
	core	4.8±1.63	4.5±1.26	4.12±1.07	3.27±0.82	/	/
15	**intact**	7.27±1.84	6.5±1.31	5.28±1.29	4.67±1.46	3.88±0.85	3.33±11.02
	core	4.62±1.6	4.35±1.23	3.98±1.07	3.15±1.81	/	/
10	**intact**	7.16±1.82	6.39±1.3	5.19±1.26	4.59±1.44	3.81±0.84	3.27±1.01
	core	4.54±1.59	4.27±1.22	3.92±1.08	3.1±0.8	/	/
3	**intact**	6.59±1.71	5.86±1.23	4.75±1.17	4.22±1.35	3.47±0.82	3±0.98
	core	4.12±1.51	3.91±1.16	3.57±1.05	2.84±0.78	/	/
1	**intact**	6.13±1.65	5.46±1.18	4.42±1.13	3.95±1.31	3.18±0.85	2.79±0.98
	core	3.8±1.49	3.65±1.15	3.33±1.07	2.66±0.79	/	/

Table 5 Loss modulus measurements (mean value ± SD) along the inner core at different distances from the tip (2, 3, 4, 5 mm) and the intact root tissue (2, 3, 4, 5, 6, 7 mm) for all frequencies (1, 3, 10, 15, 35, 85, 200 Hz). The measurements number for each distance is reported.

Freq. (Hz)	**Tissue level**	**Loss Modulus, E'' (MPa)**					
		2mm (N=15)	**3mm** (N=15)	**4mm** (N=15)	**5mm** (N=15)	**6mm** (N=10)	**7mm** (N=10)
200	**intact**	0.49±0.07	0.48±0.08	0.42±0.12	0.34±0.1	0.34±0.09	0.34±0.07
	core	0.37± 0.12	0.36±0.12	0.36±0.08	0.3±0.09	/	/
85	**intact**	0.48±0.08	0.47±0.08	0.39±0.09	0.33±0.09	0.30±0.07	0.3±0.07
	core	0.35±0.12	0.33±0.1	0.31±0.07	0.26±0.07	/	/
35	**intact**	0.49±0.09	0.47±0.09	0.38±0.09	0.32±0.08	0.29±0.06	0.28±0.06
	core	0.35±0.11	0.31±0.1	0.3±0.06	0.25±0.06	/	/
15	**intact**	0.51±0.11	0.49±0.09	0.4±0.09	0.34±0.09	0.3±0.067	0.27±0.05
	core	0.37±0.12	0.31±0.1	0.3±0.07	0.25±0.05	/	/
10	**intact**	0.54±0.13	0.51±0.1	0.42±0.1	0.35±0.1	0.32±0.07	0.27±0.05
	core	0.38±0.14	0.32±0.1	0.31±0.07	0.26±0.05	/	/
3	**intact**	0.65±0.19	0.59±0.15	0.47±0.12	0.4±0.11	0.38±0.1	0.29±0.08
	core	0.44±0.18	0.36±0.11	0.38±0.12	0.28±0.04	/	/
1	**intact**	0.86±0.28	0.73±0.23	0.56±0.16	0.47±0.12	0.46±0.11	0.34±0.12
	core	0.48±0.2	0.39±0.12	0.39±0.01	0.3±0.03	/	/

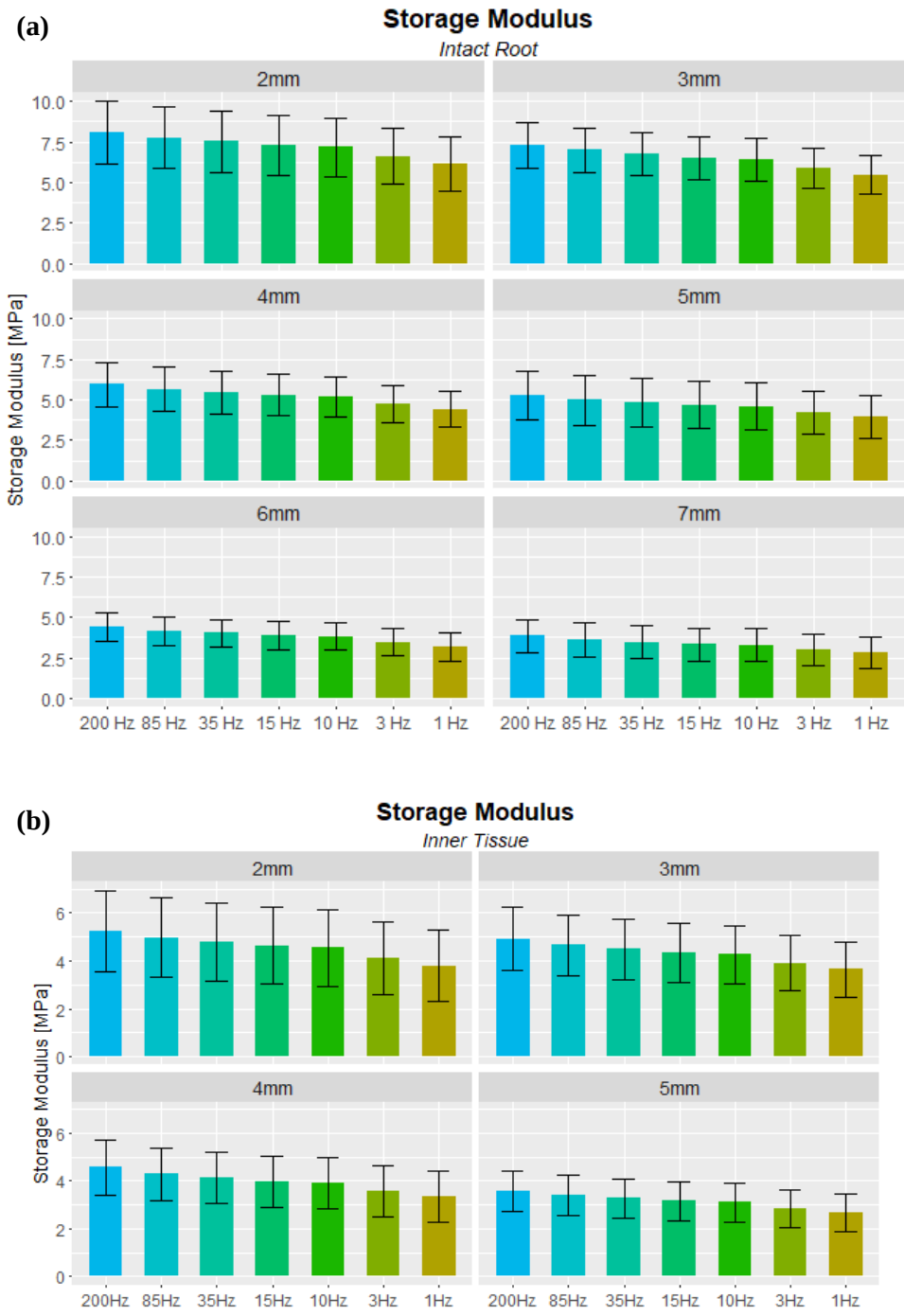

Figure 4.1.3 Plot of the mean and SD of the storage modulus at (a) the intact root and (b) the inner tissue.

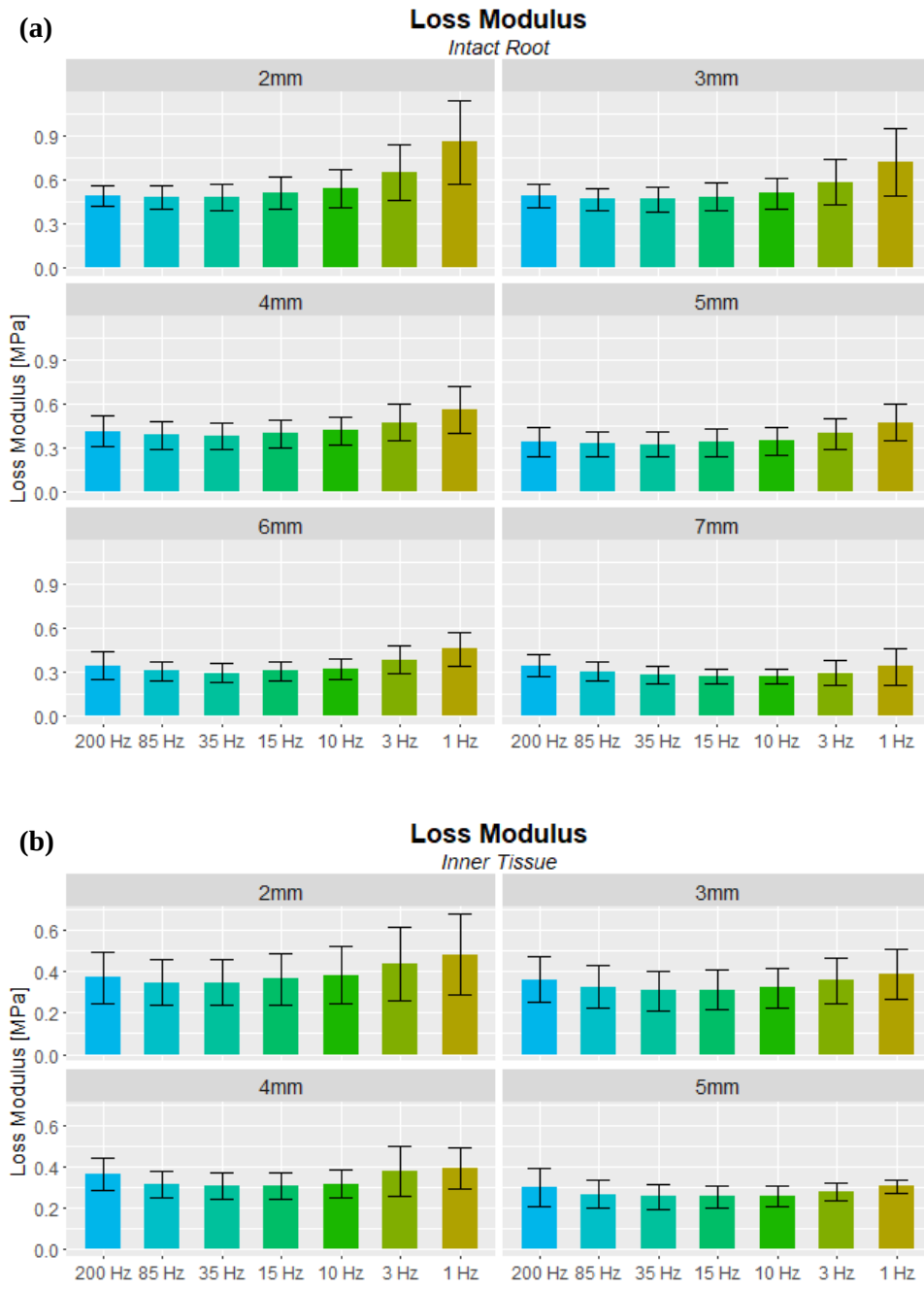

Figure 4.1.4 Plot of the mean and SD of the loss modulus at (a) the intact root and (b) the inner tissue.

Table 6 Results of the Kruskal-Wallis test for the significance of the measurements of E' obtained at inner and intact root outer tissue levels for each frequency at the distances of 2, 3, 4 and 5mm from the tip (df= degrees of freedom).

Tissue	Freq.	Kruskal-Wallis test: Storage Modulus (E') vs Distance
Inner tissue	200Hz	Kruskal-Wallis chi-squared = 12.14, df = 3, p-value = 0.006918
	85Hz	Kruskal-Wallis chi-squared = 10.922, df = 3, p-value = 0.01215
	35Hz	Kruskal-Wallis chi-squared = 11.256, df = 3, p-value = 0.01042
	15Hz	Kruskal-Wallis chi-squared = 10.862, df = 3, p-value = 0.0125
	10Hz	Kruskal-Wallis chi-squared = 10.803, df = 3, p-value = 0.01284
	3Hz	Kruskal-Wallis chi-squared = 9.6728, df = 3, p-value = 0.02156
	1Hz	Kruskal-Wallis chi-squared = 7.8297, df = 3, p-value = 0.04966
Intact root	200Hz	Kruskal-Wallis chi-squared = 19.288, df = 3, p-value = 0.0002384
	85Hz	Kruskal-Wallis chi-squared = 19.455, df = 3, p-value = 0.0002202
	35Hz	Kruskal-Wallis chi-squared = 19.255, df = 3, p-value = 0.0002421
	15Hz	Kruskal-Wallis chi-squared = 18.938, df = 3, p-value = 0.0002815
	10Hz	Kruskal-Wallis chi-squared = 18.642, df = 3, p-value = 0.0003241
	3Hz	Kruskal-Wallis chi-squared = 18.242, df = 3, p-value = 0.0003921
	1Hz	Kruskal-Wallis chi-squared = 16.844, df = 3, p-value = 0.0007609

Table 7 Results of the Kruskal-Wallis test for the significance of the measurements of E' obtained at inner and intact root outer tissue levels for each distance from the tip at all the frequencies 200, 85, 35, 15, 10, 3, 1Hz (df= degrees of freedom).

Tissue	Dist.	Kruskal-Wallis test: Storage Modulus (E') vs Frequency
Inner tissue	2mm	Kruskal-Wallis chi-squared = 12.128, df = 6, p-value = 0.05918
	3mm	Kruskal-Wallis chi-squared = 10.091, df = 6, p-value = 0.1209
	4mm	Kruskal-Wallis chi-squared = 14.486, df = 6, p-value = 0.02465
	5mm	Kruskal-Wallis chi-squared = 14.025, df = 6, p-value = 0.02936
Intact root	2mm	Kruskal-Wallis chi-squared = 10.452, df = 6, p-value = 0.1069
	3mm	Kruskal-Wallis chi-squared = 25.825, df = 6, p-value = 0.0002399
	4mm	Kruskal-Wallis chi-squared = 13.416, df = 6, p-value = 0.03688
	5mm	Kruskal-Wallis chi-squared = 11.629, df = 6, p-value = 0.07078
	6mm	Kruskal-Wallis chi-squared = 12.805, df = 6, p-value = 0.04624
	7mm	Kruskal-Wallis chi-squared = 9.5971, df = 6, p-value = 0.1427

Table 8 Results of the Kruskal-Wallis test for the significance of the measurements of E'' obtained at inner and intact root outer tissue levels for each frequency at the distances of 2, 3, 4 and 5mm from the tip (df= degrees of freedom).

Tissue	Freq.	Welch test: Loss Modulus (E'') vs Distance
Inner tissue	200Hz	F = 1.8818, num df = 3, denom df = 30.712, p-value = 0.1534
	85Hz	F = 2.6863, num df = 3, denom df = 30.488, p-value = 0.06394
	35Hz	F = 3.7163, num df = 3, denom df = 30.281, p-value = 0.02186
	15Hz	F = 4.8201, num df = 3, denom df = 29.837, p-value = 0.007454
	10Hz	F = 5.4988, num df = 3, denom df = 29.62, p-value = 0.003987
	3Hz	F = 7.8436, num df = 3, denom df = 26.941, p-value = 0.0006412
	1Hz	F = 8.6182, num df = 3, denom df = 25.923, p-value = 0.0003897
Intact root	200Hz	F = 8.7583, num df = 3, denom df = 30.756, p-value = 0.0002392
	85Hz	F = 11.084, num df = 3, denom df = 31.034, p-value = 4.16e-05
	35Hz	F = 11.243, num df = 3, denom df = 31.098, p-value = 3.698e-05
	15Hz	F = 9.9032, num df = 3, denom df = 31.043, p-value = 9.771e-05
	10Hz	F = 9.6887, num df = 3, denom df = 30.981, p-value = 0.0001153
	3Hz	F = 9.0686, num df = 3, denom df = 30.513, p-value = 0.0001915
	1Hz	F = 10.074, num df = 3, denom df = 29.91, p-value = 9.513e-05

Table 9 Results of the Kruskal-Wallis test for the significance of the measurements of E'' obtained at inner and intact root outer tissue levels for each distance from the tip at all the frequencies 200, 85, 35, 15, 10, 3, 1Hz (df= degrees of freedom).

Tissue	Dist.	Welch test: Loss Modulus (E'') vs Frequency
Inner tissue	2mm	F = 1.315, num df = 6, denom df = 43.391, p-value = 0.271
	3mm	F = 1.0713, num df = 6, denom df = 43.526, p-value = 0.3943
	4mm	F = 2.7377, num df = 6, denom df = 43.395, p-value = 0.0241
	5mm	F = 3.1199, num df = 6, denom df = 43.106, p-value = 0.01254
Intact root	2mm	F = 5.6909, num df = 6, denom df = 43.027, p-value = 0.0002016
	3mm	F = 3.7472, num df = 6, denom df = 43.245, p-value = 0.004335
	4mm	F = 3.177, num df = 6, denom df = 43.436, p-value = 0.01131
	5mm	F = 3.3021, num df = 6, denom df = 43.49, p-value = 0.00913
	6mm	F = 3.1782, num df = 6, denom df = 27.883, p-value = 0.01668
	7mm	F = 1.5232, num df = 6, denom df = 27.841, p-value = 0.2073

Table 10 Results of the one-way ANOVA test for the significance of the measurements of the storage (E') and loss (E'') moduli obtained near the root cap tip at all the frequencies 200, 85, 35, 15, 10, 3, 1Hz (Df= degrees of freedom; Sum Sq= sum square; Mean Sq= mean square).

		Measurements near the root cap				
		Df	**Sum Sq**	**Mean Sq**	**F-value**	**Pr(>F)**
Storage Modulus	**Frequency**	6	15.46	2.576	1.81	0.12
	Residuals	42	59.78	1.423		
Loss Modulus	**Frequency**	6	0.0341	0.00568	0.156	0.987
	Residuals	42	1.5275	0.03637		

4.2. Wettability Tests

4.2.1. Experimental Procedure

We tested 3/4-day old *Zea mays L.* roots and we proceeded with the same planting procedure described in the previous Section. We evaluated the wettability of the root surface close to both the tip and the seed, measuring the static contact angle. The water droplet (~0.5µl) was deposited on the surface of the root with a speed dispenser holder rate of 10000mm/min by using Hamilton 81434 Syringe. We performed measurements at the apical region and close to the seed. Since the presence and resistance of root hairs close to the seed, the needle of the syringe was immersed in the droplet in order to achieve the deposition of the water droplet directly on the root lateral surface. We carried out the test on intact roots without attack on the bottom (*Figure 4.2.1*). We converted the source image into a grayscale image with Matlab® (The Mathworks, Inc.), then we rotated and analyzed the images with ImageJ (see *Figure 4.2.2*).

4.2.2. Contact Angle Measurements

We obtained that the mean contact angle is 92.6°±18.3° at the apical region and 149.4°±11.9° at the root hair zone.

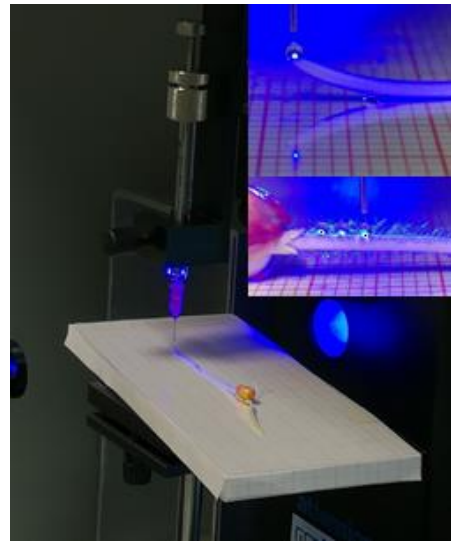

Figure 4.2.1 Overview of the contact angle measurements on the surface close to the apical and maturation zone.

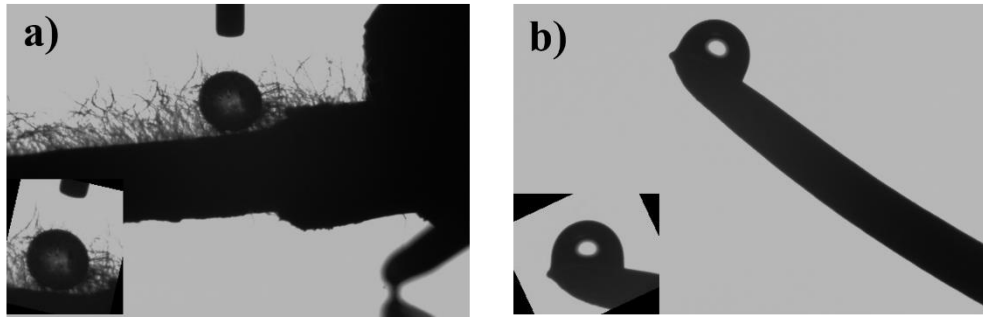

Figure 4.2.2 Grayscale images of the wettability experiments. We analysed the corresponding rotated zooms at a) the surface close to seed and b) the apical region.

4.3. Interpretation and Discussion

Recently, studies on the morphological aspects of plant development reveal the need to better understand the connection between the biochemical variations and the mechanical changes of their tissues (Hamant, Traas and Boudaoud, 2010; Potocka and Szymanowska-Pułka, 2018). Thus, the knowledge of such features is required to this aim. In this regard, studies on the mechanical properties of plant roots have been done, e.g., to explore slope stability for crop and soil sciences. In fact, protocols have been developed to exploit compression, tensile, uprooting and AFM tests, see e.g. (Whiteley and Dexter, 1981; Loades *et al.*, 2013, 2015; Edmaier *et al.*, 2014; Peaucelle, 2014; Yang, Chen and Li, 2016). In addition, non-invasive imaging techniques are used to reduce possible errors in measurements (Hamza *et al.*, 2006) and/or for novel experimental system (Bizet *et al.*, 2016). In fact, the authors of (Bizet *et al.*, 2016) combined a 3D live *in situ* imaging, kinematics and a novel mechanical sensor to study root tissues and root responses to axial mechanical forces in nutrient solution. A remaining experimental limitation is to characterize the mechanical properties of living tissues in soil-like environments. Nevertheless, such experimental investigations could quantify the functional importance of some key features involved into the root growth development. In this contest, we performed mechanical and surface characterization of root tissues. From a mechanical perspective, the variation of E' at the tissue levels suggests that the outer and inner tissue can have a different purpose: the first plays the role of a coating in the overall root stiffness, while the second can be seen as a "soft skeleton" in the root structure (*Figure 4.3.1*a-c, images of fracture due to manipulation of the root tissues are in *Figure 4.3.2*). More interestingly, the localization of the sensory and motor tissue at the apical region could lead to several classes of movements, such as circumnavigation to avoid obstacles (e.g. see (Popova, Tonazzini, *et al.*, 2016)). The investigation of curvatures produced by stimuli has been investigated by C. Darwin and F. Darwin. They showed that the

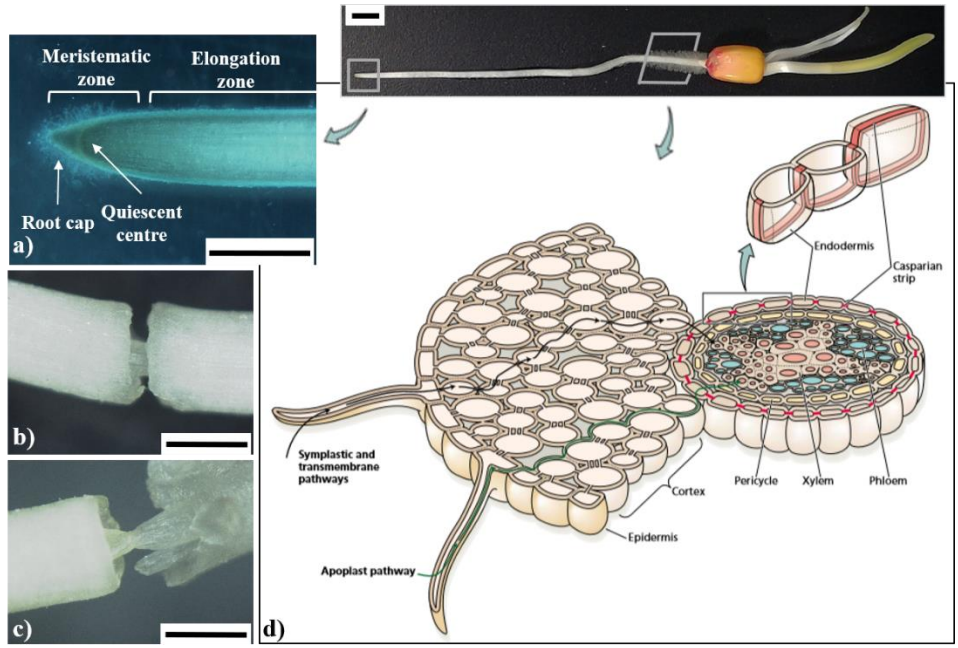

Figure 4.3.1 A 3/4-day old *Zea mays L.* root, scale bar: 5mm. (a) The apical zone is the most sensitive region of the root. Cell division and elongation occur at the apical region and allow the root to move and grow into the soil. The cell division is slower in the quiescent centre, then the cells mainly elongate and differentiate in the elongation zone. The root cap has the role of protection from the surrounding soil; (b) Fracture of the outer wall and intact inner core; (c) Twist of the inner core; (d) Water and nutrients can move across the root through different internal pathways: Apoplast, Transmembrane, and Symplast pathways. In this regard, the Casparian strip is in the Apoplast pathway, limiting the water and solute movement due to the presence of suberin (image from (Taiz and Zeiger, 1991)). The scale bar equals 1000µm in a-c.

sensitiveness of tip transmits the curvature movement to the upper part starting from 6 mm from the tip (Darwin and Darwin, 1880). In this regard, the mechanism of root curvature can be allowed due to the increase of softness with the increase of the distance from the tip (Table 4). Moreover, the authors of (Bizet *et al.*, 2016) show the presence of mechanical weakness for bending between the growing and the mature zones in poplar roots during the growth in nutrient solution. In addition, by comparing the second moment of inertia of a solid and a hollow cylindrical beam (I_S and I_H, respectively) representing the inner and outer tissues (in similar way of (Niklas, 1999)), it holds

$$I_s = \frac{\pi}{4} R_i^4 \text{ and } I_H = \frac{\pi}{4} (R_o^4 - R_i^4) \Rightarrow \frac{I_H}{I_s} = \chi^4 - 1, \qquad \frac{R_o}{R_i} = \chi \text{ with } \chi > 1,$$

where R_o is the outer radius of the intact root and R_i is the radius of the root inner core. Therefore, the outer wall could increase the stiffness of the inner core by providing a greater withstanding bending forces to the intact root. In addition, by comparing the second moment of inertia of the intact root, I_R, and the outer wall, I_H, it results $I_R / I_H = 1 - 1/\chi^4$. Thus, for $\chi \gg 1$, it holds that I_R tends I_H and $I_H \gg I_S$, i.e. the amount of outer wall could significantly increase its role in the stiffening of the whole root structure when the inner core radius is negligible with respect to the root radius. Since the cell differentiation arises more clearly with the increase of the distance from the tip, the difference between the inner and outer tissues increases with the increase of the distance to the root tip. Thus, the growing zone close to the root tip could be represented by the limiting case $\chi \gg 1$.

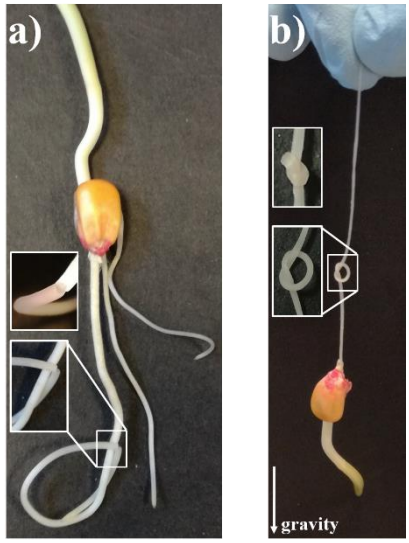

Figure 4.3.2 Images of fracture due to manipulation of the root tissues of the whole root a) and of the inner skeleton b). The tightening of the knot without fracture of the tissue is possible only at the inner tissue level.

In addition, another interesting feature to investigate is the distribution of specialized absorbing surface along the root. We found that the apical region seems

to be a surface with low wettability (92.6°±18.3°) and the root hair zone is a highly hydrophobic surface (149.4°±11.9°). The apical zone is permeable to water, while the increase in the distance from the tip leads to a higher presence of suberin, i.e. hydrophobic matter (Taiz and Zeiger, 1991). In addition, the authors of (Otten and Herminghaus, 2004) show that the presence of additional elastic hair-like structures covering a substrate could allow to exhibit superhydrophobic behaviour in Lady's Mantle leaves, even though the hairs are hydrophilic (Jiang and Feng, 2010). In fact, the bundle formation of hairs and thus its elasticity develop a repulsive interaction between the surface and the water/air interface with elastic energy costs. By considering the height of the bundle, *h*, they propose the elastic energy contribution

$$\Gamma \propto (E_{hairs} \cdot h^{-1})^{1/2} ,$$

where E_{hairs} is the hairs Young modulus (Otten and Herminghaus, 2004). In addition, the author of (Bernardino, Blickle and Dietrich, 2010) show that hydrophobicity with hydrophilic hairs is difficult to gain (e.g. see also (Mock *et al.*, 2005)) and the hairs elasticity does not provide such behaviour in the Lady's Mantle leaves, i.e. the elastic energy may not counterbalance the wetting energy. However, they do not exclude that the hairs flexibility has a key role in wetting phenomena, e.g. the water droplet bends the hairs, thus a metastable Cassie state is observed. During our experiments the buckling of the root hairs occurs due to the deposition of the water droplet. Thus, the root hairs not only extend the absorbing surface of the root but they could have also a key role as an amplifier for hydrophobicity with an air-solid state in the measurements of the contact angle (Otten and Herminghaus, 2004; Bernardino, Blickle and Dietrich, 2010; Jiang and Feng, 2010), i.e. the water drop sits on the roughness given by the root hairs (*Figure 4.3.3*, *Figure 4.3.4*). Since the hairs height and distribution along the root surface increase with increasing the distance from the root tip, the influence of these additional parameters on the hydrophobicity increases close the plant seed (*Figure 4.3.5*). The determination of factors that activate the adaptive strategies of plants could have a great potential to

be used in several applications, e.g. a recent study remarks the crucial role of the hairy surfaces in the separation of oil/water mixtures (Kavalenka *et al.*, 2017; Zeiger *et al.*, 2017). Moreover, it could be useful to exploit not only both the mechanical and wettability properties to design robots for selective absorption but also the internal transport of nutrients and water (*Figure 4.3.1d*) through the inner skeleton. Therefore, the inspiration from Nature could be essential for technologies that aim to the recycling and re-use bringing benefits to both environment and economy.

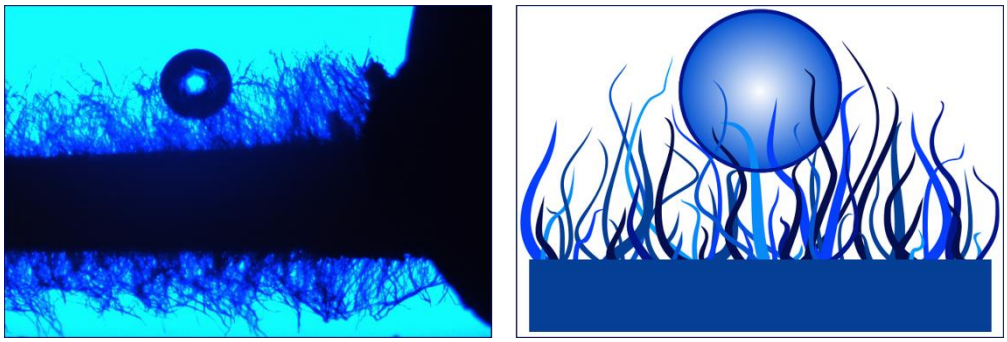

Figure 4.3.3 An example of water drops sitting on root hairs (on the left) with its schematic diagram (on the right). The surface close to the seed is covered with dense root hairs. Thus, the hydrophobic properties could be strengthened by surfaces textures and amplified by the presence of the root hairs. Moreover, an air-solid state could arise from root hairs due to the air trapped below the drop.

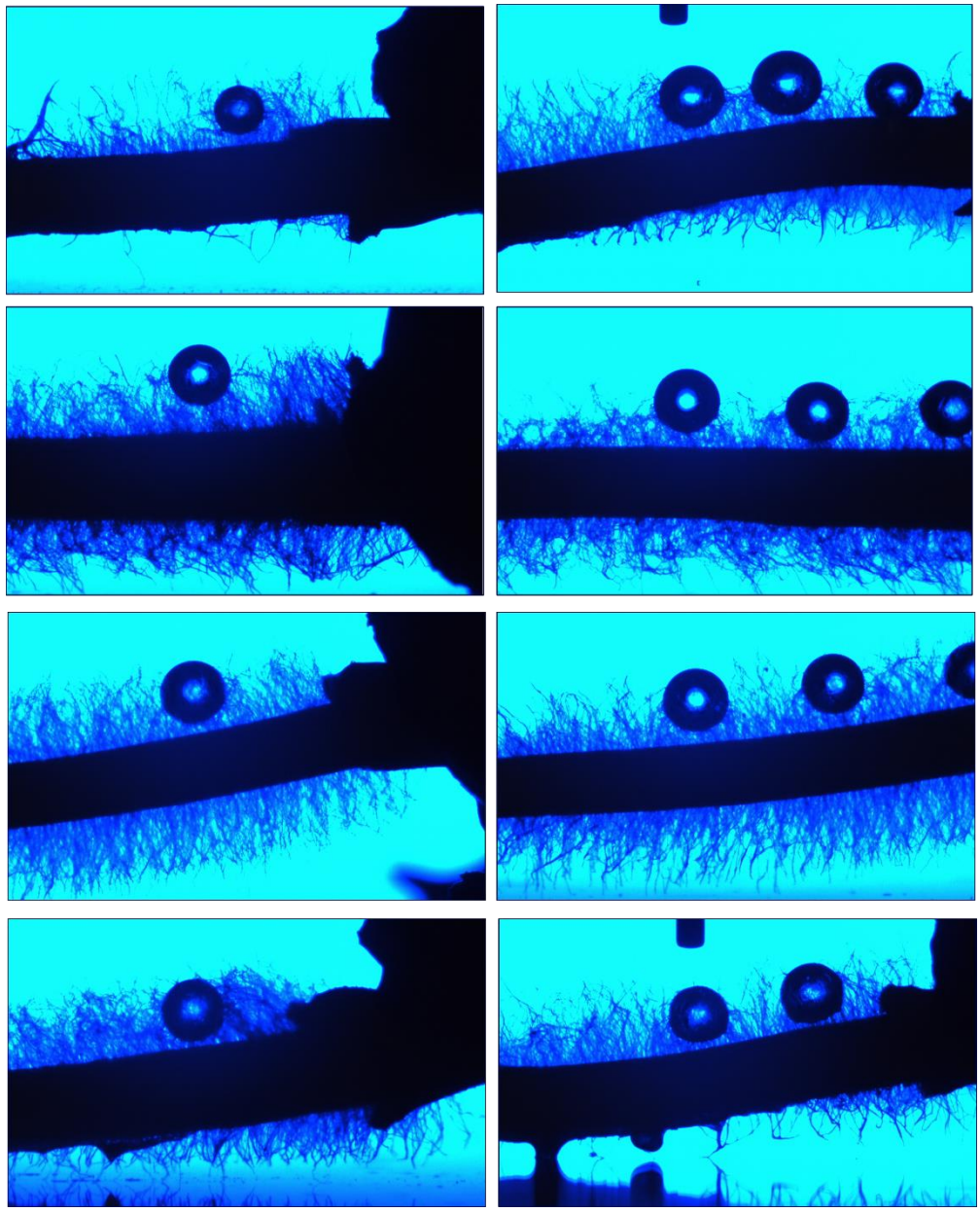

Figure 4.3.4 Images showing an air-solid state arising from the presence of root hairs on the surface close to the seed (observations on N=6 samples).

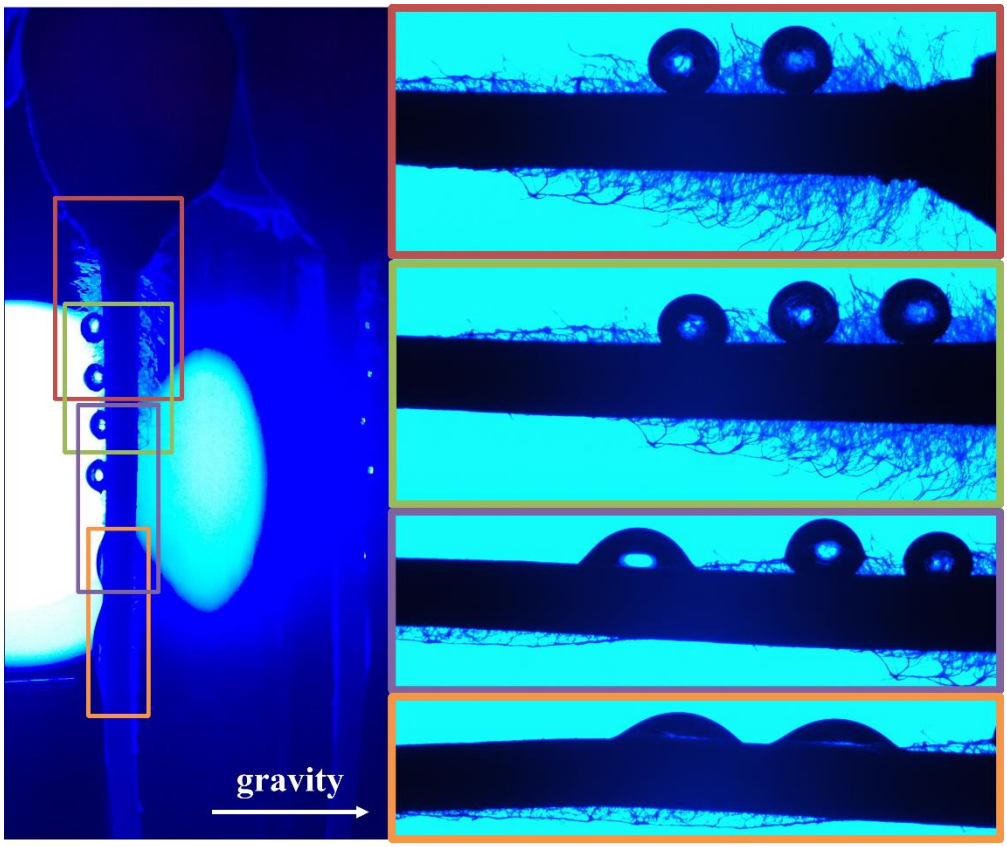

Figure 4.3.5 Droplets with different shapes along a plant root due to the variation of the height and distribution of hairs on the root surface.

Chapter 5

5. Plant Roots Growth in Photoelastic Gelatine

Plant roots represent an excellent example of successful soil penetration and exploration strategies (Popova, van Dusschoten, *et al.*, 2016). Roots can efficiently penetrate the substrate and perform key functions for growth and survival (Gilroy and Masson, 2008). Since the mechanical properties of the growth medium influence the plant root growth, the interest on the development of non-invasively technique to observe root growth is increasing (Kolb, Hartmann and Genet, 2012; Silverberg *et al.*, 2012; Tan *et al.*, 2015; Keyes *et al.*, 2016; Popova, van Dusschoten, *et al.*, 2016; Zha *et al.*, 2016). Because of its transparency, artificial substrates, e.g. agar and hydrogel, are mainly adopted to directly observe the root growth (Silverberg *et al.*, 2012; Tan *et al.*, 2015; Zha *et al.*, 2016). In addition, the development of novel non-invasive imaging techniques has a high significance to capture a more complete feedback between roots development and soil properties, see e.g. (Keyes *et al.*, 2016; Popova, van Dusschoten, *et al.*, 2016; Colombi *et al.*, 2017). In fact, in (Popova, van Dusschoten, *et al.*, 2016) a novel 3-D imaging technique, MRI, to dynamically and non–invasively investigate the influence of physical soil properties on root growth in non–transparent media has been developed. Photoelasticity can be a further powerful technique to observe the penetration strategies of plant roots. Photoelastic stress analysis is a technique once widely employed by engineers to observe stress patterns (Durelli and Riley, 1965). Moreover, the use of photoelasticity have been used also to visualize and analyse the strain in medical applications, see e.g. (Tomlinson and Taylor, 2015). In (Tomlinson and Taylor, 2015) gelatine mixed with glycerin was used for the photoelastic tests as a starting point for needle insertion. In early works forces exerted by moving organisms have been quantitatively measured by means of photoelasticity, e.g. (Harris, 1978; Full, Yamauchi and Jindrich, 1995; Goldman and Hu, 2010; Hu, David and Shelley, 2012; Dorgan, Law and Rouse, 2013;

Mirbagheri *et al.*, 2015). This technique is non-invasive and requires minimal equipment for both dynamic measurements of forces exerted by moving organisms (Harris, 1978) and direct observation of the phenomenon. In fact, gelatine has been used to study animals locomotion, e.g. in (Dorgan, Arwade and Jumars, 2007) gelatine mimics muddy sediments. Nonetheless, the photoelastic technique is also applied to living organisms in granular substrates (Kolb, Hartmann and Genet, 2012; Wendell *et al.*, 2012; Mirbagheri *et al.*, 2015). Previous studies on plant root growth have exploited photoelastic soils by means of granular systems where photoelastic grains are used to visualize and quantify the local forces in the system (Kolb, Hartmann and Genet, 2012; Wendell *et al.*, 2012). This Chapter describes the application of photoelasticity to the plant root growth in photoelastic homogeneous medium. When small forces are exerted, small stresses can be generated, thus only low fringe orders can be seen as in the case of plant root growth. Therefore, we exploited the fringe multiplication applied to the study of plant roots growing in edible gelatine. The fringe multiplication technique is especially useful for increasing the observable fringe orders. In fact, D. Post demonstrated the potential of the fringe multiplier, which consists of two partial mirrors at the front and rear of the specimen into a traditional polariscope (see e.g. (Post, 1955, 1966, 1970)). Fringe multiplication is a full-field compensation technique where the fringe fractional orders can be estimated simultaneously at all points on the sample (Dally and Riley, 1991). This technique may provide further insights into the forces exerted during root growing and bending. Since plant roots have great ability to explore and respond to environmental stimuli, a root-like growing device represents a translation of biological concepts into an engineering system not only for soil penetration but also for biomedical applications. In fact, the needle insertion (e.g. epidural puncture), guidance problems deep in the body require relatively large distance to be travelled, to penetrate and to be in close contact with tissues with different layer properties (e.g. from a hard to a soft layer). Minimally invasive penetrations may be achieved by controlling feed position or velocity using a highly sensitised tip as analogue of root tip to detect mechanical

properties of the surrounding medium. Therefore, a microdrilling that adapts to the surrounding environment and is able to avoid obstacles offers potential for improved surgery in areas of difficult access (Brett *et al.*, 1995).

5.1. Photoelasticity

We report a brief description of the photoelasticity principles in this Section and fringe multiplication in Section 5.2. For more details on the theory about photoelastic techniques we refer the reader to e.g. the book *Experimental Stress Analysis* by Dally and Riley (Dally and Riley, 1991).

Light propagates in free space with a velocity, c, approximately of $3 \times 10^8 m/s$ and in any other bodies with a lower velocity, v. The ratio between the two velocities is called index of refraction, $n = c/v$. When a ray of light enters in optically isotropic materials, the refractive index does not depend upon the direction of propagation or the plane of vibration. While optically anisotropic bodies have different indices of refraction in each of the two mutually-perpendicular planes in which the light may vibrate. Such materials are named birefringent. It is possible to obtain a temporary or artificial birefringence in certain bodies. In fact, many non-crystalline transparent materials are ordinarily optically isotropic and become anisotropic only during the application of external forces, i.e. it is temporarily birefringent. Such materials have photoelastic behaviour and are called photoelastic materials.

When a polarized light[4] pass through the body of thickness *h*, and it is divided into two components rays that are linearly polarized at right angles to each other, propagating with different velocities. Therefore, the relative retardation between the two rays is

[4] A polarized light emits waves in which the vibrations occur in a single plane. While, an ordinary light source emits waves that are vibrating in more than one plane (e.g. the light emitted by the sun and by a lamp).

$$\delta = c\ \left(\frac{h}{v_1} + \frac{h}{v_2}\right) = h(n_1 - n_2),$$

where $h/v_i = t_i$ is the time necessary of the *i*-th ray to cross the body, v_i, n_i represent the velocity of propagation and the refractive index of the *i*-th ray, respectively, with i =1, 2. Thus, the phase difference of the light components emerging is given by

$$\Delta = \frac{2\pi}{\lambda}\ (t_2 - t_1) = \frac{2\pi}{\lambda}\ h(n_1 - n_2),$$

where λ is the wavelength of the light being used.

In 1816 David Brewster discovered that "*the relative change in index of refraction is proportional to the difference of principal strain*". Then, Neumann and Maxwell studied the phenomenon of temporary birefringence and gave analogous relations in the case of linearly elastic materials. Thus, by restricting to linear elasticity, the following relationships between indices of refraction and applied loads

$$\begin{aligned} n_1 - n_0 &= c_1\sigma_1 + c_2(\sigma_2 + \sigma_3), \\ n_2 - n_0 &= c_1\sigma_2 + c_2(\sigma_3 + \sigma_1), \\ n_3 - n_0 &= c_1\sigma_3 + c_2(\sigma_1 + \sigma_2), \end{aligned}$$

hold, where n_0 is the index of refraction of the material in the unstressed state, n_1, n_2, n_3 are the principal refractive indices along the principal stress direction $\sigma_1, \sigma_2, \sigma_3$, and c_1, c_2 are constants depending on the material, namely *stress-optic coefficients*.

By subtracting the previous equation member to member and exploiting the relationship between the phase difference and the indices of refraction, in the case of two-dimensional or plane stress problems (e.g. $\sigma_3 = 0$), it holds

$$\Delta = \frac{2\pi\, hC}{\lambda}(\sigma_1 - \sigma_2),$$

where $C = c_2 - c_1$ represents the *relative stress-optic coefficient* $\left([C] = 1\ \text{Brewster} = 10^{-12}\frac{\text{m}^2}{\text{N}} = 10^{-6}\frac{1}{\text{MPa}}\right)$.

Let $N = \frac{\Delta}{2\pi}$ be the fractional phase shift (*fringe order*) and $f_\sigma = \frac{\lambda}{C}$ be a property of the material for a given wavelength (*material fringe value*), we can rewrite the latter equation as

$$(\sigma_1 - \sigma_2) = \frac{N f_\sigma}{h}.$$

If the value of *N* can be measured and f_σ can be determined through calibration, the stress difference $\sigma_1 - \sigma_2$ can be estimated.

The purpose of the polariscope is to determine the value of *N* at each point in the material. When the stressed material is placed into a polariscope, a pattern of bands is observed due to the applied loads. The bands are coloured or dark/light whether the sample is subjected to white or monochromatic light source, respectively. The displayed bands are named *fringes*, which provide the value of *N* throughout the material. The number of fringes increases in proportion to the applied forces.

A circular polariscope consist of a light source, two lenses, two polarizer filters and two quarter-wave plates (*Figure 5.1.1*). The observed fringe pattern is called isochromatic fringes and the intensity of the light emerging from the circular polariscope is given by

$$I = a^2 \sin^2 \frac{\Delta}{2},$$

where *a* is the amplitude of the wave. Therefore, the intensity of light depends only on the difference $\sigma_1 - \sigma_2$ and the formation of black bands in the photoelastic pattern

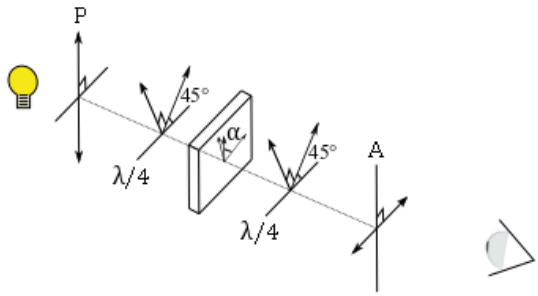

Figure 5.1.1 A circular polariscope diagram. The polarizer divides the incident light waves into vertical and horizontal components and transmit only the components parallel to the axis of polarization of the filter. The quarter-wave plate is like a photoelastic material having *N*=1/4 and its principal axis are oriented at an angle of 45° to the axis of the polarizer. α is the angle between the principal stress direction, σ_1 and σ_2, at the point under consideration in the material and the axis of polarization of the polarizer.

represents the extinction of the used monochromatic light, i.e. $\frac{\Delta}{2} = n\,\pi$, $n = 0, 1, 2, \ldots$. The observed pattern is referred as isochromatic fringe pattern. The circular polariscope can be employed with either the polarization axis of the polarizer and analyser crossed (dark field) or parallel (light field). In the first arrangement the order of fringes, *N*, coincides with *n*, while in the second arrangement the order of fringe is $N = \frac{1}{2} + n$.

By removing the two quarter-wave plates from the circular polariscope, we obtain a plane polariscope. In this system the intensity of the emerging light in the dark field arrangement is

$$I = a^2 \sin^2 2\alpha \sin^2 \frac{\Delta}{2},$$

where α is the angle between the principal stress direction at the point under consideration in the material and the axis of polarization of the polarizer. Thus, the extinction of the light depends on both the principal stress directions and the principal stress difference $\sigma_1 - \sigma_2$. The fringe pattern produced by $\sin^2 2\alpha$ is named *isoclinic fringe pattern*. Since the principal stress directions and $\sigma_1 - \sigma_2$ generally change with the point under consideration, in a plane polariscope a

superimposition of the isoclinic and isochromatic fringe pattern can be observed. Therefore, the circular polariscope is more used because it eliminates the isoclinic fringe pattern and maintains the isochromatic pattern.

5.2. Fringe Multiplication and Experimental Setup

The scope of the fringe multiplier is to increase the sensitivity of the polariscope. The optical system for fringe multiplication technique consists of a circular polariscope with the addition of a partial mirror on each side of the specimen as shown in *Figure 5.3.2*. The mirrors are slightly inclined, so that the light rays emerge in slightly different directions according to their number of passages through the sample. Light passing back and forth through the sample model is converged to different points corresponding to a specific fringe multiplication. A diaphragm stop is placed to eliminate the unwanted light beams except the specific one carrying the desired multiplication pattern to pass.

Therefore, by considering the multiplication of fringes *m* times, the intensity of light in the dark field arrangement is

$$I = a^2 T^2 R^{m-1} \sin^2 \frac{\Delta}{2},$$

where *R*, *T* are the light reflection and transmission of the employed partial mirrors, respectively. Thus, we have the value of fringe number is $N_m = \Delta/2\pi = k/m$, $k = 0, 1, 2, \ldots$.

The developed optical system for fringe multiplication technique consists of a green led as light source (with a wavelength of approximately 520-530nm), two lenses (AGL-50-39P and S-SLB-50-100P, OptoSigma Europe), two quarter-wave plates (WP140HE, ITOS), and two linear polarizing sheets (Polaroid XP44-40, ITOS). We selected partial mirrors that reflect about 50% of the incident light and transmit about 50% (Eksma Optics - Optolita UAB). Therefore, the optimum multiplication factor of the selected mirrors is *m*=3, i.e. the loss in intensity is minimized. Since the difference $\sigma_1 - \sigma_2$ is directly proportional to the applied load for a circular disk

under diametric compression, we exploited this case to verify the fringe multiplication technique. *Figure 5.2.1* shows the isochromatic pattern observed in a birefringent circular disk under diametric compression with the fringe multiplication technique.

We tested root growth in edible gelatine using a modified optical system for fringe multiplication to control the plant roots not only at constant time interval, but also at constant interval of light (Memo DW E - Vemer S.p.A.). In fact, the plant was firstly tested by keeping a light on, then 3 and 1 minutes of light every 15 minutes for all the experiment duration.

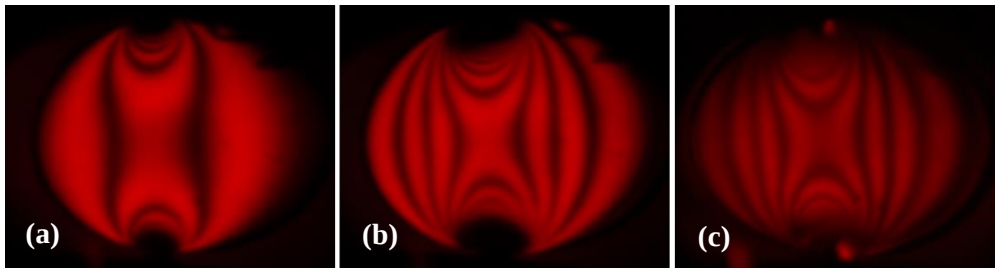

Figure 5.2.1 Isochromatic patterns observed in a birefringent circular disk under diametric compression. (a) ordinary isochromatic pattern; (b) ordinary isochromatic pattern by increasing three times the applied load; (c) three times multiplication by applying the same load as in (a).

5.3. Planting and Gelatine Preparation

We tested 3/4-day old Borlotti beans (*Phaseolus vulgaris L.*). The seed were grown in tap water and kept at ~25˚C.

The birefringent soil medium was prepared by using ~2.2gr of edible gelatine in ~50ml of boiled water. Higher concentrations of gelatine lead to an excessive and premature growth of fractures during the experiments, thus hiding the photoelastic fringes. The gelatine was placed in two types of plastic boxes (*Figure 5.3.1*). After 3/4 days, plants with root grown straight and of ~2 cm length were selected, transplanted into the gelatine, and placed into the photoelastic setup as in *Figure 5.3.2*. Therefore, the growth time t = 0 is referred to the starting time of the photoelastic experiment, i.e. the sample is a 3/4-day old primary root at t = 0.

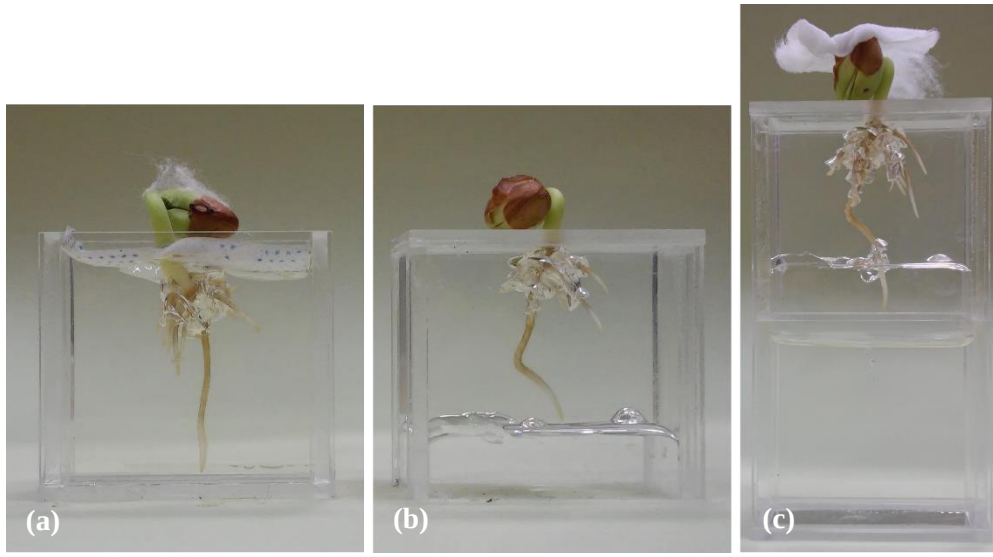

Figure 5.3.1 The plants grow in two possible types of plastic boxes. (a) The box is open at the top and close at the bottom; (b) The box is close at the top and open to the bottom to allow the possibility to extend the surface as the configuration (c), by placing a box of type (a) beside a box of type (b).

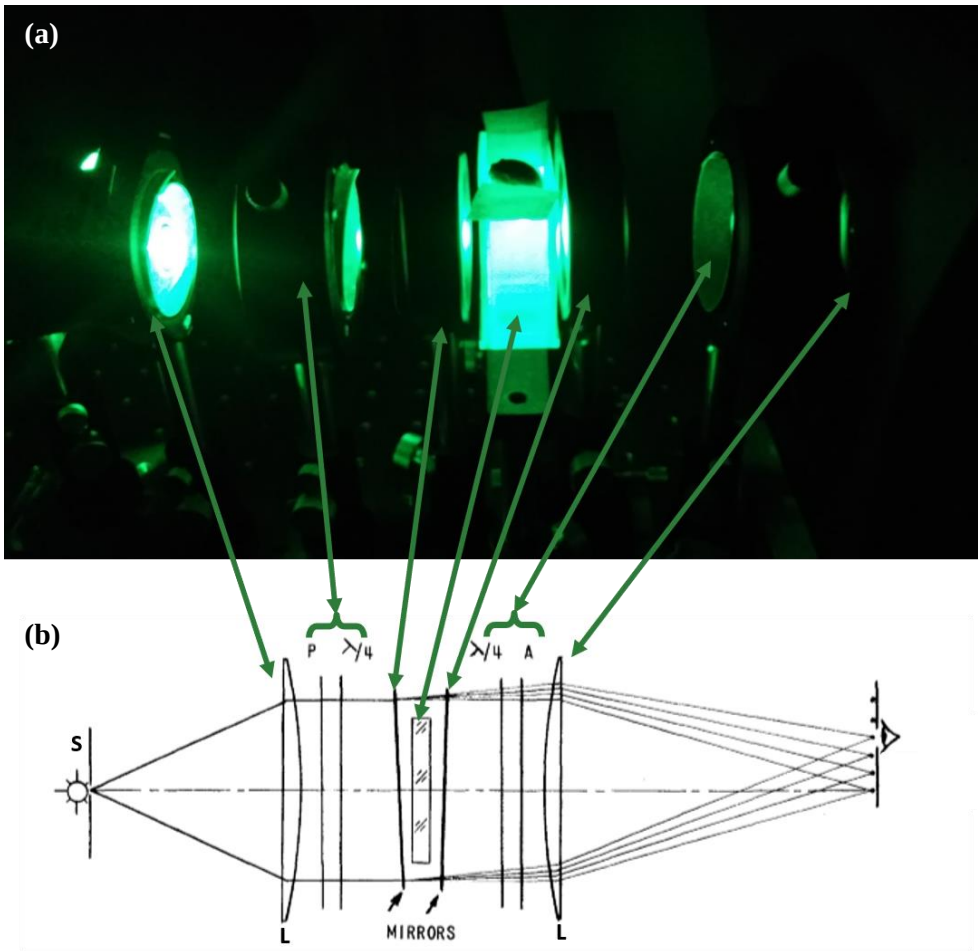

Figure 5.3.2 (a) The optical system for fringe multiplication technique and (b) its schematic diagram (modified image from (Doyle and Phillips, 1989)). S – Light Source; L – Lens; P – Polarizer; λ/4 – Quarter-wave plate; A – Analyzer.

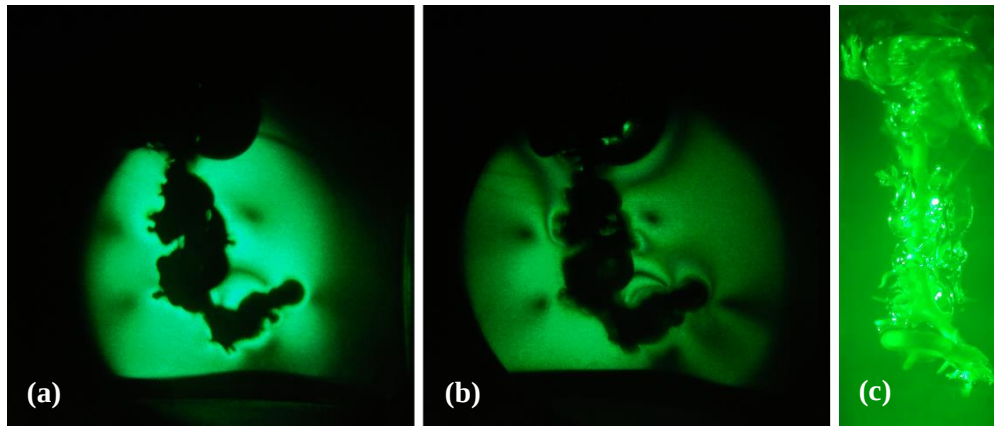

Figure 5.3.3 Isochromatic patterns developed by a Borlotti root (*Phaseolus vulgaris*) in edible gelatine illustrating photoelastic fringe multiplication by factors of (a) 1 and (b) 3. (c) The corresponding lateral view of the plant roots in the photoelastic set-up after 3 days 1h from the beginning of the photoelastic experiment.

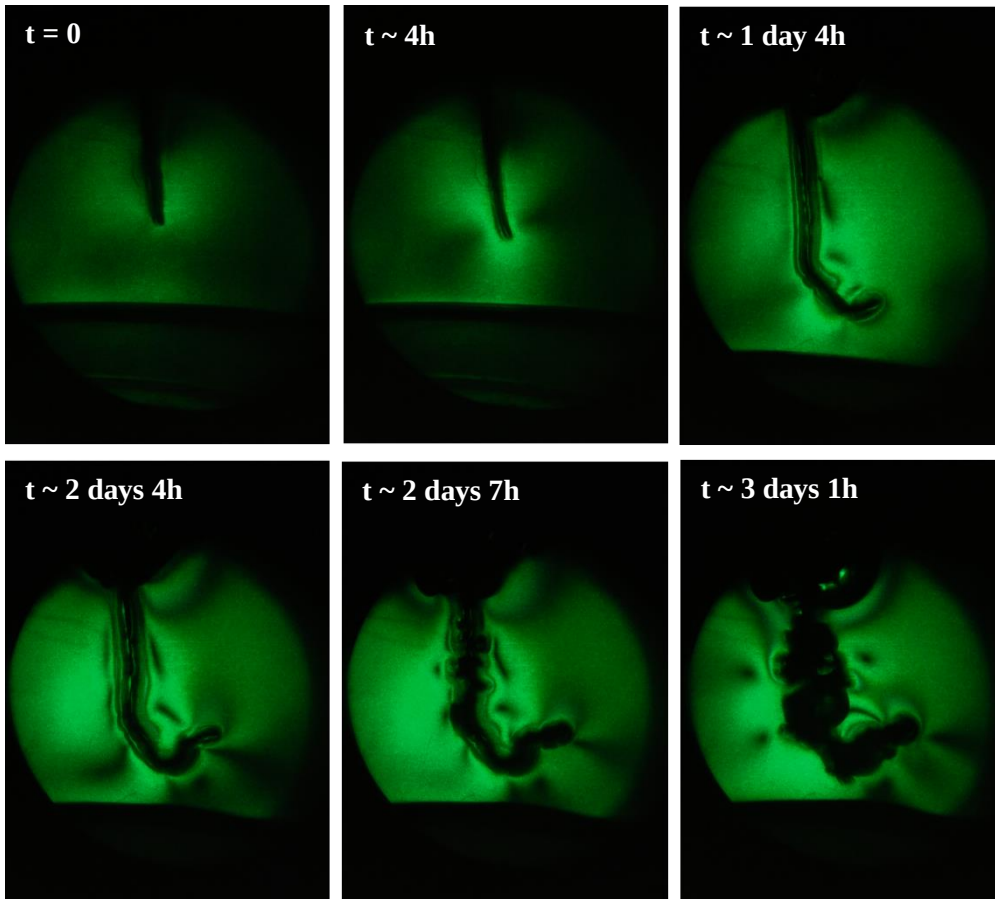

Figure 5.3.4 Development of a Borlotti root (*Phaseolus vulgaris*) in edible gelatine at different growth times with the root tested by keeping the light on during the all duration of the experiment. See Figure 5.3.3c for the lateral view of the root at t ~ 3 days 1h. The growth time t =0 is the starting time of the photoelastic experiment, i.e. the sample is a 3/4-day old primary root.

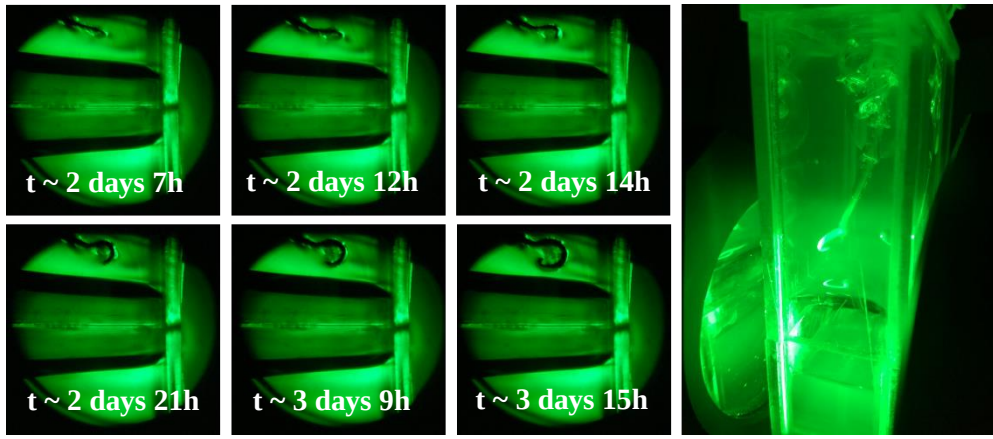

Figure 5.3.5 Development of a Borlotti root (*Phaseolus vulgaris*) in edible gelatine at different growth times with the root tested by keeping the light on for 3 minutes of light every 15 minutes for all the experiment duration. On the right the corresponding lateral view of the plant roots in the photoelastic set-up after 3 days 15h from the beginning of the photoelastic experiment.

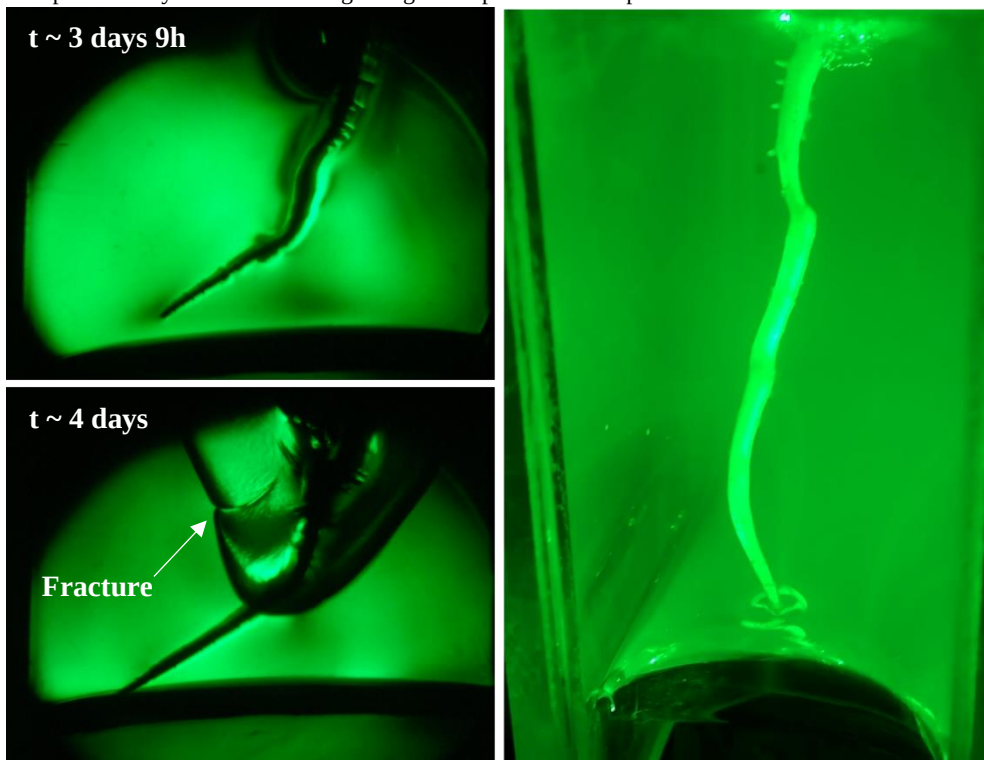

Figure 5.3.6 Development of a Borlotti root (*Phaseolus vulgaris*) in edible gelatine at different growth times with the root tested by keeping the light on for 1 minutes of light every 15 minutes for all the experiment duration. On the right the corresponding lateral view of the plant roots in the photoelastic set-up at t ~ 3 days 18h from the beginning of the photoelastic experiment and just before the arise of the fracture inside the gelatine.

5.4. Interpretation and Discussion

We firstly perform preliminary tests to investigate and choose a proper gelatine concentration and a growing method with the polariscope of our laboratory (the polariscope has been designed and manufactured at the University of Trento and used e.g. in (Noselli, Dal Corso and Bigoni, 2010; Misseroni *et al.*, 2014), see http://ssmg.unitn.it/ for more details). Then, we set up the optical system for fringe multiplication in order to increase a number of observable fringe order. We applied the fringe multiplication to the study of plant roots growing in edible gelatine. We collected the pictures into videos, by monitoring the growth of plant roots in the fringe multiplication set up keeping the light on at three different time intervals. We firstly tested keeping the light on for all the duration of the experiment. In this configuration, roots exhibited an inversion of growth direction with respect to gravity (*Figure 5.3.3, Figure 5.3.4*). To verify if the light exposition time could be a possible consequence of such phenomenon, we modified the photoelastic set-up to perform the experiments with 3 minutes and 1 minute of light every 15 minutes for all the experiment duration (*Figure 5.3.5 and Figure 5.3.6*, respectively). *Figure 5.3.6* shows the method with 1 minute of light every 15 minutes may result less invasive at reversing the green light response of the root with respect the other two methods.

To give a descriptive explanation of the presence of homogeneous fringes along the root lateral surface, we exploited the theoretical model developed in Chapter 2 with the growth data of Phytagel E. In fact, by consider the root growth as consecutive cycles of Fracture and Regrowth as in Chapter 2 and through the experimental position of the first fringe, we can obtain an estimated value of the fringe constant f_σ, e.g. at the end of the FRC. The variation of the first fringe position along the root lateral surface during a FRC is given by *Figure 5.4.1*. Then, the increase of fringes along the lateral surface of the root is due to the simultaneous growth of lateral roots and fractures of the gelatine (*Figure 5.3.3c*). We are aware that both the theoretical model and the photoelastic technique do not take into account all the

possible phenomena involved in the interaction between the plant root and soil medium, e.g. dewatering. In spite of their limitations, these studies could pay the way to give further insight on better understanding such physical phenomenon. Further experiments should be conducted to determine e.g. whether the dewatering of the soil can modify the fringe constant due to the presence of the plant root.

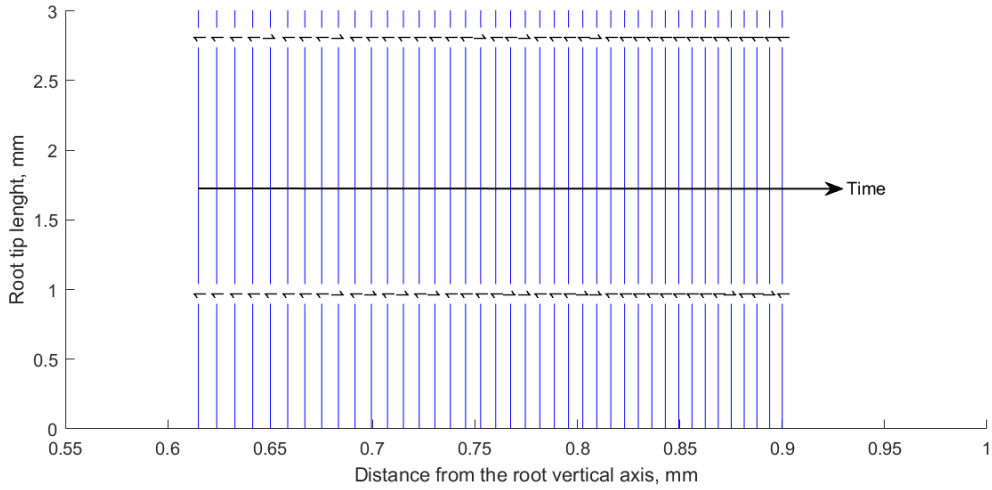

Figure 5.4.1 The evolution of the first fringe during the FRC by applying the growth model in Chapter 2 to the growth data (Phytagel E), by using f_σ= 5.22 N/m.

Chapter 6

6. Conclusion and Future Perspective

Animals and plants are in direct contact with the environment and have to face continuously several unexpected constraints and changes. On this basis, the exploitation of the movement efficiency adopted by Nature could be a key feature to provide new bioinspired concepts. Therefore, the interest of science and engineering is increasing to understand the principles exploited by Nature.

The present thesis aims at creating a synergy between different fields, such as biology, engineering and mathematics in order to investigate on the adaptive strategies adopted by plant roots for new potential devices. In particular, mathematical models applied to plant science can be crucial for both explaining biological phenomena and better designing robotic systems enabled with penetration capabilities and adaptive movements. There is a great potential for a possible extension of such models to develop new methodologies for robots with adaptive movements based on soft materials. In the present work, both the theoretical and experimental studies could lead to deeper investigations to gain a better understanding of the adaptive strategies of plant roots to the outer stimuli.

In Chapter 2, we studied the growth of plant roots in artificial and real soils. Since the ability of plant roots to penetrate soils is affected by the mechanical stresses exerted by the surrounding medium, we investigated and modelled the biomechanical response of the *Zea mays L.* primary roots, grown in soils with different impedances. In this regard, we developed a growth mathematical model based on a modified version of the extended universal law of West, Brown, and Enquist. Our model, in agreement with our experimental results, showed a different root elongation compared to data from both real and artificial soil by varying the soil medium compactness.

Then, in Chapter 3 we extended the mathematical model, developed in Chapter 2, to the growth of plant roots in artificial soils with different concentrations of nutrient. In order to avoid the soil heterogeneity, we used experiments in artificial soil with only the presence of different nutrient stimuli. In fact, we proposed a model, in combination with experimental data, in order to better understand the adaptation process of roots in presence of high nutrient concentrations. Our findings indicated that the root length decreases whereas its radius increases in higher nutrient concentration. The theoretical framework aims at coupling continuum mechanics with plant roots response to nutrient availability.
Understanding the mechanisms that control root growth is essential to model the key biological processes and translate them into possible bio-inspired engineering applications. Therefore, the two theoretical studies may provide further insights into the adaptive ability of plant roots at various impedance and nutrient constraints and could be improved by including and considering a more complete and complex scenario of the root growth inside a soil medium.

In addition, some theories and hypotheses about the function of the root tip and the mechanism of transmitted stimuli by the tip along the whole root have not been completely understood and explained. The investigation of how the mechanical and surface properties could vary with respect to the outer stimuli is closely related to the role of root tip as a "motor zone" (Dougal, 1987). Thus, in Chapter 4, we used the dynamic nanoindentation technique and wettability tests to study the mechanical properties and surface features of *Zea mays L.* root tissues. As new cells are continuously created in the apical region, the cellular differentiation is at an early stage, close to the root tip. Therefore, the results of the mechanical tests could reveal root penetration strategies during the growth from the tip. The combination of soft and stiff materials may enhance plant roots to simultaneously penetrate and adapt to soil constraints. Accordingly, this experimental study could improve the current knowledge in the tip function to control the adaptive mechanisms for the development of bioinspired engineering applications. Future developments will be

the study of the whole plant tissues in various plant species in order to gain a better understanding of the role of mechanical tissue properties in penetrating soil at different outer stimuli.

Finally, in Chapter 5, we presented a set-up for the primary root growth in homogeneous birefringent media using photoelastic technique. An accurate picture of stress distribution at various points in a photoelastic material can be determined, by studying the fringe pattern by means of photoelastic technique. Several attempts have been made due to the difficulties of controlling bacterial activities and gelatine concentration. Lastly, we obtained a working method to use edible gelatine as a growing medium for *Phaseolus vulgaris* primary roots. We selected optical products for the fringe multiplication technique in order to improve the results on observable fringe order. Further experiments, exploiting the created non-standard boxes, could be useful to investigate how the penetration angle of the root could evolve during the penetration with different soil constraints, e.g. as the tip-to-barrier angle (observed in (Popova, Tonazzini, *et al.*, 2016)). This study showed that photoelasticity may be an alternative and potentially useful technique to investigate the primary root growth. In fact, despite its exploratory nature, this study could offer some insights into the stress distribution developed by roots inside a birefringent medium thanks to the monitoring of the root growth by keeping the light on at different time interval.

Bibliography

Agrawal, R., Peng, B. and Espinosa, H. D. (2009) 'Experimental-computational investigation of ZnO nanowires strength and fracture', *Nano Letters*, 9(12), pp. 4177–4183. doi: 10.1021/nl9023885.

Agudelo, C., Packirisamy, M. and Geitmann, A. (2016) 'Influence of Electric Fields and Conductivity on Pollen Tube Growth assessed via Electrical Lab-on-Chip', *Scientific Reports*. Nature Publishing Group, 6(January), pp. 1–15. doi: 10.1038/srep19812.

Alessa, L. and Earnhart, C. (2000) 'Effects of soil compaction on root and root hair morphology: implications for campsite rehabilitation', in *Wilderness science in a time of change conference-Volume 5: Wilderness ecosystems, threats, and management*, pp. 99–104.

Atwell, B. (1989) 'Physiological responses of lupin roots to soil compaction', in Loughamn, B. C., Gašparíková, O., and Kolek, J. (eds) *Structural and Functional Aspects of Transport in Roots: Third International Symposium on 'Structure and Function of Roots' Nitra, Czechoslovakia, 3–7 August 1987*. Kluwer Academic Publishers, pp. 251–255.

Baluska, F. *et al.* (1993) 'Cellular Dimorphism in the Maize Root Cortex : Involvement of Microtubules , Ethylene and Gibberellin in the Differentiation of Cellular Behaviour in Postmitotic Growth Zones', pp. 394–403.

Baluška, F., Jasik, J., *et al.* (2001) 'Latrunculin B-induced plant dwarfism: Plant cell elongation is F-actin-dependent', *Developmental Biology*. doi: 10.1006/dbio.2000.0115.

Baluška, F., Busti, E., *et al.* (2001) 'Lilliputian mutant of maize lacks cell elongation and shows defects in organization of actin cytoskeleton', *Developmental Biology*, 236(2), pp. 478–491. doi: 10.1006/dbio.2001.0333.

Baluška, F. *et al.* (2009) 'The "root-brain" hypothesis of Charles and Francis Darwin', *Plant Signaling & Behavior*, 4(12), pp. 1121–1127. doi: 10.4161/psb.4.12.10574.

Baluska, F., Hauskrecht, D. V. M. and Barlow, P. W. (1996) 'Root Cap Mucilage and Extracellular Calcium as Modulators of Cellular Growth in Postmitotic Growth Zones of the Maize Root Apex *', 109, pp. 25–34.

Baluska, F., Parker, J. S. and Barlow, P. W. (1993) 'A role for gibberellic-acid in orienting microtubules and regulating cell-growth polarity in the maize root cortex.', *Planta*, 191(2), pp. 149–157.

Baluška, F., Parker, J. S. and Barlow, P. W. (1993) 'The microtubular cytoskeleton in cells of cold-treated roots of maize (Zea mays L.) shows tissue-specific responses', *Protoplasma*, 172(2–4), pp. 84–96. doi: 10.1007/BF01379366.

Bar-Cohen, Y. (2006) 'Biomimetics - Using nature to inspire human innovation', *Bioinspiration and Biomimetics*. doi: 10.1088/1748-3182/1/1/P01.

Barley, K. P. (1963) 'Influence of soil strength of growth of roots', *Soil Science*, 96(3), pp. 175–180. doi: 10.1097/00010694-196309000-00004.

Bartsch, M. *et al.* (2001) 'Exploring Insect Biomechanics with Micromachined Force Sensors', *Transducers '01 Eurosensors XV*, pp. 1634–1637.

Bartsch, M. S. *et al.* (2003) 'Small insect measurements using a custom MEMS force sensor', in *TRANSDUCERS 2003 - 12th International Conference on Solid-State Sensors, Actuators and Microsystems, Digest of Technical Papers*, pp. 1039–1042. doi: 10.1109/SENSOR.2003.1216946.

Bartsch, M. S. *et al.* (2007) 'A multiaxis force sensor for the study of insect biomechanics', *Journal of Microelectromechanical Systems*, 16(3), pp. 709–718. doi: 10.1109/JMEMS.2007.893677.

Bengough, A. G. *et al.* (2006) 'Root responses to soil physical conditions; growth dynamics from field to cell', in *Journal of Experimental Botany*, pp. 437–447. doi: 10.1093/jxb/erj003.

Bengough, A. G. *et al.* (2011) 'Root elongation, water stress, and mechanical impedance: A review of limiting stresses and beneficial root tip traits', *Journal of Experimental Botany*, pp. 59–68. doi: 10.1093/jxb/erq350.

Bengough, A. G. (2012) 'Root elongation is restricted by axial but not by radial pressures: So what happens in field soil?', *Plant and Soil*, 360(1–2), pp. 15–18. doi: 10.1007/s11104-012-1428-8.

Bengough, A. G., Croser, C. and Pritchard, J. (1997) 'A biophysical analysis of root growth under mechanical stress', *Plant and Soil*, 189(1), pp. 155–164. doi: 10.1023/A:1004240706284.

Bengough, A. G. and Mackenzie, C. J. (1994) 'Simultaneous measurement of root force and elongation for seedling pea roots', *Journal of Experimental Botany*, 45(1), pp. 95–102. doi: 10.1093/jxb/45.1.95.

Bengough, A. G. and Mullins, C. E. (1990) 'Mechanical impedance to root growth: a review of experimental techniques and root growth responses', *Journal of Soil Science*, 41(3), pp. 341–358. doi: 10.1111/j.1365-2389.1990.tb00070.x.

Bengough, A. and Mullins, C. (1990) 'Mechanical impedance to root growth: a review of experimental techniques and root growth responses', *Journal of soil*

science, 41, pp. 341–358. doi: 10.1111/j.1365-2389.1990.tb00070.x.

Bennet, R., Breen, C. and Fey, M. (1985a) 'Aluminium uptake sites in the primary root of Zea mays L.', *South African Journal of Plant and Soil*, 2(1), pp. 1–7.

Bennet, R., Breen, C. and Fey, M. (1985b) 'The primary site of aluminium injury in the root of Zea mays L.', *South African Journal of Plant and Soil*, 2(1), pp. 8–17.

Bernardino, N. R., Blickle, V. and Dietrich, S. (2010) 'Wetting of surfaces covered by elastic hairs', *Langmuir*, 26(10), pp. 7233–7241. doi: 10.1021/la904345r.

Bettencourt, L. M. A. *et al.* (2007) 'Growth, innovation, scaling, and the pace of life in cities', *Proceedings of the National Academy of Sciences*, 104(17), pp. 7301–7306. doi: 10.1073/pnas.0610172104.

Bizet, F. *et al.* (2016) '3D deformation field in growing plant roots reveals both mechanical and biological responses to axial mechanical forces', *Journal of Experimental Botany*, 67(19), pp. 5605–5614. doi: 10.1093/jxb/erw320.

Blengino Albrieu, J. L., Reginato, J. C. and Tarzia, D. A. (2015) 'Modeling water uptake by a root system growing in a fixed soil volume', *Applied Mathematical Modelling*. doi: 10.1016/j.apm.2014.11.042.

Bombelli, P., Howe, C. J. and Bertocchini, F. (2017) 'Polyethylene bio-degradation by caterpillars of the wax moth Galleria mellonella', *Current Biology*, pp. R292–R293. doi: 10.1016/j.cub.2017.02.060.

Bowles, J. E. (1997) *Foundation Analysis and Design, Engineering Geology*. doi: 10.1016/0013-7952(84)90010-3.

Bradshaw, A. D. (1965) 'Evolutionary Significance of Phenotypic Plasticity in Plants', *Advances in Genetics*, 13(C), pp. 115–155. doi: 10.1016/S0065-2660(08)60048-6.

Brett, P. N. *et al.* (1995) 'Automatic Surgical Tools for Penetrating Flexible Tissues', *IEEE Engineering in Medicine and Biology Magazine*, 14(3), pp. 264–270. doi: 10.1109/51.391778.

Budíková, S. (1999) 'Structural changes and aluminium distribution in maize root tissues', *Biologia Plantarum*, 42(2), pp. 259–266. doi: 10.1023/A:1002116803679.

Chavarría-Krauser, A., Jäger, W. and Schurr, U. (2005) 'Primary root growth: A biophysical model of auxin-related control', *Functional Plant Biology*. doi: 10.1071/FP05033.

Clark, L. J. *et al.* (1996) 'Complete mechanical impedance increases the turgor of cells in the apex of pea roots', *Plant, Cell and Environment*, 19(9), pp. 1099–1102. doi: 10.1111/j.1365-3040.1996.tb00217.x.

Clark, L. J. *et al.* (1999) 'Maximum axial root growth pressure in pea seedlings: Effects of measurement techniques and cultivars', *Plant and Soil*, 209(1), pp. 101–109. doi: 10.1023/A:1004568714789.

Clark, L. J., Whalley, W. R. and Barraclough, P. B. (2003) 'How do roots penetrate strong soil?', in *Plant and Soil*, pp. 93–104. doi: 10.1023/A:1026140122848.

Colombi, T. *et al.* (2017) 'Root Tip Shape Governs Root Elongation Rate under Increased Soil Strength', *Plant Physiology*, 174(4), pp. 2289–2301. doi: 10.1104/pp.17.00357.

Cranford, S. W. *et al.* (2012) 'Nonlinear material behaviour of spider silk yields robust webs', *Nature*, pp. 72–76. doi: 10.1038/nature10739.

Crick, J. C. and Grime, J. P. (1987) 'Morphological plasticity and mineral nutrient capture in two herbaceous species of contrasted ecology', *New Phytologist*, 107(2), pp. 403–414. doi: 10.1111/j.1469-8137.1987.tb00192.x.

Crouzy, B., Edmaier, K. and Perona, P. (2014) 'Biomechanics of plant anchorage at early development stage', *Journal of Theoretical Biology*, 363, pp. 22–29. doi: 10.1016/j.jtbi.2014.07.034.

Dally, J. and Riley, W. (1991) *Experimental Stress Analysis*. Third Edit. McGraw Hill.

Darwin, C. and Darwin, F. (1880) *The power of movement in plants*, *The Power of Movement in Plants*. doi: 10.1017/CBO9780511693670.

Das, B. M. (2014) *Advanced Soil Mechanics 4th edition, CRC press, Taylor & Francis Group*. doi: 10.1029/EO066i042p00714-02.

Dexter, A. R. (1987) 'Mechanics of root growth', *Plant and Soil*, 98(3), pp. 303–312. doi: 10.1007/BF02378351.

Dietrich, D. *et al.* (2017) 'Root hydrotropism is controlled via a cortex-specific growth mechanism', *Nature Plants*. doi: 10.1038/nplants.2017.57.

Dorgan, K. M., Arwade, S. R. and Jumars, P. A. (2007) 'Burrowing in marine muds by crack propagation: kinematics and forces', *Journal of Experimental Biology*, 210(23), pp. 4198–4212. doi: 10.1242/jeb.010371.

Dorgan, K. M., Law, C. J. and Rouse, G. W. (2013) 'Meandering worms : mechanics of undulatory burrowing in muds', *Proceedings of the Royal Society B: Biological Sciences*, 280(February), pp. 1–9. doi:

http://dx.doi.org/10.1098/rspb.2012.2948.

Dougal, D. T. (1987) ‘The curvature of Roots’, *Botanical Gazette*, 23(5), pp. 307–366.

Doyle, J. F. and Phillips, J. W. (1989) ‘Manual on Experimental Stress Analysis Fifth Edition Society for Experimental Mechanics’, *Society for Experimental*.

Drew, M. C. and Saker, L. R. (1978) ‘Nutrient supply and the growth of the seminal root system in barley: III. Compensatory increases in growth of lateral roots, and in rates of phosphate uptake, in response to a localized supply of phosphate’, *Journal of Experimental Botany*, 29(2), pp. 435–451. doi: 10.1093/jxb/29.2.435.

Dupuy, L., Gregory, P. J. and Bengough, A. G. (2010) ‘Root growth models: Towards a new generation of continuous approaches’, *Journal of Experimental Botany*. doi: 10.1093/jxb/erp389.

Durelli, A. and Riley, W. (1965) *Introduction to Photomechanics*. Prentice-Hall.

Dyson, R. J. and Jensen, O. E. (2010) ‘A fibre-reinforced fluid model of anisotropic plant cell growth’, *Journal of Fluid Mechanics*. doi: 10.1017/S002211201000100X.

Edmaier, K. *et al.* (2014) ‘Influence of root characteristics and soil variables on the uprooting mechanics of Avena sativa and Medicago sativa seedlings’, *Earth Surface Processes and Landforms*, 39(10), pp. 1354–1364. doi: 10.1002/esp.3587.

Filleur, S. *et al.* (2005) ‘Nitrate and glutamate sensing by plant roots.’, *Biochemical Society transactions*, 33(Pt 1), pp. 283–6. doi: 10.1042/BST0330283.

Foehse, D. and Jungk, A. (1983) ‘Influence of phosphate and nitrate supply on root hair formation of rape, spinach and tomato plants’, *Plant and Soil*, 74(3), pp. 359–368. doi: 10.1007/BF02181353.

Forterre, Y. (2013) ‘Slow, fast and furious: Understanding the physics of plant movements’, *Journal of Experimental Botany*, pp. 4745–4760. doi: 10.1093/jxb/ert230.

Full, R. J. (2002) ‘Quantifying Dynamic Stability and Maneuverability in Legged Locomotion’, *Integrative and Comparative Biology*, 42(1), pp. 149–157. doi: 10.1093/icb/42.1.149.

Full, R., Yamauchi, a and Jindrich, D. (1995) ‘Maximum single leg force production: cockroaches righting on photoelastic gelatin’, *The Journal of experimental biology*, 198(Pt 12), pp. 2441–2452. Available at: http://www.ncbi.nlm.nih.gov/pubmed/9320366.

Gagliano, M. (2017) 'The mind of plants: Thinking the unthinkable', *Communicative & Integrative Biology*. Taylor & Francis, 10(2), p. e1288333. doi: 10.1080/19420889.2017.1288333.

Gilroy, S. and Masson, P. (2008) *Plant Tropisms*. Blackwell Publishing.

Goldman, D. I. and Hu, D. L. (2010) 'Wiggling Through the World - The mechanics of slithering locomotion depend on the surroundings', *American Scientist*, 98, pp. 314–323.

Goodman, A. M. and Ennos, A. R. (1999) 'The effects of soil bulk density on the morphology and anchorage mechanics of the root systems of sunflower and maize', *Annals of Botany*, 83(3), pp. 293–302. doi: 10.1006/anbo.1998.0822.

Goriely, A. and Neukirch, S. (2006) 'Mechanics of climbing and attachment in twining plants', *Physical Review Letters*, 97(18). doi: 10.1103/PhysRevLett.97.184302.

Greacen, E. L. and Oh, J. S. (1972) 'Physics of root growth', *Nature New Biology*, 235(53), pp. 24–25. doi: 10.1038/newbio235024a0.

Grime, J. P. and Mackey, J. M. L. (2002) 'The role of plasticity in resource capture by plants', *Evolutionary Ecology*, 16(3), pp. 299–307. doi: 10.1023/A:1019640813676.

Gross, K. L., Peters, A. and Pregitzer, K. S. (1993) 'Fine root growth and demographic responses to nutrient patches in four old-field plant species', *Oecologia*, 95(1), pp. 61–64. doi: 10.1007/BF00649507.

Guiot, C., Pugno, N. and Delsanto, P. P. (2006) 'Elastomechanical model of tumor invasion', *Applied Physics Letters*, 89(23), pp. 23–25. doi: 10.1063/1.2398910.

Hamant, O., Traas, J. and Boudaoud, A. (2010) 'Regulation of shape and patterning in plant development', *Current Opinion in Genetics and Development*. doi: 10.1016/j.gde.2010.04.009.

Hamza, O. *et al.* (2006) 'Biomechanics of Plant Roots: estimating Localised Deformation with Particle Image Velocimetry', *Biosystems Engineering*, 94(1), pp. 119–132. doi: 10.1016/j.biosystemseng.2006.02.006.

Harris, J. K. (1978) 'A photoelastic substrate technique for dynamic measurements of forces exerted by moving organisms', *Journal of Microscopy*, 114(2), pp. 219–228. doi: 10.1111/j.1365-2818.1978.tb00132.x.

Hawkes, E. W. *et al.* (2014) 'Human climbing with efficiently scaled gecko-inspired dry adhesives', *Journal of The Royal Society Interface*, 12(102), pp. 20140675–20140675. doi: 10.1098/rsif.2014.0675.

Herbert, E. G. *et al.* (2009) 'Measuring the constitutive behavior of viscoelastic solids in the time and frequency domain using flat punch nanoindentation', *Journal of Materials Research*, 24(3), pp. 626–637. doi: 10.1557/jmr.2009.0089.

Herbert, E. G., Oliver, W. C. and Pharr, G. M. (2008) 'Nanoindentation and the dynamic characterization of viscoelastic solids', *Journal of Physics D: Applied Physics*, 41(7). doi: 10.1088/0022-3727/41/7/074021.

Hu, David and Shelley, M. (2012) 'Slithering Locomotion', *Natural locomotion in fluids and on surfaces; swimming, flying and sliding*, 155, pp. 35–51. doi: 10.1007/978-1-4614-3997-4.

Huang, C. X. and van Steveninck, R. F. M. (1990) 'Salinity induced structural changes in meristematic cells of barley roots', *New Phytologist*, 115(1), pp. 17–22. doi: 10.1111/j.1469-8137.1990.tb00916.x.

Isnard, S. and Silk, W. K. (2009) 'Moving with climbing plants from Charles Darwin's time into the 21st century', *American Journal of Botany*, pp. 1205–1221. doi: 10.3732/ajb.0900045.

Jackson, R. B. and Caldwell, M. M. (1989) 'The timing and degree of root proliferation in fertile-soil microsites for three cold-desert perennials', *Oecologia*, 81(2), pp. 149–153. doi: 10.1007/BF00379798.

Jackson, R. B. and Caldwell, M. M. (1996) 'Integrating Resource Heterogeneity and Plant Plasticity: Modelling Nitrate and Phosphate Uptake in a Patchy Soil Environment', *The Journal of Ecology*, 84(6), p. 891. doi: 10.2307/2960560.

Jiang, L. and Feng, L. (2010) *Bioinspired Intelligent Nanostructured Interfacial Materials*. World Scientific Publishing Co. Pte. Ltd. and Chemical Industry Press.

Kavalenka, M. N. *et al.* (2017) 'Adaptable bioinspired special wetting surface for multifunctional oil/water separation', *Scientific Reports*, 7. doi: 10.1038/srep39970.

Keyes, S. D. *et al.* (2016) 'Mapping soil deformation around plant roots using in vivo 4D X-ray Computed Tomography and Digital Volume Correlation', *Journal of Biomechanics*. Elsevier, 49(9), pp. 1802–1811. doi: 10.1016/j.jbiomech.2016.04.023.

Kirby, J. and Bengough, A. (2002) 'Influence of soil strength on root growth : experiments and analysis using a critical-state model', *European Journal of Soil Science*, 53(March), pp. 119–128. doi: 10.1046/j.1365-2389.2002.00429.x.

Kolb, E., Hartmann, C. and Genet, P. (2012) 'Radial force development during root growth measured by photoelasticity', *Plant and Soil*, 360(1–2), pp. 19–35. doi: 10.1007/s11104-012-1316-2.

Kolb, E., Legué, V. and Bogeat-Triboulot, M. B. (2017) 'Physical root-soil

interactions', *Physical Biology*, 14(6). doi: 10.1088/1478-3975/aa90dd.

Kurth, E. *et al.* (1986) 'Effects of NaCl and CaCl2 on Cell Enlargement and Cell Production in Cotton Roots', *PLANT PHYSIOLOGY*, 82(4), pp. 1102–1106. doi: 10.1104/pp.82.4.1102.

Kynast, R. (2012) 'Handbook of maize: its biology', in. Bennetzen Jeff L., Hake Sarah C. eds. 2009 . Springer, pp. vii–viii.

Laschi, C. *et al.* (2012) 'Soft robot arm inspired by the octopus', *Advanced Robotics*, 26(7), pp. 709–727. doi: 10.1163/156855312X626343.

Li, H. *et al.* (2014) 'Histone acetylation associated up-regulation of the cell wall related genes is involved in salt stress induced maize root swelling', *BMC Plant Biology*, 14(1). doi: 10.1186/1471-2229-14-105.

Loades, K. W. *et al.* (2013) 'Biomechanics of nodal, seminal and lateral roots of barley: Effects of diameter, waterlogging and mechanical impedance', *Plant and Soil*, 370(1–2), pp. 407–418. doi: 10.1007/s11104-013-1643-y.

Loades, K. W. *et al.* (2015) 'Effect of root age on the biomechanics of seminal and nodal roots of barley (Hordeum vulgare L.) in contrasting soil environments', *Plant and Soil*, 395(1–2), pp. 253–261. doi: 10.1007/s11104-015-2560-z.

Lockhart, J. A. (1965) 'An analysis of irreversible plant cell elongation', *Journal of Theoretical Biology*, 8(2), pp. 264–275. doi: 10.1016/0022-5193(65)90077-9.

Margheri, L. *et al.* (2011) 'Non-invasive study of Octopus vulgaris arm morphology using ultrasound', *Journal of Experimental Biology*, 214(22), pp. 3727–3731. doi: 10.1242/jeb.057323.

Materechera, S. A., Dexter, A. R. and Alston, A. M. (1991) 'Penetration of very strong soils by seedling roots of different plant species', *Plant and Soil*, 135(1), pp. 31–41. doi: 10.1007/BF00014776.

Mazzolai, B. (2017) 'Plant-inspired growing robots', *Biosystems and Biorobotics*, 17, pp. 57–63. doi: 10.1007/978-3-319-46460-2_8.

Mazzolai, B., Beccai, L. and Mattoli, V. (2014) 'Plants as Model in Biomimetics and Biorobotics: New Perspectives', *Frontiers in Bioengineering and Biotechnology*, 2. doi: 10.3389/fbioe.2014.00002.

Mirbagheri, S. A. *et al.* (2015) 'Sensitively Photoelastic Biocompatible Gelatin Spheres for Investigation of Locomotion in Granular Media', *Experimental Mechanics*, 55(2), pp. 427–438. doi: 10.1007/s11340-014-9958-z.

Misra, R. K., Dexter, A. R. and Alston, A. M. (1986) 'Maximum axial and radial growth pressures of plant roots', *Plant and Soil*, 95(3), pp. 315–326. doi: 10.1007/BF02374612.

Misseroni, D. *et al.* (2014) 'Stress concentration near stiff inclusions: Validation of rigid inclusion model and boundary layers by means of photoelasticity', *Engineering Fracture Mechanics*, 121–122, pp. 87–97. doi: 10.1016/j.engfracmech.2014.03.004.

Mock, U. *et al.* (2005) 'Towards ultrahydrophobic surfaces: A biomimetic approach', *Journal of Physics Condensed Matter*, 17(9). doi: 10.1088/0953-8984/17/9/021.

Murashige, T. and Skoog, F. (1962) 'A Revised Medium for Rapid Growth and Bio Assays with Tobacco Tissue Cultures', *Physiologia Plantarum*. doi: 10.1111/j.1399-3054.1962.tb08052.x.

Nezhad, A. S. *et al.* (2013) 'Quantification of the Young's modulus of the primary plant cell wall using Bending-Lab-On-Chip (BLOC)', *Lab on a Chip*, 13(13), p. 2599. doi: 10.1039/c3lc00012e.

Niklas, K. J. (1999) 'The mechanical role of bark', *American Journal of Botany*, 86(4), pp. 465–469. doi: Doi 10.2307/2656806.

Normand, V. *et al.* (2000) 'New insight into agarose gel mechanical properties.', *Biomacromolecules*. doi: 10.1021/bm005583j.

Noselli, G., Dal Corso, F. and Bigoni, D. (2010) 'The stress intensity near a stiffener disclosed by photoelasticity', *International Journal of Fracture*, 166(1–2), pp. 91–103. doi: 10.1007/s10704-010-9502-9.

Okada, K. and Shimura, Y. (1990) 'Reversible Root Tip Rotation in Arabidopsis Seedlings Induced by Obstacle-Touching Stimulus', *Science*, 250(4978), pp. 274–276. doi: 10.1126/science.250.4978.274.

Otten, A. and Herminghaus, S. (2004) 'How Plants Keep Dry: A Physicist's Point of View', *Langmuir*, 20(6), pp. 2405–2408. doi: 10.1021/la034961d.

Pantano, M. F. *et al.* (2015) 'Multiphysics Design and Implementation of a Microsystem for Displacement-controlled tensile testing of nanomaterials', *Meccanica*, 50, pp. 549–560.

Peaucelle, A. (2014) 'AFM-based Mapping of the Elastic Properties of Cell Walls: at Tissue, Cellular, and Subcellular Resolutions', *Journal of Visualized Experiments*. doi: 10.3791/51317.

Pelesko, J. and Bernstein, D. (2003) *Modeling MEMS and NEMS*. Boca Raton, FL: Chapman & Hall/CRC.

Pharr, G. M., Oliver, W. C. and Brotzen, F. R. (1992) 'On the generality of the relationship among cantact stiffness,contact area, and elastic-modulus during indentation', *Journal of Materials Research*, 7(3), pp. 613–617. doi: 10.1557/JMR.1992.0613.

Pierret, A. *et al.* (2007) 'Root Functional Architecture: A Framework for Modeling the Interplay between Roots and Soil', *Vadose Zone Journal*, 6(2), p. 269. doi: 10.2136/vzj2006.0067.

Pietola, L. and Smucker, A. J. M. (1998) 'Fibrous carrot root responses to irrigation and compaction of sandy and organic soils', *Plant and Soil*, 200(1), pp. 95–105. doi: 10.1023/A:1004294330427.

Pope, M. T. *et al.* (2017) 'A Multimodal Robot for Perching and Climbing on Vertical Outdoor Surfaces', *IEEE Transactions on Robotics*, 33(1), pp. 38–48. doi: 10.1109/TRO.2016.2623346.

Popova, L., van Dusschoten, D., *et al.* (2016) 'Plant root tortuosity: an indicator of root path formation in soil with different composition and density', *Annals of Botany*, 118(4), pp. 685–698. doi: 10.1093/aob/mcw057.

Popova, L., Tonazzini, A., *et al.* (2016) 'Unveiling the kinematics of the avoidance response in maize (Zen mays) primary roots', *Biologia (Poland)*, 71(2), pp. 161–168. doi: 10.1515/biolog-2016-0022.

Post, D. (1955) 'Isochromatic fringe sharpening and fringe multiplication in photoelasticity', *Proc. SESA*, 12(2).

Post, D. (1966) 'Fringe multiplication in three-dimensional photoelasticity', *The Journal of Strain Analysis for Engineering Design*, 1(5), pp. 380–388. doi: 10.1243/03093247V015380.

Post, D. (1970) 'Photoelastic-fringe multiplication-For tenfold increase in sensitivity - Author concludes that fringe multiplication offers economy and improved accuracy of results', *Experimental Mechanics*, 10(8), pp. 305–312. doi: 10.1007/BF02320808.

Potocka, I. and Szymanowska-Pułka, J. (2018) 'Morphological responses of plant roots to mechanical stress', *Annals of Botany*, (May), pp. 1–13. doi: 10.1093/aob/mcy010.

Roppolo, D. *et al.* (2011) 'A novel protein family mediates Casparian strip formation in the endodermis', *Nature*, 473(7347), pp. 381–384. doi: 10.1038/nature10070.

Sadeghi, A. *et al.* (2014) 'A novel growing device inspired by plant root soil penetration behaviors', *PLoS ONE*, 9(2), pp. 1–10. doi: 10.1371/journal.pone.0090139.

Sadeghi, A. *et al.* (2017) 'A plant-inspired robot with soft differential bending capabilities', *Bioinspiration and Biomimetics*. IOP Publishing, 12(1). doi: 10.1088/1748-3190/12/1/015001.

Sánchez-Calderón, L., Ibarra-Cortés, M. E. and Zepeda-Jazo, I. (2013) 'Root

Development and Abiotic Stress Adaptation', in *Agricultural and Biological Sciences, 'Abiotic Stress - Plant Responses and Applications in Agriculture'*. doi: 10.5772/55043.

Schiavi, A., Cuccaro, R. and Troia, A. (2016) 'Strain-rate and temperature dependent material properties of Agar and Gellan Gum used in biomedical applications', *Journal of the Mechanical Behavior of Biomedical Materials*, 53, pp. 119–130. doi: 10.1016/j.jmbbm.2015.08.011.

Silverberg, J. L. *et al.* (2012) '3D imaging and mechanical modeling of helical buckling in Medicago truncatula plant roots', *Proceedings of the National Academy of Sciences*, 109(42), pp. 16794–16799. doi: 10.1073/pnas.1209287109.

Strogatz, S. (2000) 'Nonlinear dynamics and chaos: with applications to physics, biology, chemistry and engineering', *Cambridge, MA: Westview Press*. Available at: http://www.citeulike.org/group/4585/article/2606929%5Cnpapers://30dd8192-3a85-4010-af1a-3e33b620a902/Paper/p7760.

Taiz, L. and Zeiger, E. (1991) *Plant physiology*, *EE. UU. California: Sinauer*. Available at: http://pdf115.nikubooks.com/plant-physiology-fifth-edition-PDF-341715.pdf.

Tan, T. H. *et al.* (2015) 'How grow-and-switch gravitropism generates root coiling and root waving growth responses in *Medicago truncatula*', *Proceedings of the National Academy of Sciences*, 112(42), pp. 12938–12943. doi: 10.1073/pnas.1509942112.

Taylor, H. M. and Ratliff, L. F. (1969) 'Root elongation rates of cotton and peanuts as a function of soil strength and soil water content', *Soil Science*, 108(2), pp. 113–119. doi: 10.1097/00010694-196908000-00006.

Tian, X. and Doerner, P. (2013) 'Root resource foraging: does it matter?', *Frontiers in Plant Science*, 4. doi: 10.3389/fpls.2013.00303.

Tomlinson, R. A. and Taylor, Z. A. (2015) 'Photoelastic materials and methods for tissue biomechanics applications', *Optical Engineering*, 54(8), p. 081208. doi: 10.1117/1.OE.54.8.081208.

Tramacere, F. *et al.* (2014) 'Hairy suckers: The surface microstructure and its possible functional significance in the octopus vulgaris sucker', *Beilstein Journal of Nanotechnology*, 5(1), pp. 561–565. doi: 10.3762/bjnano.5.66.

Tricinci, O. *et al.* (2015) '3D Micropatterned Surface Inspired by Salvinia molesta via Direct Laser Lithography', *ACS Applied Materials and Interfaces*, 7(46), pp. 25560–25567. doi: 10.1021/acsami.5b07722.

Volkmar, K. M. (1994) 'Pre-germination effects on mechanically impeded root growth of barley (Hordeum vulgare L)', *Plant and Soil*, 163(2), pp. 197–202. doi:

10.1007/BF00007968.

Wang, J. *et al.* (2017) 'Bioinspired shape-memory graphene film with tunable wettability', *Science Advances*. doi: 10.1126/sciadv.1700004.

Wei, C. and Lintilhac, P. M. (2007) 'Loss of Stability: A New Look at the Physics of Cell Wall Behavior during Plant Cell Growth', *PLANT PHYSIOLOGY*, 145(3), pp. 763–772. doi: 10.1104/pp.107.101964.

Wendell, D. M. *et al.* (2012) 'Experimental Investigation of Plant Root Growth Through Granular Substrates', *Experimental Mechanics*, 52(7), pp. 945–949. doi: 10.1007/s11340-011-9569-x.

West, G. B., Brown, J. H. and Enquist, B. J. (1997) 'A general model for the origin of allometric scaling laws in biology', *Science*. doi: 10.1126/science.276.5309.122.

West, G. B., Brown, J. H. and Enquist, B. J. (2001) 'A general model for ontogenetic growth', *Nature*, 413(6856), pp. 628–631. doi: 10.1038/35098076.

Whiteley, G. M. and Dexter, A. R. (1981) 'Elastic response of the roots of field crops', *Physiologia Plantarum*, 51(4), pp. 407–417. doi: 10.1111/j.1399-3054.1981.tb05578.x.

Wilson, A. J. and Robards, A. W. (1978) 'The ultrastructural development of mechanically impeded barley roots. Effects on the endodermis and pericycle', *Protoplasma*, 95(3), pp. 255–265. doi: 10.1007/BF01294454.

Wilson, A. J., Robards, A. W. and Goss, M. J. (1977) 'Effects of mechanical impedance on root growth in barley, Hordeum vulgare L.: II. Effects on cell development in seminal roots', *Journal of Experimental Botany*, 28(5), pp. 1216–1227. doi: 10.1093/jxb/28.5.1216.

Yang, Y., Chen, L. and Li, N. (2016) 'How gauge length and loading rate influence the root tensile strength of Betula platyphylla', *Journal of Soil and Water Conservation*, 71(6), pp. 460–466. doi: 10.2489/jswc.71.6.460.

Zacarias, L. and Reid, M. S. (1992) 'Inhibition of ethylene action prevents root penetration through compressed media in tomato (Lycopersicon esculentum) seedlings', *Physiologia Plantarum*, 86(2), pp. 301–307. doi: 10.1034/j.1399-3054.1992.860217.x.

Zeiger, C. *et al.* (2017) 'Selective filtration of oil/water mixtures with bioinspired porous membranes', *RSC Adv.*, 7(52), pp. 32806–32811. doi: 10.1039/C7RA05385A.

Zha, G. *et al.* (2016) 'Mechanical touch responses of Arabidopsis TCH1-3 mutant roots on inclined hard-agar surface', *International Agrophysics*, 30(1), pp. 105–111. doi: 10.1515/intag-2015-0065.

Zhu, M. Y., Ahn, S. J. and Matsumoto, H. (2003) 'Inhibition of growth and development of root border cells in wheat by Al', *Physiologia Plantarum*, 117(3), pp. 359–367. doi: 10.1034/j.1399-3054.2003.00036.x.

Zidan, I., Azaizeh, H. and Neumann, P. M. (1990) 'Does Salinity Reduce Growth in Maize Root Epidermal Cells by Inhibiting Their Capacity for Cell Wall Acidification?', *PLANT PHYSIOLOGY*, 93(1), pp. 7–11. doi: 10.1104/pp.93.1.7.

Appendix

A. Additional Related Activity: Load Sensor Instability in MEMS-based Tensile Testing Devices

Quantitative and qualitative approaches involve experiments at the different length scales from micro/nanoscale to macroscale in the context of biomechanics and biomimetics.

The ability of animal and plant movements and how their tissues adapt to external constraints and changes can be collected through experimental data. Experimental methods can be tissue mechanical tests and surface properties characterizations. Mechanical tests include nanoindentation, tensile and compression tests that provide information about the strength, stiffness, and hardness of the considered tissues. Indeed, such properties affect the ability of the whole animal/plant structure to perform specific movements. The aim of such experiments is to unlock the secrets of the biological tissue structures that could significantly affect the stability of movements and anchorage. While the second type of characterization will provide information about wettability and adhesion of the tissue during a specific movement. To this aim direct measurements of animal ground forces and plant ground anchorages can be carried out by means of force sensors and tracking tools to study the adaptive movement ability of plants and animals as a whole, see e.g. the Full and Tu force platform at Berkeley (Bartsch *et al.*, 2001, 2003, 2007), the Bending-Lab-On-Chip and the Electrical Lab-on-Chip (Nezhad *et al.*, 2013; Agudelo, Packirisamy and Geitmann, 2016). In addition, mathematical modelling is useful to analyse and verify the plausibility of experimental findings. Theoretical frameworks have a key role to highlight and explain natural phenomena in several fields. Moreover, an analytical approach can be useful in potential predictions for performances of bio- and non-bioinspired devices. In fact, dynamical systems theory could shed light on the potential implementation of strategies adopted by Nature into the physical key parameters of novel devices, e.g. to prevent the

possible onset of instability in devices during measurements (Agrawal, Peng and Espinosa, 2009).

In this regard, MEMS-based tensile testing devices are very powerful tools for mechanical characterization of nanoscale materials, as they allow for testing of micro/nano-sized components *in situ* electron microscopes. In a typical configuration, they consist of an actuator, to deliver force/displacement, and a load sensor, which is connected to the sample like springs in series. Such configuration, while providing a high-resolution force measurement, can cause the onset of instability phenomena, which can later compromise the test validity. In the present Chapter, such phenomena are quantitatively discussed through the development of an analytical model, which allows to find a relationship between the rise of instability and the sensor stiffness, which is the key parameter to be optimized. In addition, a potential bio-inspired design can be an effective solution to avoid such instability phenomena.

The work in this Chapter arises from the collaboration with Dr. Ing. Maria Fiorella Pantano of the University of Trento.

Analytical modeling of MEMS-based tensile testing devices

In most of MEMS tensile testing devices, the load sensor and the sample to be tested are connected like springs in series, as in the lumped parameters model reported in *Figure A.1*a. This is a 2-degrees-of-freedom system, where the sample is represented as a spring with a generic characteristic (its mass is negligible with respect to that of the load sensor), while the load sensor is modeled through a mass (M_{LS}) connected to the substrate through a damper (with damping constant D) and a spring (with spring constant k_{LS}). The sample undergoes a displacement x_S, as a consequence of the actuator movement (not reported in the present model), whereas x_{LS} is the load sensor's displacement.

For simplicity, let us first neglect both the damping and inertial contribution, and let us evaluate the global force-displacement relationship characterizing the system comprising the load sensor and sample springs (*Figure A.1*b).

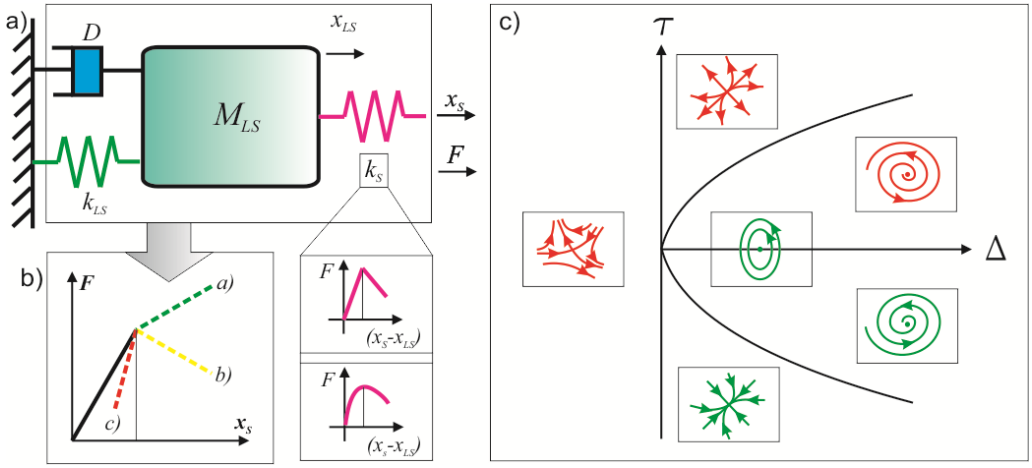

Figure A.1 a) Lumped parameters model of a typical tensile testing device, where the sample can be modeled like a spring whose characteristic shows a softening branch; b) Global behavior of the system consisting of both the load sensor and the sample, showing the relationship between the force (F) corresponding to the applied displacement (x_S). When the sample enters in the softening regime, F may increase (line a)) or decrease (either line b) or c)) with x_S, depending on the magnitude of the slope of the sample characteristic, $\partial F/\partial(x_S-x_{LS})$, compared to the load sensor stiffness, k_{LS}. In particular, line b) corresponds to $\partial F/\partial(x_S-x_{LS})<0$ and $k_{LS}>|\partial F/\partial(x_S-x_{LS})|$, c) $\partial F/\partial(x_S-x_{LS})<0$ and $k_{LS}<|\partial F/\partial(x_S-x_{LS})|$. In order to evaluate the stability of the equilibrium position of the load sensor, its dynamic behavior can be linearized and modeled about such position through a Jacobian matrix. c) The sign of the trace, τ, and the determinant, Δ, of the Jacobian matrix determine the stability of the equilibrium point.

Global system behavior

The overall deformation undergone by the system is $x_S=x_{LS}+(x_S-x_{LS})$, where x_{LS} is the load sensor deformation and (x_S-x_{LS}) the sample deformation. If infinitely small displacements are considered, the overall system deformation becomes:

$$dx_S = dx_{LS} + d(x_S - x_{LS}). \quad \text{(A1)}$$

Since k_{LS} is the load sensor spring constant, then $dx_{LS}=dF/k_{LS}$. If a general characteristic is assumed for the sample, it follows that $d(x_S - x_{LS}) = \partial(x_S - x_{LS})/\partial F\, dF$, where dF is the force acting on the system, which is the same on both the sample and load sensor (since they are connected in series). Thus, eq. (A1) can be rewritten as:

$$dx_S = \frac{dF}{k_{LS}} + \frac{\partial(x_S - x_{LS})}{\partial F}\,\mathrm{dF}\,, \tag{A2}$$

or,

$$\frac{dx_S}{dF} = \frac{1}{k_{LS}} + \frac{\partial(x_S - x_{LS})}{\partial F}\,. \tag{A3}$$

At the beginning, the sample characteristic has a linear increasing trend, (e.g., $\partial(x_S - x_{LS})/\partial F$ or $\partial F/\partial(x_S - x_{LS})$ are constant, and the sample can be modeled like a linear spring), and the slope of the system characteristic ($\partial F/\partial x_S$) is equal to the equivalent stiffness of the sample and load sensor spring constants. Then, the system characteristic may either increase or decrease with increasing x_S, depending on the sample's behavior. In particular, either of the following cases may occur (*Figure A.1*b):

(a) Overall system hardening as a consequence of sample hardening, e.g, if $\partial(x_S - x_{LS})/\partial F > 0$;

(b) Overall softening with negative slope, if the sample exhibits softening (e.g., $\partial F/\partial(x_S - x_{LS}) < 0$) and its slope in modulus is smaller than the load sensor spring constant. In fact, from eq. (A3):

$$\frac{dx_S}{dF} < 0 \;\Leftrightarrow \frac{1}{k_{LS}} + \frac{\partial(x_S - x_{LS})}{\partial F} < 0\,, \tag{A4}$$

which is equivalent to

$$k_{LS} > \left|\frac{\partial F}{\partial(x_S - x_{LS})}\right|, \tag{A5}$$

(c) Overall softening with positive slope if the sample exhibits softening (e.g., $\partial F/\partial(x_s - x_{LS}) < 0$) and its slope in modulus is bigger than the load sensor spring constant. In fact, from eq. (A3):

$$\frac{dx_S}{dF} > 0 \;\Leftrightarrow \frac{1}{k_{LS}} + \frac{\partial(x_S - x_{LS})}{\partial F} > 0\,, \tag{A5}$$

which is equivalent to

$$k_{LS} < \left|\frac{\partial F}{\partial(x_S - x_{LS})}\right|. \tag{A7}$$

Thus, in this latter case, the system would tend to come back to smaller values of x_S, displaying a snap-back branch with positive slope. However, since in a typical tensile test, x_S is progressively increased, the sample is broken without the possibility to follow the snap-back branch and, thus, the corresponding region of the sample characteristic. As a consequence, the optimal design value for the load sensor stiffness depends on the steepest point of interest to be expected during softening regime in the sample characteristic curve. Thus, as a compromise between high resolution during the elastic regime and stability requirement, we can define an optimal load sensor stiffness as

$$k_{LS,opt} = \eta \left|\frac{\partial F}{\partial(x_S - x_{LS})}\right|_{MAX},$$

where η is a partial factor for stability, which could be set equal to 10%.

Load sensor stability

It is now interesting to study what happens to the load sensor when its stiffness is smaller than the sample characteristic slope during softening. To this aim, it is convenient to refer to the model depicted in *Figure A.1*a and write the load sensor's equilibrium equation:

$$M_{LS}\frac{d^2x_{LS}}{dt^2} = \sum_i F_i\,, \tag{A8}$$

where F_i is the i-th force acting on the load sensor. In this case, three forces have to be considered:

$$F_S = F(x_S - x_{LS}), \tag{A9}$$

$$F_{LS} = -k_{LS}x_{LS}\,, \tag{A10}$$

$$F_D = -D\frac{dx_{LS}}{dt}\,, \tag{A11}$$

where F_S is the force transmitted to the load sensor by the sample and depends on the actual sample deformation $(x_S\text{-}x_{LS})$, F_{LS} is the elastic force exerted by the load sensor spring, and F_D the damping force. Thus, considering the (A9)-(A11), eq. (A8) can be rewritten as:

$$M_{LS}\frac{d^2x_{LS}}{dt'^2} = -D\frac{dx_{LS}}{dt'} - k_{LS}x_{LS} + F(x_S - x_{LS}). \tag{A12}$$

In steady-state condition, the equilibrium points of equation (A12) are given by the roots of $f(x_{LS}) = -k_{LS} + F(x_S - x_{LS})$. In order to infer about the stability of a load sensor equilibrium point, x_{LS}^* (solution of eq. (A12)), it is convenient to linearize $f(x_{LS})$ through Taylor expansion as $f(x_{LS}) \approx f'(x_{LS}^*)(x_{LS} - x_{LS}^*)$, where $f'(x_{LS}^*) = \left(-k_{LS} - \frac{dF}{d(x_S - x_{LS})}\right)\Big|_{x_{LS}^*}$ (Pelesko and Bernstein, 2003). From this, it follows that the sign of the slope of $f(x_{LS})$ depends on the magnitude of the slope of $F(x_S - x_{LS})$ compared to k_{LS}, providing two possible cases:

1) $f'(x_{LS}^*) > 0 \;\Leftrightarrow\; \dot{F}(x_S - x_{LS}^*) < -k_{LS}$,
2) $f'(x_{LS}^*) < 0 \;\Leftrightarrow\; \dot{F}(x_S - x_{LS}^*) > -k_{LS}$.

It is now convenient to rewrite eq. (A12) through the following system

$$\begin{cases} \dfrac{dx_{LS}}{dt} = v, \\ \dfrac{dv}{dt} = -\dfrac{D}{M_{LS}}v + \dfrac{f(x_{LS})}{M_{LS}}, \end{cases}$$

that we can linearize near the equilibrium point, x_{LS}^*, as $\frac{d\boldsymbol{u}}{dt} = J\,\boldsymbol{u}$, with $J = \left(\begin{matrix} 0 & 1 \\ \frac{f'}{M_{LS}} & -\frac{D}{M_{LS}} \end{matrix}\right)\Big|_{x_{LS}^*}$, $\boldsymbol{u} = \binom{x_{LS}-x_{LS}^*}{v}$.

The stability of the solution, x_{LS}^*, depends on the trace and determinant of the Jacobian matrix (Strogatz, 2000; Pelesko and Bernstein, 2003), $\tau = tr(J), \Delta = det(J)$, respectively, that on turn depend on f'. In particular, in our system $\tau = -D/M_{LS}<0$, whereas $\Delta = -f'/M_{LS}$. Therefore, when $f'>0$ (previous case 1) $\Delta<0$, meaning that the equilibrium point is unstable (saddle point from *Figure A.1*c). On the contrary, when $f'<0$ (previous case 2), $\Delta>0$, corresponding to always stable equilibrium points (*Figure A.1*c). As a conclusion, when the sample characteristic slope is negative (e.g., softening in the sample) and its modulus is smaller than k_{LS}, stable equilibrium points are allowed to the load sensor (case 2); while instead the sample characteristic slope is negative and its modulus is bigger than k_{LS}, no stable equilibrium points are possible (case 1). Indeed, in such case, as shown in the previous Section, the system of the sample and load sensor springs show a snap-back branch with a positive slope, which cannot be followed during the tensile test.

In some simple cases, the previous generic equation (A12) can be solved analytically. As an example, let us consider a piecewise linear expression of $F(x_S - x_{LS})$, that is characterized by an initial region, where the force increases with the deformation, followed by a second region with a decreasing trend (softening region), that can be defined as (*Figure A.1*a):

$$F(x_S - x_{LS}) = \begin{cases} k_0(x_S - x_{LS}), & if\ x_S - x_{LS} < x^* \\ k_0 x^* - k_1(x_S - x_{LS} - x^*), & if\ x_S - x_{LS} > x^* \end{cases} \quad (A13)$$

Its first region defines the sample elastic regime, while the second one corresponds to the softening region. In order to study what happens to the sensor as soon as the sample enters within the softening regime, we substitute the second of equations (A13) in equation (A12), which then becomes:

$$M_{LS}\frac{d^2x_{LS}}{dt'^2} = -D\frac{dx_{LS}}{dt'} - k_{LS}x_{LS} + k_0x^* - k_1(x_S - x_{LS} - x^*). \quad (A14)$$

It is convenient rewrite Eq. (A14) in dimensionless form. To this aim, we introduce the dimensionless time, $t=t'\sqrt{\frac{|k_1-k_{LS}|}{M_{LS}}}$, and length, $y=x_{LS}/l$, being l the sample gage length and $k_1 \neq k_{LS}$. With these positions, Eq. (A14) can be rewritten as:

$$\frac{d^2y}{dt^2} = -\alpha\frac{dy}{dt} + sgn(k_1 - k_{LS})y + \frac{x^*(k_0 + k_1) - k_1x_S}{l|k_1 - k_{LS}|}. \quad (A15)$$

Where $\alpha = \frac{D}{\sqrt{M_{LS}|k_1-k_{LS}|}}$ is a corrected quality factor, that takes into account the presence of the sample through the term k_1.

Considering a typical MEMS, like that one reported in (Pantano *et al.*, 2015), the damping contribution can be neglected with respect to the inertial effects, meaning that $\alpha \ll 1$. Thus, in the inertia-dominated regime, Eq. (A15) simplifies as:

$$\frac{d^2y}{dt^2} = sgn(k_1 - k_{LS})y + \frac{x^*(k_0 + k_1) - k_1x_S}{l|k_1 - k_{LS}|}. \quad (A16)$$

In general, $x_s=x_s(t)$, but in the hypothesis of a negligible variation of x_s with time, Eq. (A16) can be solved analytically depending on the positive (a) or negative (b) sign of (k_1-k_{LS}).

(a) If $k_1>k_{LS}$, the general solution of Eq. (25) is:

$$y = Ae^{t} + Be^{-t} - \frac{x^*(k_0 + k_1) - k_1 x_S}{l(k_1 - k_{LS})}, \tag{A17}$$

(b) If $k_1<k_{LS}$, the general solution of Eq. (25) is instead:

$$y = A\cos t + B\sin t - \frac{x^*(k_0 + k_1) - k_1 x_S}{l(k_1 - k_{LS})}, \tag{A18}$$

A, B are constants depending on the initial conditions.

In order to infer about the stability of the load sensor equilibrium positions defined by equations (A17) and (A18), it is useful to write the second-order differential equation (A16) as a nonhomogeneous linear system:

$$\begin{cases} \dfrac{dy_1}{dt} = y_2, \\ \dfrac{dy_2}{dt} = sgn(k_1 - k_{LS})y_1 + \dfrac{x^*(k_0 + k_1) - k_1 x_S}{l|k_1 - k_{LS}|}. \end{cases}$$

This latter can be turn in a homogeneous system, by introducing the translations $\chi_1 = y_1 - \frac{x^*(k_0+k_1)-k_1x_S}{l(k_1-k_{LS})}$, $\chi_2 = y_2$, i.e.

$$\begin{cases} \dfrac{d\chi_1}{dt} = \chi_2, \\ \dfrac{d\chi_2}{dt} = sgn(k_1 - k_{LS})\chi_1. \end{cases}$$

The above homogeneous linear system has a fixed point, χ^*, at $\chi_1=0$, $\chi_2=0$, i.e. the origin corresponds to the equilibrium position of the system. Repeating the same logic as before, the trace, τ, and the determinant, Δ, of the Jacobian matrix associated to the linear system provides the stability of the fixed point. In this case, $\tau=0$, while $\Delta=-sgn(k_1-k_{LS})$. Thus, with reference to *Figure A.1*c,

(a) If $k_1>k_{LS}$, $\Delta<0$, thus the equilibrium point, χ^*, is a saddle point, i.e., unstable.
(b) If $k_1<k_{LS}$, $\Delta>0$the equilibrium point, χ^*, is a center, i.e., neutrally stable.

Since $\frac{dF}{d(x_s-x_{LS})} = k_1$ and k_1 represents the slope of the decreasing branch of the sample characteristic, the results found now match the conclusions derived previously in case of a sample with a generic characteristic.

The ability of plant roots to penetrate soils is affected by several stimuli from the surrounding medium such as mechanical stresses and chemical changes. Therefore, roots have developed multiple responses to the several outer stimuli. Since plant roots have to face very complex problems to grow deeply into the ground, they are remarkable examples of problem-solving behaviour and adaptation to the outer constraints. The adaptation strategies of a natural root are not yet completely known and understood with exhaustive explanations. For this reason, mathematical models and experimental techniques applied to biological phenomena can perform a key role in translating the Nature adaptive solutions into engineering applications. The aim of this thesis is to provide further insights in understanding biological phenomena for the development of new technologies inspired by the adaptive ability of plant roots. Accordingly, both theoretical and experimental explanations to the adaptive behaviour of plant roots are proposed. The mathematical modelling is based on a modified version of the extended West, Brown and Enquist universal law, considering the root growth as an inclusion problem. The proposed equation has as a particular case a growth equation exploiting an approach similar to Lockhart taking into account the soil impedance. The influence of mechanical stresses and nutrient availability on the root growth are studied. The solutions of the analytical model are compared with experimental data collected in real and artificial soils.
In addition, the theories and hypotheses of the root ability to grow in the apical region through nanoindentation, wettability, and photoelasticity are investigated. The first technique provided insights for the possible role and function at both different tissues levels and distances from the tip in the root movement and penetration during the growth. The investigation of root tissue properties revealed that the penetration and adaptation strategies adopted by plant roots could be enhanced by a combination of soft and stiff tissues. The second technique aimed to highlight the wettability of the apical zone and root hairs for the acquisition of water and nutrients. Finally, photoelastic experiments provided a non-invasive and *in situ* observation of plant roots growth and, by exploiting the fringe multiplication, a set up for the study of plant roots growing in edible gelatine is proposed.